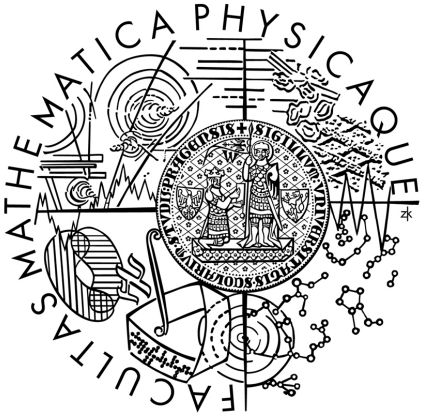

STUDY OF THERMAL PLASMA JETS GENERATED BY DC ARC PLASMA TORCHES USED IN PLASMA SPRAYING APPLICATIONS

Ph.D. Thesis

Mgr. Tetyana Kavka

Supervisor: doc. RNDr. Milan Hrabovský, CSc.

Faculty of Mathematics and Physics
Charles University in Prague

Prague 2006

Devoted to my grandfather
I wish you were here with me at this moment

Content

Acknowledgement

With great pleasure I would like to thank to my supervisors and all coworkers without whom this work could not come into the world.

I would like to thank my supervisor Doc. Milan Hrabovský who introduced me into the world of thermal plasma and guided me through all obstacles, helping and encouraging me during my study, giving worthwhile advice and keeping the main way of the work. I wish to thank RNDr. Miloš Konrad who makes me familiar with the enthalpy probe diagnostics and gave me the first experience with Czech language.

My great thanks are for Doc. Rudolf Henne for the invitation and enabling working in the Institute for Technical Thermodynamics of DLR-Stuttgart, where a big part of the work was done. He is thanked for being my supervisor during my staying in DLR, for his great ideas and assistance. I am grateful to Doc. Johannes Arnold and Doc. Matthias Müller for their willingness to help with work any time and also for their support out of work during my stays in Stuttgart.

I would like to thank Oleksiy Chumak who was not only a compatriot and very good friend during these years. I appreciate his advice and long discussions about all aspects of plasma science. I would like to thank Doc. Vladimír Kopecký, Doc. Viktor Sember, Ing. Vaclav Březina and all other members of the department for their help.

Special thanks are to my family, who supported my decision to study in Charles University in Prague, and to my husband Robert, who always countenanced me and made me stronger when my faith in myself was shacked. Thank you for being loving and patient.

Introduction

Thermal plasma jets interact very intensively with surrounding atmosphere. Unavoidable entrainment of the cold ambient gas alters not only the plasma jet temperature and velocity but the plasma jet composition as well. As a result, the entrainment process puts restrictions onto applications of such jets. The main problem is connected with plasma spraying of metallic powders. Entrainment of the surrounding cold gas into the plasma jet can alter the properties and the quality of the produced coatings. Powder particles are heated to their melting temperature in the plasma jet. Thus, due to fast chemical reactions in-flight oxidation of the metal particles may occur. Oxides in coatings are considered to influence the structure and properties of the deposits. For these reasons, mastering methods of controlling the entrainment to the plasma jet is highly desirable. Efforts are continuously being made to develop practical methods for flow control not only in the core region but in the turbulent region as well.

The present work is aimed to study the entrainment process occurring in thermal plasma jets generated by DC arc plasma torches with gas and gas-water stabilization of the arc. These torches are widely used for thermal plasma processing and mainly for plasma spraying applications. Properties of the generated plasma can be varied in a wide range by supply of different plasma forming gases and setting different arc power values. The plasma jets can be generated at the open atmosphere and under low pressure conditions if the torch is positioned inside a low pressure chamber. The plasma jet surrounding can be also altered by application of a shrouding system with different shroud gases making a protective envelope around the jet.

The reported results refer to studies conducted in the laboratory of Thermal Plasma Department of the Institute of Plasma Physics in Prague (Czech Republic) and work performed in the Electrochemical Energy Department of the Institute of Technical Thermodynamic of DLR-Stuttgart (Germany).

The first chapter of the thesis considers the present state of the solved problem. The mechanism of air entrainment is described for both isothermal and thermal plasma jets. Methods how to eliminate or at least reduce the entrainment process are considered. Next chapter describes the experimental arrangements. Both DC arc plasma torches with gas and hybrid gas-water stabilization of arc are depicted together with their working parameters. Methods of the plasma diagnostics are described as well, including enthalpy probe, mass spectrometry and Schlieren imaging. The last chapter represents the results of the present work. Properties of the plasma jet have been measured and analyzed combining and comparing the information obtained from different techniques. The plasma jets generated under atmospheric and low pressure conditions have been studied. The effect of arc current, plasma gas composition, surrounding pressure and shrouding on the cold air entrainment process is discussed.

1. Generation of thermal plasma jets, their properties and applied diagnostic tools

1.1 Thermal plasma and its properties

1.1.1 The plasma state

The plasma state is frequently referred to as a fourth state of matter in the sequence: solid, liquid, gas, and plasma. The term 'plasma' was given by Irwing Langmuir in 1923. Under the normal conditions gases are good insulators. The insulating properties can be disturbed by applying strong electrical field making a gas electrically conducting. In fact, plasmas may reach electrical conductivities exceeding those of metals at room temperature. For example, hydrogen plasma at one atmosphere heated to a temperature of 10^6 K has approximately the same electrical conductivity as copper at room temperature.

The gas becomes electrically conducting due to the presence of free charge carriers. Plasma consists of a mixture of electrons, ions, neutral particles in the ground and excited states and photons. Such a mixture, however, is only qualified as a plasma if the negative and positive charges balance each other, i.e., overall plasma must be electrically neutral. Some of the neutrals in the exited state are able to return to their ordinary or ground state by photon emission, which is at least partially responsible for the luminosity of plasmas.

The most common way to generate and maintain a plasma is by means of an electric discharge. In such a discharge the high-mobility electrons pick up energy from the applied electric field and then transfer part of this energy to the heavy particles through elastic collisions. The electron temperature is set in such a way as to provide that the energy received by electrons per unit time transfers to heavy particles during the same period of time. But even with excellent collisional coupling (high collision frequency) between electrons and heavy particles, there will always be a difference between the electron temperature and the temperature of the heavy species in the plasma. Thus, it is difficult to reach complete kinetic equilibrium.

The relation, expressing kinetic equilibrium in a plasma is:

$$\frac{T_e - T_h}{T_e} \approx \left(\frac{E}{p}\right)^2, \tag{1.1}$$

where T_e and T_h is the temperature of electrons and heavy particles, respectively, E is the electric field and p is the pressure. This relation shows that the parameter E/p plays a governing role for determining the kinetic equilibrium situation in plasma. For small values of E/p, the electron temperature approaches the heavy particle temperature - this is one of the basis requirements for the existence of Local Thermodynamic Equilibrium (LTE) in a plasma.

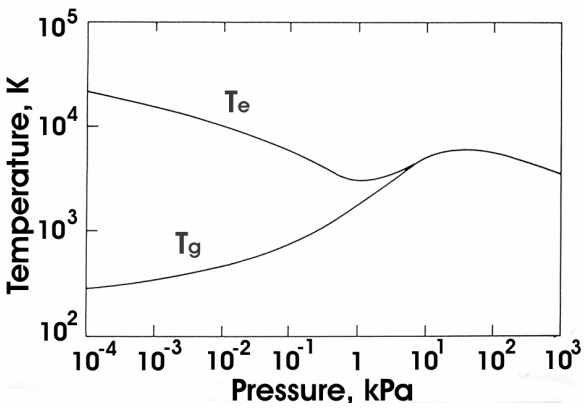

Figure 1.1 Dependence of the electron and heavy particle temperatures on pressure [1].

The Complete Thermodynamic Equilibrium never exists in real plasmas as plasmas usually show inhomogeneities and is affected by the external forces. That is why a classification of plasmas is based on the existence of LTE. A plasma that is in kinetic equilibrium and simultaneously meets all LTE requirements is classified as thermal plasma. Additional conditions for LTE include excitation and chemical equilibrium as well as certain limitations on the gradients in the plasma. Typically, pressures in LTE plasmas exceed 10 kPa, as illustrated for arc plasmas in Figure 1.1. For pressures below 10 kPa, the electron and heavy-particle temperatures separate ($T_e > T_h$) and at 0.1 Pa, the gas temperature is 300 K, while the electron temperature is 10^4 K. At low pressures gas is weakly ionized and the electron density ranges between 10^8 and 10^{13} cm^{-3}. Under these conditions, the collision rate between electrons and neutral molecules is insufficient to bring about thermal equilibrium. Consequently, the electron temperature T_e can be one or two orders of magnitude higher than the neutral and ion temperatures T_h. Such a plasma with strong deviation from kinetic equilibrium ($T_e >> T_h$) is classified as nonthermal or nonequilibrium plasma. As the pressure increases, the collision rate will rise to a point where effective energy exchange occurs between electrons and neutral molecules, so that the temperature of electrons and heavy particles merge together above 10 kPa to an average value of about 5000 K.

Thus, nonequilibrium plasma systems are in most cases operated at pressures below 10 kPa, while thermal plasma systems operate under pressures higher than 10 kPa. The pressure for achievement LTE could be sensitively depend on gas composition because the probability for energy exchange by collision of an electron and molecule depends on the nature of the molecule [1-2].

1.1.2 Properties of thermal plasmas

As it follows from the previous section, a thermal plasma has to meet all LTE requirements, which include:

1. The velocity distribution function is described by Maxwellian distribution;
2. The population density of exited states for each species is described by Boltzmann distribution;
3. The concentration of the present species can be calculated assuming chemical equilibrium.

Over the past years, it has become clear that even the existence of LTE in plasmas is the exception rather than the rule. One of the main reasons of deviation from complete

LTE is the lack of the excitation equilibrium. In particular, the lower energy levels of atoms may be underpopulated due to the high radiative transition probability of these levels, resulting in a corresponding overpopulation of the ground state. Because of the small contribution of excited species to the enthalpy of the plasma, this type of deviation from LTE is unimportant for most applications. For this reason, such plasmas are still treated as thermal plasma. More serious deviations from LTE may be expected in the fringes of a plasma in the vicinity of walls or electrodes. For example, in the electrode regions of electric arcs there are wide deviations from thermal equilibrium, both due to the electric field [3-4] and also due to convection [5]. Moreover, in high-speed plasma flows, deviation from chemical equilibrium takes place because chemical reactions cannot follow the rapid macroscopic motion of the species.

It is accepted that the physical state of the plasma in thermodynamic equilibrium is given by any pair of the state functions: T, V; T, s; s, V; s, p, where T, V, s, p are temperature, volume, entropy and pressure of a plasma element, respectively. The other macroscopic characteristics can be derived from the mentioned independent functions by means of the thermodynamic equations [48].

The most important thermodynamic and transport properties of thermal plasmas are dependent directly on the plasma composition [6]. That is why the overview starts with the plasma composition. The temperature range, which has to be considered in investigations of thermal plasmas, is typically from near room temperature in the edge regions of the plasma to 20000 K or even more in the central regions. Within this range, many different species have to be considered.

The local composition of a plasma in LTE is determined only by the local temperature, pressure and concentrations of the present chemical elements. The composition may be calculated using the method of minimization of Gibbs free energy (the free enthalpy) for a given temperature and pressure, which is the standard technique in equilibrium chemistry [7]. When a gas such as hydrogen (a molecular gas at room temperature and atmospheric pressure) is progressively heated, the molecules first dissociate following the endothermic reaction $H_2 \leftrightarrow 2H - E_d$, where E_d is the energy of dissociation. At higher temperatures ionization starts through the endothermic reaction $H \leftrightarrow H^+ + e - E_i$, where E_i is the first ionization energy. The composition of such a plasma is shown in Figure 1.2 for atmospheric pressure conditions[1]. With increasing temperature the mole fraction of the hydrogen molecules decreases

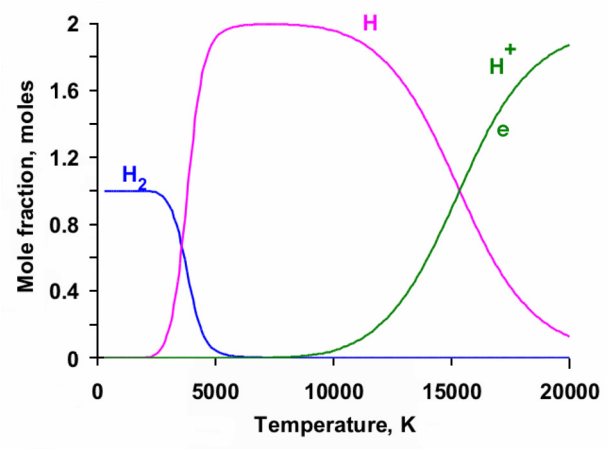

Figure 1.2 Composition of the hydrogen plasma.

[1] The thermodynamic and transport properties shown in the section were calculated by means of ADEP computer code [143]

due to the progressive dissociation, which is completed near 4000 K. The total mole number increases as the molecule of hydrogen divides into two hydrogen atoms. At temperatures about 10000 K the ionization of the hydrogen atoms starts. As only hydrogen atoms are the source of the electrons the mole fractions of the hydrogen atoms and electrons are the same. If the gas contains atoms with higher electron number, further temperature increase causes ions to lose one more electrons and double ionized atoms appear (second ionization) and so on. The composition of the gas depends strongly on its temperature, which is a result of the energy balance between the electrical energy dissipated and the heat losses that occur mainly at the fringes of the plasma. In a complex mixture, where dynamic equilibrium exists between dissociation, ionization, and recombination, the total energy content depends on the energy of the various particles and on chemical reactions among them. Thus the thermodynamic properties depend strongly on the composition of the plasma.

Thermodynamic properties, such as enthalpy, specific heat and density, may be calculated in a relatively simple way once the composition is known, using the mass, enthalpy and number density of each species present.

The enthalpy is defined as

$$h = U + pV\,, \tag{1.2}$$

where U is the inner energy of the system, p is the pressure and V is its volume. The enthalpy of a substance increases as its temperature rises. The relation between the increase in enthalpy and the increase in temperature depends on the conditions (for example, constant pressure or volume). The most important condition is constant pressure. At constant pressure the changes in enthalpy are equal to the heat supplied to the system:

$$dh = dq\,. \tag{1.3}$$

The heat capacity at constant pressure is used to relate the change in enthalpy to a change in temperature: $h_g - h_0 = \int_{T_0}^{T} C_p(T)dT$, where h_g is the total enthalpy of the mixture at the given temperature and pressure, h_0 – the total enthalpy at the reference state at the temperature T_0 and C_p is the heat capacity at constant pressure. The enthalpy can also be calculated directly by introduction of the frozen enthalpy of each species contained in the gas and the reactive enthalpy. The frozen

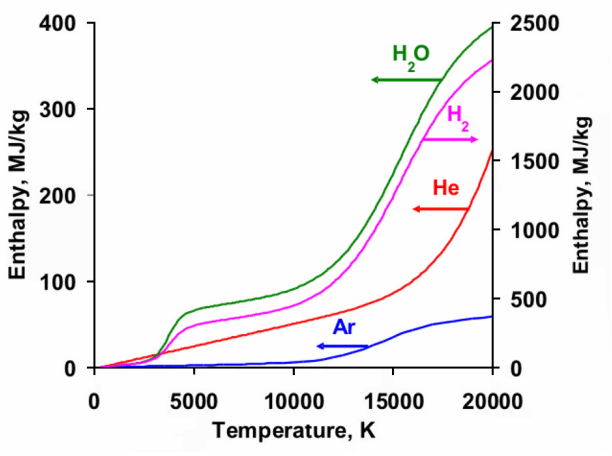

Figure 1.3 Enthalpy as a function of temperature.

enthalpy represents the enthalpy when no reaction occurs (no dissociation or ionization), while the gas is heated to the fixed temperature. The reactive enthalpy involves enthalpy changes that accompany chemical reactions, dissociation, and ionization. As enthalpy is a state function, a change in enthalpy is independent of the path between the two states [8]. Figure 1.3 represents the specific enthalpy (in *MJ/kg*) as a function of temperature for various gases (H_2, H_2O, *Ar*, *He*) at atmospheric pressure. The steep variations in enthalpy are essentially due to the heat of reaction. The first steep increase of enthalpy for H_2O and H_2 is due to dissociation of molecules. The increase of enthalpy for temperatures higher than 10000 K for all gases is because ionization starts. The very high enthalpy of the hydrogen is provided also by its low mass. Helium has a low mass as well, but its enthalpy is much lower in comparison to H_2 because it is an atomic gas with high ionization potential. The ionization of the *He* atoms has really not started yet, but due to its low mass *He* still has higher specific enthalpy than argon.

In practice it is difficult or even impossible to produce a uniform plasma and an actual plasma reveals gradients concerning particle number density, electrical potential, temperature and velocity. These gradients can be considered as driving forces generating fluxes due to diffusion, electrical conductivity, thermal conductivity and appearance of frictional force. The linear relationships between fluxes and driving forces incorporate the so-called transport coefficients, which are known as diffusion coefficient, electrical conductivity, thermal conductivity and viscosity. The calculation of the transport coefficients is more difficult. They are calculated using the Chapman-Enskog method [9], which is based on an approximate solution of the Boltzmann equation. Expressions for the transport coefficients are derived as a function of the collision integrals, which are required for each pair of present species. The evaluation of the transport properties is further described.

In a real fluid in addition to the normal forces, tangential forces also occur both between layers in the fluid and between the fluid and the walls. These tangential or friction forces are connected to the physical property called the viscosity of the fluid. Viscosity becomes apparent as the resistance against the mutual movement of the particles. Viscosity represents the constant of the proportionality in the elementary law of fluid friction:

$$\tau = \mu \frac{dV}{dy}, \tag{1.4}$$

where τ is shear stress, and *dV/dy* is the gradient of the velocity perpendicular to the direction of the main flow. The value μ is a physical property and represents viscosity of the fluid. Since viscosity establishes the momentum transport perpendicular to the main flow direction, it is a transport property of the fluid. The viscosity is in general a function of temperature and pressure, although the temperature dependence is dominant. As the temperature increases, the viscosity of gases generally increases particularly following the factor: $\mu \approx nl\bar{v} \sim \sqrt{T}$, where l is the mean free path, n – particle density, and $\bar{v}$ - particle velocity [10]. Viscosity is independent of pressure until ionisation takes place. The fact

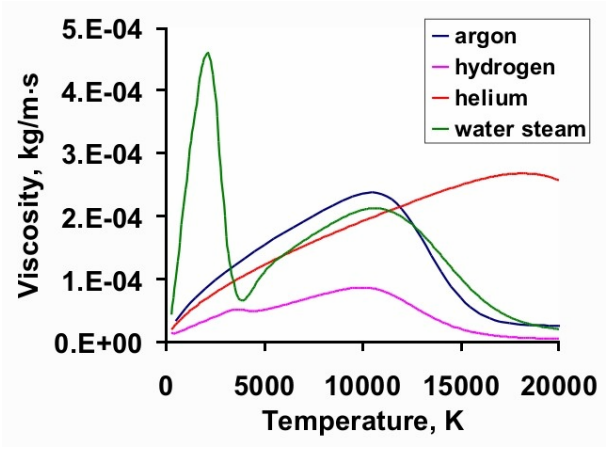

Figure 1.4 Viscosity as a function of temperature.

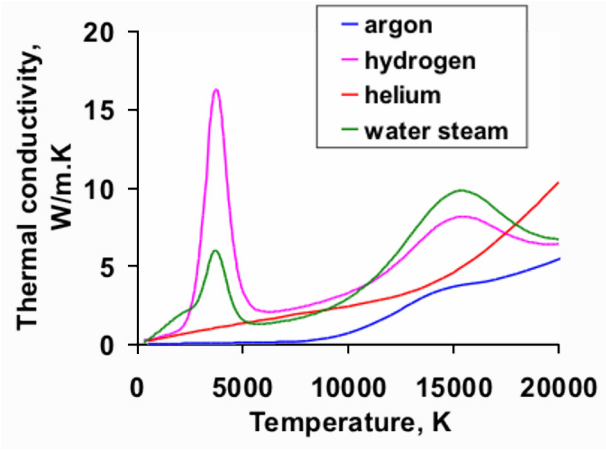

Figure 1.5 Thermal conductivity as a function of temperature.

could be explained by the two opposites: if the number of particles is doubled in the same volume, there are twice as many particles available to transport momentum, but the mean free path of each molecule is halved, so they can transport this momentum only half as effectively, and thus the net rate of momentum transfer is unchanged. When the temperature increases beyond room temperature, the values of μ are first controlled by the interaction between neutral molecules (for diatomic molecules), then, as dissociation starts, they are controlled by the neutral atoms and at higher temperatures by the charged particles [11]. On Figure 1.4 there is a dependence of the viscosity on temperature for different gases. First, the viscosity rises with the temperature increase, particularly water vapour viscosity increases very quickly. But at the temperature near 2200 K the dissociation of water molecule takes place and there is a steep decrease of μ. The same is the case for hydrogen molecules, which dissociates as well but the effect is not as strong as in the case of water vapour. When ionisation starts, μ decreases with increasing temperatures. This drop in viscosity is due to ionisation of the gas, resulting in Coulomb forces of relatively long range between particles. The mobility of the charged particles decreases when charged-particles density increases. Helium is ionized at a higher temperature compared to the other gases, and hence the decrease in viscosity occurs at the higher temperature for helium.

The thermal conductivity is of primary importance for thermal plasmas as it controls the energy losses. If q_z is the heat flux due to temperature gradients in the z direction, the thermal conductivity k is defined by

$$q_z = -k\frac{\partial T}{\partial z}. \tag{1.5}$$

The dependence of thermal conductivity on temperature for different gases is shown on Figure 1.5 in which it is seen that the thermal conductivity shows strong maxima. The dissociation and ionization phenomena make a large contribution to energy

transport, and the corresponding peaks occur at temperatures where these phenomena happen (reaction thermal conductivity). In addition to reaction the thermal conductivity contains more terms. Since each species has an internal energy component (due to vibrational, rotational, and electronic excitation) at high temperature, energy is transferred through inelastic collisions of the second kind. This effect is taken into account by the internal thermal conductivity. The translational thermal conductivity is related to elastic collisions and can be written as the sum of two terms, one due to electrons and the other due to heavy particles. Thus, the total thermal conductivity is the sum of three terms, the translational, internal and reaction.

The electrical conductivity is connected with the motion of charge carriers and refers to the flux due to electrical conduction:

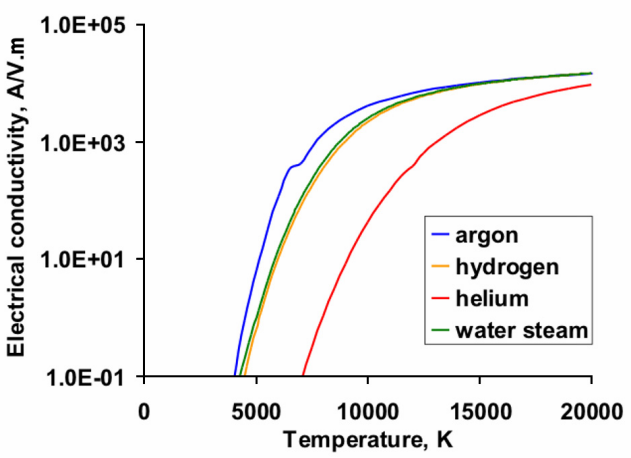

Figure 1.6 Electrical conductivity as a function of temperature.

$$j = -\sigma \ gradV\,, \qquad (1.6)$$

where j represents the electric current density, σ the electrical conductivity and V the electrical potential. The electrical conductivity is determined as: $\sigma = en_e\mu_e$. The electrical conductivity depends mainly on the electron density n_e, which varies almost exponentially with temperature. That is why σ is almost negligible for the most common plasma gases below 6000 K as illustrated in Figure 1.6. For helium σ reaches significant values only for temperatures higher than 13000 K due to the high ionization potential.

1.2 Thermal plasma generation and its applications

1.2.1. Thermal plasma sources

Plasmas can be generated by passing an electric current through a gas. Since gases at room temperature are excellent insulators, a sufficient number of charge carriers must be generated to make the gas electrically conducting. This process is known as electrical breakdown, and there are many possible ways to accomplish this breakdown. Breakdown of the originally non conducting gas establishes a conducting path between a pair of electrodes. The passage of an electrical current through the ionized gas leads to an array of phenomena known as gaseous discharges, which are most common with plasma generation.

The most widely used electrical methods for producing a thermal plasma employ high-intensity arcs or inductively-coupled high-frequency discharges; more recently

microwave discharges have been also considered. In all types of the discharges the electrons are primarily responsible for the absorption of energy from the electric field.

A high-intensity arc is defined as a discharge operated at current levels $I>50\ A$ and pressures $p>10\ kPa$. The arc is established between two electrodes. An arc column approaches to a state of LTE, while anode and cathode regions show strong deviations from LTE. The arc properties are determined by the arc parameters, including the arc geometry. High temperature plasmas generated by both a direct current (DC) and alternating current (AC) arc are heat sources of enormous power and versatility, combining the clean and almost mass-less heat of an electric arc with the stability and control of a gas flame. The result is heat without combustion and chemical reactions without contamination up to impressive temperatures [1, 2, 11-12]. That is why such arcs find wide use in actual applications. Mechanism of the arc formation as well as the design of arc devices will be given later in details as this method of generation of the thermal plasma was used in the present work.

An RF discharge can be maintained either by capacitive or inductive coupling with the power source. In capacitive coupling the high-frequency electric field is responsible for maintaining the discharge. An inductively coupled discharge is maintained by the time varying magnetic field. For generation of thermal plasmas, inductively coupled discharges are far more important. The plasma torch consists of a confinement tube which is surrounded by several turns of an induction coil connected to the RF power supply. The upper part of the torch is the gas distribution head, responsible for the introduction of different gas streams into the discharge chamber. The minimum power to sustain the discharge depends on frequency and gas composition. The lower power level corresponds to monatomic gases like argon. Typical torch efficiencies are in the 40-50% range. This lower thermal efficiency of the torch is compensated by a few remarkable advantages as are flexibility of gas chemistry and axial injection of the products to be treated allowing a better mixing of the reactant. Such torches can be operated between 25 and 400 kPa. The temperature of the resulting plasma jet is in the range of 5000 to 10000 K, while the flow velocity varies in the range from 40 to 50 m/s up to 2000 to 3000 m/s, which could be reached by use of supersonic de Laval nozzles [13-14].

Microwave discharges are not as widely used as thermal plasma sources as discharges mentioned above. Conventional microwave discharges require that the discharge is an integral part of the microwave circuit. This requirement imposes limitations on the flexibility of the discharge parameters, in particular on the configuration and size of the plasma volume. The more flexible microwave devices make use of traveling wave discharges (TWD) for sustaining stable and reproducible plasma. The key component of the TWD is the wave launcher, which excites the surface wave. After breakdown of the initially non conducting gas in the discharge tube, the surface wave travels along the interface between the plasma and the discharge tube, supplying power for sustaining the discharge. The wave supplies energy to the plasma, but without the plasma, the wave could not exist. Since the traveling wave looses energy continuously as it moves along the tube, less and less energy is supplied to the plasma with increasing distance from the wave

launcher. In a steady-state situation there is a local balance between the power supplied by the wave and the power lost from the plasma [15-17].

1.2.2 Thermal plasma technology

The high energy content of a plasma compared to that of solids, liquids, or ordinary gases accounts for a number of important applications. The initial interest in thermal plasma technologies took place in the 1960's and was associated with aerospace programs. The 1970's have seen the development of industrial applications in the fields of cutting, welding, spraying, transferred arc reclamation, analysis by inductively coupled plasmas, and tentative developments in melting and refining, extractive metallurgy, ultrafine particle synthesis, powder spheroidisation, and lightning. Whereas in the 1980's the established industrial applications experienced a remarkable increase in their economic importance, there has been a decrease in development of other potential applications. The fundamental research in the field has made great progress by understanding the phenomena in thermal plasma conditions. This effort in fundamental research has renewed the interest for applying thermal plasmas in material processing and waste treatment as demonstrated by the drastic increase in the number of papers and patents published since the middle of the 1980's [18].

Thermal plasma technology covers today a wide spectrum of applications as well as development efforts which may be classified to

- Thermal plasma coating technology,
- Thermal plasma synthesis,
- Thermal plasma waste destruction,
- Thermal plasma densification.

Coating technology includes plasma spraying [19-22], wire arc spraying [23-24] and thermal plasma chemical vapor deposition (TPCVD) [25-26]. Today, applications of plasma spraying include corrosion-, temperature-, and abrasion-resistant coatings and production of monolithic and near net shapes that also takes advantage of the rapid solidification process. The material to be sprayed is introduced into the plasma jet in the form of powder. Powder particles are heated in the hot environment to their melting point and accelerated towards the substrate. Powders of glassy metals can be plasma sprayed without changing their amorphous characteristics. Recently, high temperature superconductive materials have been deposited by the plasma spray process [27]. Wire arc spraying is usually restricted to spraying of metals and alloys. Here the deposited material is introduced into the arc in the form of the two wires serving as consumable arc electrodes. A gas jet across the arc removes molten droplets from the wire tips, atomizes droplets and drives them to the substrate. In a TPCVD process high-energy-density plasma produces high-density vapour-phase precursors for the deposition of relatively thick films. TPCVD finds applications for fabrication diamonds and dense ceramic or superconducting films as well nanostructured films.

In thermal plasma synthesis either the discharge itself or the plasma flame downstream of the discharge may be used for synthesizing the powders [28-29]. Precursor materials injected as a fine mist into the plasma undergo complete vaporization and dissociation. The rapid quench downstream of the hot zone induces supersaturation of the dissociated precursor vapour, which in turn, leads to a desired chemistry and to the formation of fine powder particles via homogeneous nucleation. During last 10 years the synthesis of nanoparticles and nanotubes in the thermal plasma field has got a rapid development [30].

During the past years, industrial processes have shown little care for environmental aspects and as consequence a huge accumulation of pollution and hazardous products resulted. High energy-density and temperature associated with thermal plasmas and the corresponding fast reaction time offer unique advantages for the destruction of hazardous waste in thermal plasma reactors [31-32]. The feedstock is treated by thermal plasma in a reactor chamber, whereby organic components are converted into a synthetic gas of high caloric value, and inorganic components are converted into non-leachable vitrified lava.

Powder densification, which thermal plasma densification technology refers primarily to, involves in-flight melting of the material in particulate form, followed by graduate cling and freezing before being collected at the bottom of the densification chamber. The process has been successfully used for the densification and spheroidisation of a large number of materials, ranging from low-melting-point metals (copper, nickel) to oxide ceramics (alumina, yttria-stabilized zirconia) and refractory metals (molybdenum, tungsten) [33].

1.3 DC arc plasma torches

1.3.1 Electric arc generation and stabilization

The main characteristics of the arc are already seen under visual observation. The arc column is contracted and homogeneous along the axis. The contraction of the arc is larger near the electrodes. Measurements showed that the temperature is very high at the center of the arc and drops towards the fringes. The conductivity of the plasma changes even more sharply in section of the arc column because of the exponential dependence of conductivity on temperature. The distribution of the electrical field along the arc without external influence is usually uniform (Fig. 1.7). It is seen from the plot that the arc can be divided into three main regions: cathode region, arc column and anode region also called anode attachment.

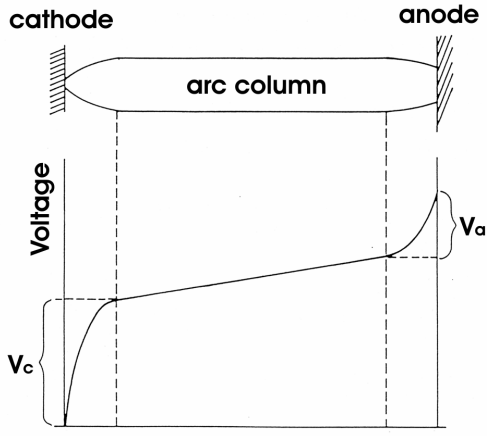

Figure 1.7 The distribution of the electrical field along the arc [1].

The arc voltage is a sum of the voltages in these three regions. The largest part of voltage drop refers to cathode and anode regions. The most important characteristic of the arc represents the volt-ampere characteristic. Examples of volt-ampere characteristics of arcs burning in channels of two different diameters are shown in Figure 1.8. If the arc ignites in the wide diameter channel so that the influence of the walls is very small, the volt-ampere characteristic is falling and an increase of arc current leads to a decrease of arc voltage. If the influence of channel walls is evident and a part of the arc energy is consumed by the walls or the walls confine growth of the arc diameter with arc current increase, volt-ampere characteristic becomes rising [1,34].

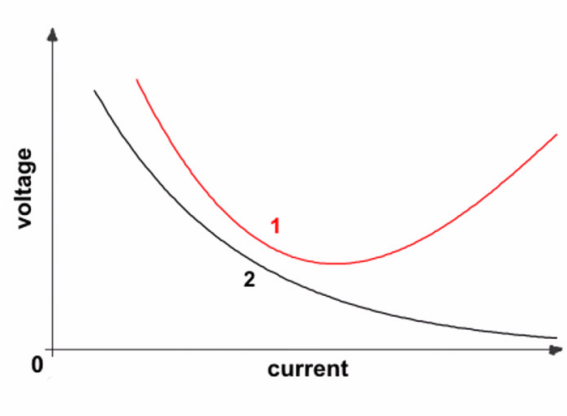

Figure 1.8 Volt-ampere characteristics of the arc in channel with:
1 – smaller diameter confined by walls;
2 – larger diameter [34].

The conversion of electrical energy to thermal energy is effected by the heating of the gas in the plasma. The specific enthalpy of the gas assists in determining the gas as best suited for the specific application. In fact, power dissipated in the arc column is divided between Joule heating effect (heat generation) and the heat losses by conduction, convection and radiation.

The electrodes serve as the termination points of the arc, and thus are an interface between high temperature plasma and a solid material. But the role of arc cathodes differs from the role of arc anodes. While the anode is a passive collector of electrons to assure current continuity, the cathode has to provide electrons needed by the arc attachment.

There exists no universal plasma heater. Very often in industry any arc is generated by a plasma torch. Most of the plasma torch principles used in industry were developed before 1975. They are very flexible instruments and operate simultaneously as an electrochemical and a thermal apparatus. The essential components, which determine the functional design of the plasma torch and consequently the plasma properties, are an arc electrode design and a plasma forming gas [18].

Cathode region. The cathodes differ according to the mechanisms by which the electrons are emitted: by thermionic emission (thermionic cathodes) or by a field emission (cold cathodes). Thermionic cathodes provide the electrons by having surface temperatures, which are sufficiently high for emission of a sufficient number of electrons. Refractory materials are required, usually in a form of a rod or button, and frequently a low work function material is added to increase the electron emission at lower cathode spot temperatures. In 1914 Langmuir already investigated the positive effect of thorium oxide addition to tungsten. A small concentration of thorium in the cathode affects the work function considerably. But for operation with oxidizing gases tungsten cannot be used because of the formation of volatile oxides. Tungsten cathodes with addition of a low work function material are standard for most applications.

The cold cathode usually consists of a water-cooled metal. In most practical applications, copper, steel, silver or an alloy of these materials are used. The electrons are supplied to the arc by evaporation and ionization of a metal in a very small cathode spot. Consequently, electron emission is necessarily associated with material loss [40].

The cathode region has a thickness of about 0,1 mm. Electrons are emitted from the cathode surface (several tenths of mm^2) and are accelerated by the electric field and heat the injected plasma gas (Joule effect heating). The energy transfer in the cathode region is carried out by electrons emitted from the cathode and ions from the arc column. Electrons get such a high kinetic energy in the region of the potential drop that they are able to ionize neutral atoms. Positive ions are accelerated towards the cathode, where they give up their energy. The current density can reach in this region $10^7 - 10^8$ $A.m^{-2}$. Thanks to the widening of the arc column, a strong cathodic jet is created having a stabilizing influence on the arc column. Here a zone of laminar flow exists resulting in a strong pumping of cold plasma gas into the arc column from the cathode region.

Anode region. The anode region is the most problematic region of the arc. The anode configuration can be divided according to the geometrical arrangement of the plasma generator: the anode surface being perpendicular to the arc axis or the anode surface parallel to the arc axis. The transferred arc will not be discussed here. The electric current is carried out in the anode region mostly by electrons outgoing form the arc column. Thermal fluxes at the arc attachment can reach 10^{11} $W.m^{-2}$ and thus the anode must be cooled. Despite intensive cooling of the anode, the erosion would be catastrophic due to a high heat transfer without arcs fluctuations [35]. Depending on the conditions, either a constricted or a diffuse attachment develops. The voltage drop in the constricted attachment is higher than in the diffuse one. The constricted anode attachment also leads to the formation of an anodic jet, similar to the cathodic jet. The gas acts on the attachment by exerting a drag force, which pushes the attachment downstream, while electromagnetic forces may pull the attachment upstream [36]. The imbalance between these forces may the reason for the movement of the arc attachment. This movement may result in arc fluctuations and the character of this movement determines a mode of plasma torch operation – restrike, takeover or steady. In the steady mode the voltage fluctuations are very small. The drag force of the plasma gas and the electromagnetic forces causing the arc attachment are in equilibrium. The anode attachment stays at one spot, close to the cathode. In the takeover mode the fluctuation of the arc voltage becomes significant, but smaller than in the restrike mode. The name comes from the idea that a new attachment is not created by breakdown but instead the new attachment gradually “takes over” the role of the old attachment. The restrike mode is characterized by the highest voltage fluctuation and an asymmetric saw tooth-like shape of the voltage trace. The arc voltage is rising slowly and then dropping very fast as a new current path is suddenly created by an electric breakdown. This phenomenon was described in detail by Wutzke et al. [37].

A new theory of the anode attachment formation was formulated in our working group in IPP (Prague) a year ago. The presence of diffusive currents between the arc column and the anode surface was demonstrated. These currents could lead to the heating

of the layer of cold gas and consequently to the thermal breakdown in the location of highest *jE* [38-39].

The torch geometry, the level of electrode erosion as well as the arc generation conditions (plasma gas, arc current, pressure) determines the mode of the plasma torch operation. For a given anode nozzle diameter, the boundary layer thickness will change due to a change in the plasma gas mixture or a change in arc current. Increasing the hydrogen content or reducing the current usually results in establishment of the restrike mode. On the other hand, a reduced boundary layer thickness e.g. through increasing the arc current or using helium instead of hydrogen as the secondary gas will facilitate a breakdown between the arc column and the anode surface. A more random variation of the arc length is the consequence (takeover mode). Further increasing of the arc current will result in a decrease in the boundary layer thickness and a change in operation mode to a steady may occur. While the movement of the anode attachment has the advantage of reducing anode erosion, the resulting variation in arc voltage and power will produce variations in the enthalpy levels in the plasma jet and, therefore, result in fluid dynamic instabilities of the jet [40].

Arc column. The arc column is the place where energy is delivered and the gas is heated. The voltage drop in the arc column depends on the length of the arc, the arc column width, the conductivity of the plasma in the arc and the arc current. The basic understanding of the arc column can be achieved under the assumption that the flow is fully developed (i.e. all variables are independent of the axial distance), radially symmetric and stabilized by walls. Under these conditions, it can be described by the Elenbaas-Heller equation:

$$\frac{1}{r}\frac{d}{dr}\left(rk\frac{dT}{dr}\right)+\sigma E_z^2-P_r=0\,, \tag{1.7}$$

where r is the radial coordinate and T, k, σ, E_z, P_r are temperature, thermal conductivity, electrical conductivity, axial component of the electric field and power loss due to radiation, respectively. The equation represents a balance between the energy generated by the arc current with Joule heating and the energy carried out by heat conduction and radiation. The voltage along the arc column is then equal to $E_z dl$. From the solution of the Elenbaas-Heller equation 1.7 it follows that for lower current values, the V-A characteristic of the arc column is decreasing as the arc is widening while for higher currents the V-A characteristic is increasing as the conduction of the heat by walls becomes more important. The explanation of this fact is following. The plasma temperature is defined by the energy balance of the arc. The increasing of the arc current results in increasing of the plasma temperature and thus the electrical conductivity as well. This results in a decrease of the potential difference. The amount of energy losses is proportional to the diameter of the arc and thus the increasing of the arc current results in the increase of the arc diameter. The presence of the wall confines the spreading of the arc column, providing an increase of temperature and electrical conductivity, but a higher potential difference is needed to maintain the current value because of increased losses to the walls by the thermal conductivity of the plasma [48].

The arc oscillates constantly and some of its parts could approach very closely to the channel walls and could close onto the walls if they are metallic. The length and thus the power of the arc then could essentially decrease. To eliminate or at least diminish this effect most electric arcs require some kind of stabilizing mechanism, which must be either provided externally or produced by the arc itself. For arc applications, it is useful to classify arc columns in terms of their methods of stabilization. There is a direct link between the method of arc column stabilization and the options available for the design of arc devices. Here the term stabilization refers to a particular mechanism that keeps the arc column in a given, stable position, i.e., any accidental excursion of the arc from its equilibrium position causes an interaction with stabilizing mechanisms such a way that the arc column is forced to return to its equilibrium position. This stable position is not a stationary one; the arc may, for example, rotate or move along rail electrodes with a certain velocity. Stabilization implies in this situation that the arc column can only move in a well-defined pattern controlled by the stabilizing mechanism [1].

With ***free-burning arcs*** no external stabilizing mechanism is imposed; but that does not exclude the possibility that this arc generates its own stabilizing mechanism. Although high-intensity arcs may be operated in the free-burning arc mode, they are frequently classified as self stabilized arcs. In such arcs the interaction of the self-magnetic field and the arc current is the dominating stabilizing mechanism.

The principle of ***wall stabilization*** has been known for more than 80 years. A long arc enclosed in a narrow tube with circular cross section will assume a rotationally symmetric, coaxial position within the tube. Any accidental excursion of the arc column toward the wall will be compensated by the increased heat conduction to the wall, which reduces the temperature and therefore the electrical conductivity in this location. In short, the arc will be forced to return to its equilibrium position. In this situation, increased thermal conduction and the associated secondary effects provide the stabilizing mechanism. The maximum possible temperature or enthalpy attainable in a wall-stabilized arc is limited by the highest permissible heat flux the wall is able to withstand.

The most easy and effective way of stabilization is ***convectional vortex stabilization***. The arc is confined to the center of a tube in which an intense vortex of gas or liquid is maintained. Centrifugal forces drive the cold fluid towards the walls of the arc chamber, which therefore is thermally well protected. There is also a superimposed axial component, which continuously supplies cold fluid and because of it stability can be achieved. Various gases and gas mixtures are used as working fluids in actual applications. Convective heat transfer from the arc to the cold gas surrounding plays essentially the same role as conduction in the case of a wall-stabilized arc.

Since an arc is an electrically conducting medium, it will interact not only with its own magnetic field but also with externally applied magnetic fields, which is used in ***magnetically stabilized arcs***. The interaction of arcs with magnetic fields can be divided into the three categories: magnetic stabilization of arcs in cross flow, then a magnetic field is applied so that the drag force exerted on the arc is balanced by the $\vec{j} \times \vec{B}$ force; magnetically deflected arcs and magnetically driven arcs.

1.3.2 Gas stabilized plasma torches

The essential elements of a plasma torch with gas stabilization of the arc are shown in Figure 1.9. A DC arc is maintained between the electrodes – the anode and the cathode. The anode is usually copper and the cathode tungsten. A gas, usually argon or nitrogen or a mixture of these with hydrogen or helium flows around the cathode and through the anode which serves as a constricting nozzle which is properly cooled by pressurized water. Very important is the perfect centering of the cathode with respect to the anode to avoid overheating of one side of the nozzle. The plasma gas is supplied under pressure along the cathode either axially or tangentially. The amount of gas has to be high enough to provide a relatively cold gas layer between the arc and the nozzle wall. The tangential injection results in a rotation of the gas around the electrode. The rotating movement continues within the nozzle as well and leads to a prolongation of the arc which in turn results in higher arc voltage. The cold gas moves along the wall while the hot gas stays at the center due to the centrifugal forces. The axial velocity component predominates over the radial one and at the nozzle exit the radial component is suppressed and thus the laminar plasma jet flows in axial direction. The power used varies from about 5 to 80 kW depending on the type of the torch and operating parameters. The plasma generated by the arc consists of free electrons, ionized atoms, and some neutral atoms and non dissociated diatomic molecules if nitrogen or hydrogen is used [41, 48].

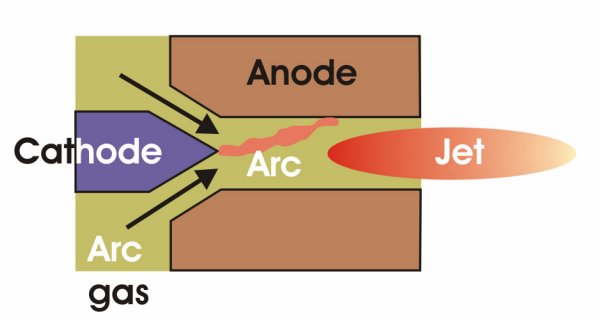

Figure 1.9 Gas stabilized plasma torch.

It has to be emphasized that the arc behavior strongly depends on nozzle design and operating parameters, in particular on nozzle diameter, arc current, plasma gas nature and mass flow rates. The plasma gas nature affects the voltage of the arc. Noble gases, such as argon or helium, are not molecular and require therefore less energy for their heating to the ionization temperature than molecular gases. Molecular gases as hydrogen or oxygen have first to be dissociated before being ionized and consume much more energy to get the same temperature as atomic gases. The solution of the Elenbaas-Heller equation (1.7) depends on the properties of the plasma gas but it does not explain the effect of the plasma gas flow rate because the changes in temperature in the direction of the axis are neglected.

In real situations, part of the energy generated by the arc current is used for heating of the gas before the flow becomes fully developed. An increase of the plasma gas flow rate requires more energy for the heating of the gas which in turn needs a higher electric field. Moreover, if the flow rate is increased then the arc column close to the cathode becomes more constricted and the cold gas boundary layer will be thicker which can lead to a longer arc. Both of these effects contribute to the increase of the arc voltage when the plasma gas flow rate is increased [83].

Plasma gas velocities with most conventional torches are subsonic, but supersonic velocities can be generated by using converging-diverging nozzles with critical exit contours and pressure drops [42]. Usually temperatures in torches with non-transferred electric arc with gas stabilization are somewhat in the range from 8000 K to 14000 K. The corresponding plasma enthalpies, determined as ratio of the useful power of the plasma generator to the flow rate of plasma forming gas, vary from 1 to 100 MJ/kg. Further increase of plasma temperatures and enthalpies is limited by the fact that flowing gas protects the arc chamber walls from thermal overloading and thus a minimum possible gas flow rate exists for a given arc power. Higher thermal loading is possible if the walls are created by a water vortex and the arc is stabilized by wall evaporation. Thus, water stabilized arcs can be utilized as sources of thermal plasmas with high temperatures and enthalpies.

1.3.3 Plasma torches with water stabilization of arc

The electric arc with stabilization by a water vortex was first described more than eighty years ago by Gerdien and Lotz [43-44]. The basic stabilizing mechanism of the arc column is the cooling of the arc fringes by water vapor evaporated from the wall region. Basic experimental investigations of the water stabilized arcs were performed in the 1950's. Maecker et al. [45-46] measured electric characteristics of the arc and studied the effect of the length and the diameter of the stabilizing channel. Several investigators measured arc plasma temperatures using methods of emission spectroscopy [47]. All authors reported very high plasma temperatures in the arc column with a maximum about 50000 K in the centerline position. The principle of arc stabilization by water vortex was utilized in plasma torches designed for plasma spraying and cutting. [48] Despite of the possibility of achieving extreme performance characteristics, the development of water stabilized torches was limited especially due to their more complex structure and due to the lack of understanding of physical processes in the arc which is necessary for improvement of the torch design.

The investigation of water stabilized plasma torches has been established at the

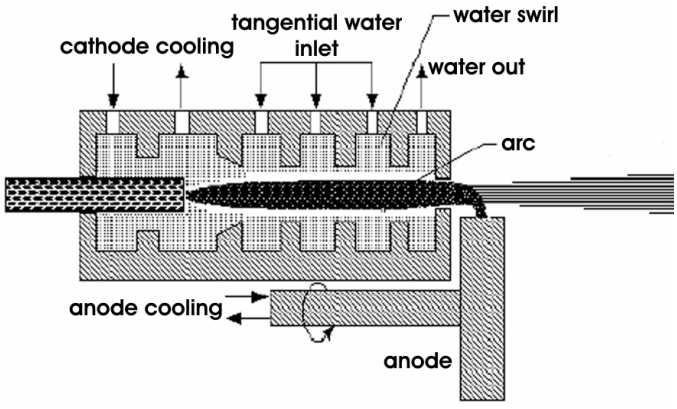

Figure 1.10 Plasma torch with water stabilization of arc [50].

beginning of the 1990's in the Thermal Plasma Department of the Institute of Plasma Physics in Prague with the aim of better understanding of the arc processes, of development of better plasma torches and of determination of characteristics of the generated plasma jets.

A schematic picture of the arc chamber is shown in Figure 1.10. The chamber is divided into several sections by baffles with central holes. Water is injected tangentially into the sections where the vortex is created. The inner diameter of the vortex is determined by the diameter of the holes in the baffles. Water is exhausted at two positions along the arc chamber. The water flow rates through the system have to be exactly adjusted and kept constant to ensure stable operation of the torch. The cathode is created either by a graphite rod, which is automatically moved into the chamber to compensate erosion, or by a small rod of zirconium, which is pressed into a copper sleeve rod. If active stabilizing gases as water vapor are used an anode has to be placed outside the plasma torch chamber and moved fast to cope with the incoming energy load on a big area. Thus, the anode representing a rotating cooper disc with internal cooling is located outside the arc chamber downstream of the nozzle exit. An arc is ignited in the center of a vortex of water. The evaporation from the inner surface of the vortex, the heating and ionization of vapor are principle mechanisms which produce the arc plasma. Energy, dissipated in the conducting arc core by Joule heating, is transported radially to the inner surface of vortex by radiation, heat conduction and turbulent transfer. The evaporation rate is determined by the fraction of total power reaching the liquid. The other part of transferred energy is absorbed in a vapor zone (between the arc column and the surface of water) causing heating and ionization of vapor. The part of the energy which is transferred into the liquid represents a power loss.

The basic parameter which determines arc and plasma characteristics is the mass flow rate through the arc chamber. In contrast to the gas stabilized plasma torches, in liquid-stabilized torch this parameter can not be controlled independently, but it is determined by the power balance of the radial transfer of energy in the arc chamber. The arc evaporates its needed amount of water vapor to create the plasma. The torches based on this principle are sources of oxygen-hydrogen plasmas with high temperature. The high content of hydrogen results in high enthalpy of the plasma. The arc voltage and consequently the arc power are substantially higher compared to gas stabilized torches. The power input reaches 170 kW with a bulk enthalpy of 320 MJ/kg. High efficiency at utilizing of the plasma enthalpy for powder heating and high heat fluxes to the powder particles enable a large throughput of powder, about one order of magnitude higher

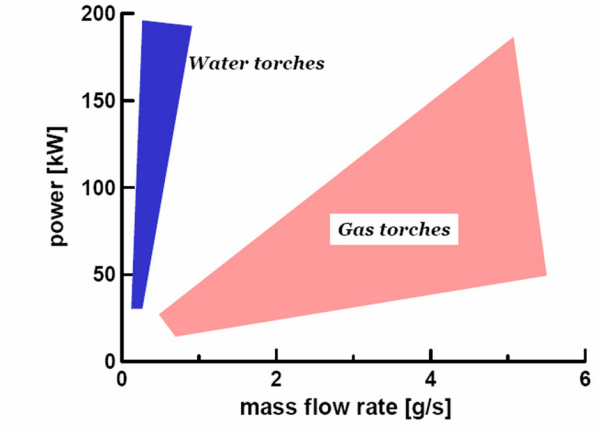

Figure 1.11 Parameters of the gas and water stabilized torch.

than for common gas stabilized torches [49].

Physical limits of the two principles, the gas and the liquid arc stabilization, do not allow generation of plasmas with parameters in the wide range between the two principles (Figure 1.11). Plasma torches with gas stabilization of the arc have low enthalpy values and high gas flow rates and densities, while water torches are characterized by very high enthalpy values but low density and flow rates. For plasma spraying applications the high enthalpy jets generated in water torches ensure high efficiency of the particle heating and thus high throughputs, while low plasma flow rates and densities result in lower efficiency of particle acceleration [50]. The plasma torch which combines both principles of stabilization has been designed in IPP in Prague. The idea was to develop the torch with hybrid gas-liquid stabilization of arc.

1.3.4 Hybrid gas-water plasma torches

The idea to combine two types of stabilization, the stabilization by water vortex and by gas flow, is rather new. The hybrid torch with gas-water stabilization of the arc has been developed in the Institute of Plasma Physics in Prague in the course of the last years. The plasma torch configuration is shown in Figure 1.12 [51]. The arc is generated between the tip of the stick cathode and passes through the channel inside the water vortex towards the external rotating anode. The cathode part of the torch is arranged similarly like in gas torches. Gas is supplied along the cathode. A vortex component of the gas flow assures proper stabilization of the arc in the cathode nozzle. The consumable graphite cathode used in water-stabilized torches is replaced by the cathode made from thoriated tungsten as the cathode is prevented from the contact with aggressive water vapor by the gas sheath. Plasma created in the cathode region flows through the cathode nozzle into the second part of the torch where the arc column is surrounded by a water vortex. The vortex is formed in three cylindrical segments with tangential water injection in the same way like in water-stabilized torches. Water is exhausted from the arc chamber through two exhaust gaps. Interaction of arc column with the water vortex causes evaporation at the inner surface of the vortex. The steam mixes with gas plasma, the overpressure produced in the arc chamber due to evaporation accelerates the arc plasma, created by a mixture of steam and

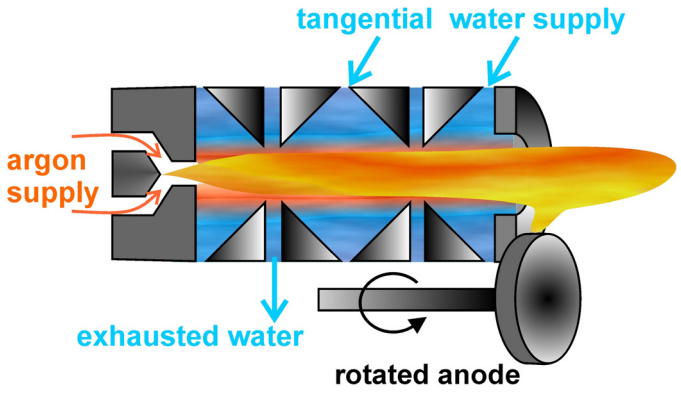

Figure 1.12 Hybrid torch with gas-liquid stabilization of arc [51].

gas, towards the exit nozzle. The anode of the torch is formed by a rotating cooper disc that is located outside of the arc chamber. Hence, the arc column is divided into two parts – an upstream gas stabilized and a downstream water stabilized part. The plasma jet properties such as velocity, enthalpy, mass flow rate, and others can be varied in significantly wider range by changing the gas flow rate compared to pure gas- or liquid-stabilized torches. The achieved arc powers reach 130 kW, producing plasma jets with temperatures up to 22000 K.

1.4 Thermal plasma jets

1.4.1 Turbulent isothermal jet

The phenomenon of jets is the result of complex interactions of physical and chemical processes. When fluid emerges from a nozzle it interacts with fluid from the surrounding to form the jet. Jet flows are classified as fully separated flows because, after separation from solid surfaces, the solid surfaces no longer play a significant role in their development. Most flows which occur in practical applications are turbulent. In such flows irregular fluctuations (mixing or eddying motion) are superimposed on the main stream and the flow shows highly irregular transverse motions. In laminar flows the layers of the fluid move with different velocities without great exchange of fluid particles perpendicular to the flow direction. Figure 1.13 represents regions of the turbulent free jet [52]. Immediately downstream from the nozzle there is a region, the potential core, within which the velocity and concentration of nozzle fluid remain unchanged. Outside this region a free boundary layer develops in which momentum and mass is transferred perpendicular to the direction of the flow. The fully developed region of the jet is preceded by a transition region.

Changes in the jet shape can be observed when the flow rate of the jet gas issuing from a nozzle is progressively increased. When gas discharges at velocities below a critical value from the nozzle into a surrounding stagnant air, the flow of gas is laminar and the mixing of gas and air occurs by molecular diffusion in a thin layer. With increasing flow velocity the jet increases in length until a critical velocity is reached and the tip of the jet becomes unsteady and begins to flutter. With further increase in velocity, this unsteadiness

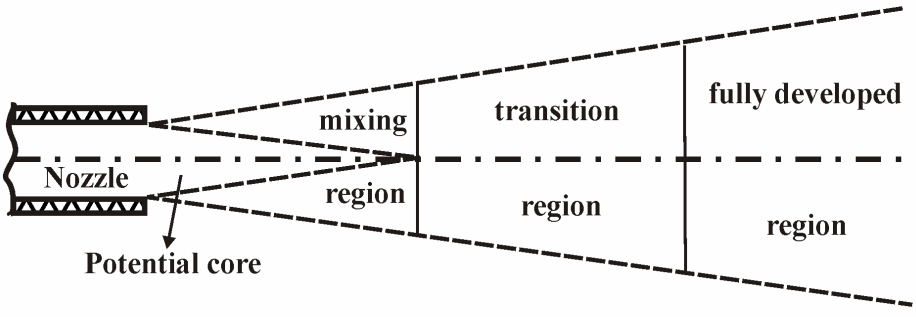

Figure 1.13 Regions of a jet [52].

develops into a noisy turbulent brush of jet starting at a definite point along the jet where a breakdown of the laminar flow occurs and a turbulent jet develops. A characteristic jet length as initially determined by Hawthorne et al. [53] is shown in Figure 1.14. As the flow velocity increases from zero, initially there is an almost proportional increase in jet length and, at any velocity in this region, the jet has sharp edges and is constant in shape. When a significantly high velocity is reached, the tip of the jet changes in character indicating the jet break point. With further increase in velocity, the jet breakpoint moves towards the nozzle and the jet length is slightly reduced. When the breakpoint has approached quite close to the nozzle, the fully developed turbulent flow conditions are reached. Further increase in velocity has practically no effect on jet length, but the noise continues to increase.

There is much known about turbulence, but there is still a lot to be discovered. The turbulence plays two roles, as a random exciter of waves, and as an ensemble of the waves themselves. When turbulent flow is analyzed more closely, one striking characteristic has to be noted that velocity and pressure at a fixed point in space don't remain constant in time but perform irregular fluctuations. The velocity fluctuations may amount only a few percent of the average velocity, but they are still the deciding factor in the whole course of the motion.

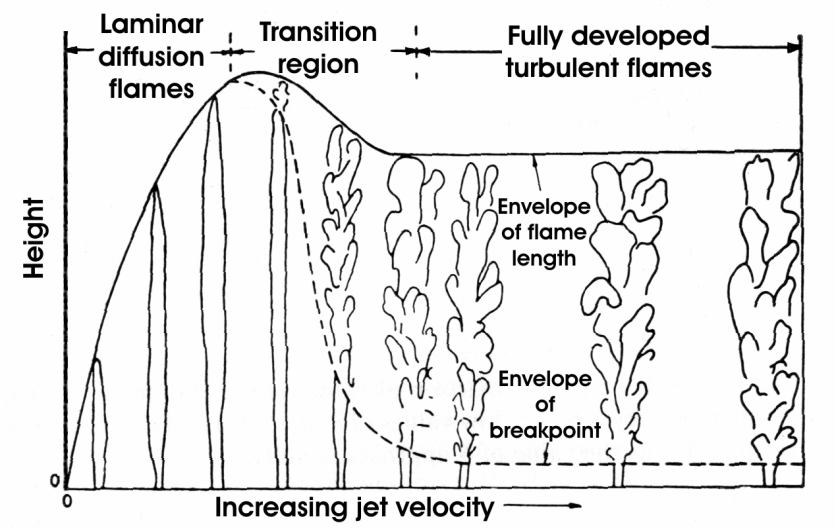

Figure 1.14 Changes in the flame shape with velocity increase [53].

An important aspect of the understanding of a turbulent flow lies in the quantification of the turbulence. In the initial region of the jet, Boguslawsksi and Popiel [54] determined that the highest turbulence value appears at an axial distance of approximately 6 exit nozzle diameters downstream and a radial distance of 0.7 to 0.8 diameters, and that the highest turbulent kinetic energy on the axis occurs at a distance of 7.5 to 8.5 diameters. The location of these maximum values near the end of the core region correlate nicely with the location of maximum noise generation, which is commonly given as less than 10 diameters from the nozzle exit.

Osborne Reynolds derived the original criterion for turbulence. In 1883, he published his famous paper entitled `An experimental investigation of the circumstances which determine whether motion of water shall be direct or sinuous and of the law of resistance in parallel channels'. This paper proved to be a classic in the literature of the science of fluid motion and had a profound effect on the development of fluid mechanics in the widest sense. It contained the formulation of the dimensionless number, the Reynolds Number. The Reynolds number is used in momentum, heat, and mass transfer to account for dynamic similarity and indicates the relative significance of the viscous effect compared to the inertia effect. The condition of this similarity (when two similar objects of possibly different sizes in perhaps different fluids with different flow rates will have similar fluid flow around them.) is that the ratio of inertial to friction forces must be the same at similarly situated points and the dimensionless Reynolds number can be written as:

$$\mathrm{Re} = \frac{inertial \quad force}{friction \quad force} = \frac{VD}{\nu}, \tag{1.8}$$

where V means the free stream velocity, D the exit nozzle diameter and ν the cinematic viscosity. The Reynolds number is important in analyzing any type of flow when there is a substantial velocity gradient. There is a critical *Re* reaching which leads to dramatical changes of the flow portrait resulting in a transition of the flow from laminar to turbulent. The critical *Re* depends on the exact flow configuration and must be determined experimentally. Within a certain range around this point there is a region of gradual transition where the flow is neither fully laminar nor fully turbulent, and the predictions of fluid behavior can be difficult. The viscosity is of great importance in the transition from non-turbulent to fully turbulent flow.

The structure of the turbulent jet in the first few diameters has always attracted the attention of researchers to understand the mechanism by which noise is generated in the jet and to study the possibility of the influence on the general flow field in the jet by control the regular pattern existing close to the nozzle. The boundary layer depends on the

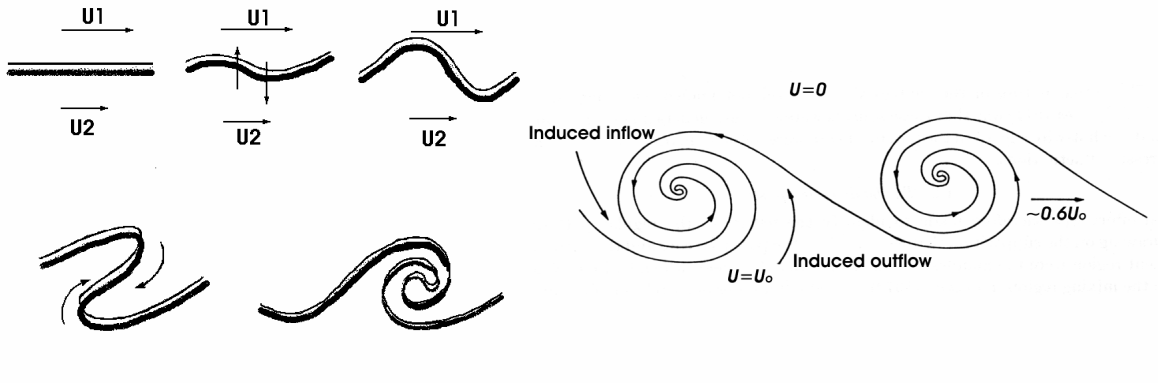

Figure 1.15 Kelvin-Helmholtz instability: a) development of the instability [57]; b) basic vortex model [61].

contraction upstream of the nozzle, as well as on the Reynolds number [55]. The turbulent boundary layer at the edges is characterised by the transition from the non fluctuating (or weakly fluctuating) non rotational outer flow to the turbulent and thus rotational boundary-layer flow. The edge of the turbulent boundary layer is actually a spatially and temporally strongly fluctuating surface. The velocity jump creates a vortex sheet, which develops to Kelvin-Helmholtz instabilities and performs a classical roll-up into vortex tube-like structures.

The instability of the free borders of the jets was already known by Helmholtz, who noticed that the edges of the jets are rolling up into periodical spirals. But Kelvin was the person, who showed the quantitative investigation of the phenomenon [56]. The most common example of Kelvin-Helmholtz instability is provided by a wind blowing over a water surface undulating it. Consider the basic flow of incompressible inviscid immiscible fluids (1) and (2) in two horizontal parallel infinite streams of different velocities and densities, the faster stream above the other (Fig. 1.15 a)). The horizontal boundary, corresponding to a sharp difference of velocity in the fluid is a shearing layer. An external perturbation may give an oscillation on the fringes. Pressure in concavities is higher than pressure in convexities so the amplitude of the oscillation grows up and the upper part of the sheet is carried by the upper fluid, while the lower part of the sheet is carried by the lower fluid. So a tautening of the front occurs and there is a phenomenon of rolling up of the interface in a direction corresponding to the vorticity direction of the mixing layer (here in positive direction for the figure) [57]. In the jets the leading edge of each vortex induces an outflow of high velocity fluid from the potential-core side of the mixing region across into the low velocity region (Figure 1.15 b). In the same way relatively low velocity fluid is transported radially inwards towards the potential core by the trailing edge of each vortex [61]. Now the fluid elements which carry out fluctuations both in the direction of main flow and at right angles to this direction are not individual molecules, but rather are macroscopic ‘fluid balls’ of varying size called *eddies*. This process named *entrainment*, i.e. a ‘negative displacement effect’, is typical to free boundary layers.

As far as vorticity passes from the boundary into the flow, as occurs continuously from a jet orifice, the flow depends not only on instantaneous surface conditions, but on the entire history of vortex passing from the boundary [55].

Townsend was the first who proposed a mechanism of entrainment process [58]. He emphasized the important role of the *large eddies*, which define the whole process. The large eddies might arise from the general turbulent motion, but their degree of organization suggests that they derive energy from the organized mean flow, and that the remaining turbulent motion of smaller scales resists their growth by absorbing some of their energy. Then a sufficiently high intensity of the turbulent motion may prevent further growth of the large eddied or even destroy existing ones. Further, transversal spreading of a free turbulent flow is accompanied necessarily by transfer of energy from the mean flow to the turbulent motion, and the greater the rate of spread the greater the rate of energy transfer. So, if an unusually vigorous set of large eddies appeared in the flow, they would cause a large increase in the rate of production of turbulent energy which, in turn, might lead to destroy them. Townsend proposed the equilibrium hypothesis, which assumes that the

large eddies are the principle agents of the entrainment process and that their average intensity is set by the operation of a control cycle whose elements are:

- During periods of quiescence, the turbulent intensity is too large to permit a growth of large eddies, but it decreases making the flow unstable enough to develop the large eddies of suitable scale;
- Once the flow is unstable, the existing turbulence grows and develops into a large eddy system, which causes rapid entrainment;
- The rapid entrainment leads to an increase of turbulence intensity, and the existing eddies lose energy to the main turbulent motion, and another period of quiescence begins.

The explanation of the sudden appearance of large eddies after a quiescent period was given by Grant [59] in terms of stress-releasing behavior, in which Reynolds stresses stored in the fluid are re-aligned by the large eddies so that they can release energy.

One of the earliest indications suggesting the possible existence of a regular flow pattern in the turbulent subsonic jet came from the work of Bradshaw et al. [60]. They carried out a survey in the general region of the potential core and the mixing layer situated in the distance of first few nozzle diameters, and made statistical measurements of various properties in this region. The results suggested that the fluctuations detected in the potential core were the result of the passage of a fairly regular pattern. Crow et al. [55] supposed that an incompressible turbulent jet can sustain orderly modes of axisymmetric flow, including preferred frequency. Lau et al. [61-62] obtained a picture of the regular pattern, named the 'basic vortex model'. The picture consisted essentially of an array of discrete vortices spaced about one and a quarter nozzle diameters apart. This array of vortices was assumed to move downstream in the region of maximum turbulence at a speed of $0.65U_j$ (U_j - jet velocity). As the array moved downstream, it caused fluctuations

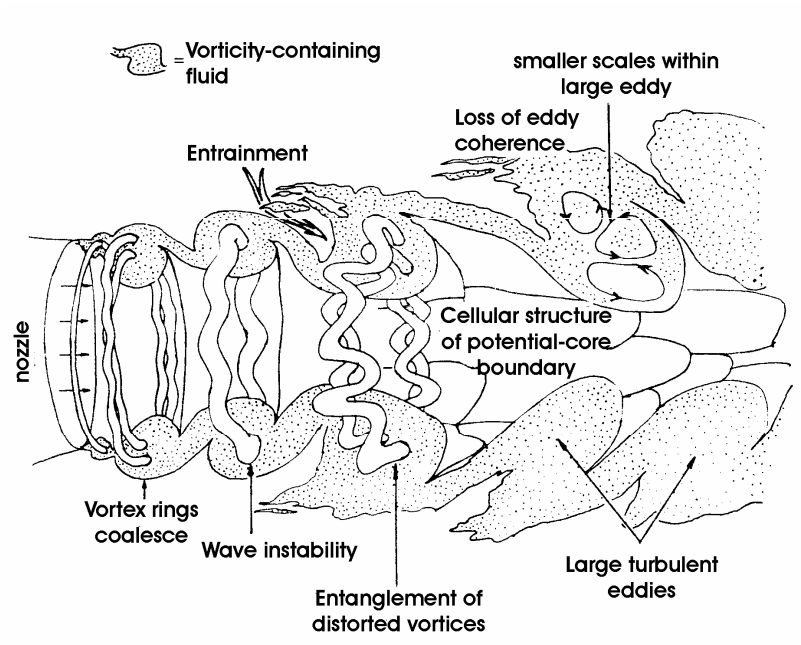

Figure 1.16 Physical structure of transitional jet [65].

in its vicinity. Since the jet was cylindrical, it was assumed that the vortices would be toroidal in shape. For instance, it appeared that the vortices might not show exactly the same distance apart at all times and that they did not move along a definite path. As these vortices move downstream they sweep fluid from the high velocity side of the jet to the other and vice versa. Dahm et al. [63] found unmixed ambient fluid throughout the jet. The time-varying probability of detecting ambient fluid within the jet increased markedly at approximately regular intervals, consistent with the idea of a periodic, large-scale entrainment mechanism.

Brown et al. [64] considered the process of entrainment as entanglement, which appears to occur primarily in the formation of the large coherent eddies. Thus, each eddy contains and is transporting fluid from both sides of the layer which has been entangled into it in earlier stages of its formation.

Yule [65] created a picture of the ring structure entanglement, which provides an excellent physical description to support the quantitative findings of Boguslawski mentioned above (Fig. 1.16). At the end of the potential core, the regular vortex ring breakdown can be characterized as the entanglement and wave deformation of the common large-structured rings into collapsed, unruly, three-dimensional state. The location of this complete entanglement marks the beginning of fully developed turbulence in the jet. A breakdown in the generally organized shear layers at the end of the core results in high kinetic energy [66].

1.4.2 Thermal plasma jets: entrainment and development of turbulences

The flow of plasma issuing from the torch are in form of a jet, which is dependent upon the pressure energy that is converted into kinetic energy at the torch exit and thus, the flows are fully separated from walls. Thermal plasma jets are usually generated in air atmosphere. Cylindrical jets are formed as result of plasma discharges from nozzles of cylindrical cross section.

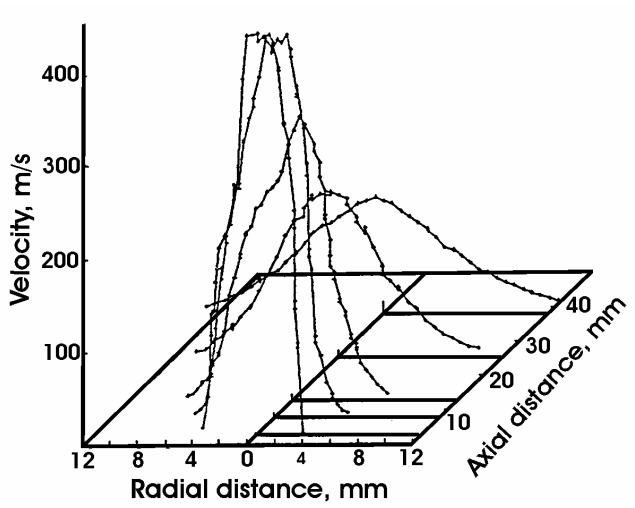

Figure 1.17 Evaluation of the velocity along plasma jet [74].

In thermal plasma jets not only velocity gradients but also temperature and density gradients occur as well, which makes its study more difficult than isothermal one. Although low density jets with $S<1.0$ ($S = \rho_j / \rho_a$, ρ_j - jet density, ρ_a - density of the surrounding) have received relatively little attention in the literature compared to their constant density counterpart ($S=1.0$), the available information suggests that mixing and entrainment are increased

as the jet density is reduced. Ricou and Spalding [67] found that hydrogen jets exhausting into air (*S=0.07*) entrained external air more rapidly than constant density jets. Tombach [68] found that helium jets issuing into air (*S=0.14*) and sulfur hexafluoride (*S=0.03*) produced larger spread rates and more rapid axial velocity decay than homogeneous jets (*S=1.0*).

Unfortunately, in case of thermal plasma the measurements are restricted by high jet temperatures and impossibility of making diagnostics in the most interesting regions – close to the exit nozzle. The extremely high density ratio of the jet is thought to be of primary importance in producing large amount of entrainment and mixing with the ambient air. Russ et al. [69] examined the behavior of both the low density flow and plasma jets and compared mixing and entrainment in both jets. He found that mixing and entrainment in low density jets are quite dependent on the formation of vortex structures in the surrounding close to the jet, which, in turn, sensitively depends on the initial conditions of the jet. When the conditions were laminar, the jet displayed very coherent vortex structures and so-called side jets, formations of which it is believed to be due to the break down of vortex rings leading to the rapid expulsion of jet fluid. Initial turbulent conditions disrupted the side jet formation and produced a more rapid mixing. For very low density jets mixing between the jet fluid and surrounding air was relatively insensitive to the jet initial conditions.

The main difference in mixing of low density jets and plasma jets is due to arc fluctuations. Because of them the plasma jet core becomes unsteady with large temperature and velocity variations. High core turbulence level can be expected to disrupt the regular formation of coherent structures in the shear layer. The shear layer could break down rapidly into small scale turbulence without forming large coherent structures [70]. In spite of this, the model of the entrainment into the thermal plasma jet is heavily based on the model of the isothermal jet described above. The main reason for such a correlation is similarity in development of characteristics of both jets, confirmed by the flow visualization [71-73]. Significant gains in the understanding of the flow structure have been made over the last several years by research performed in the High Temperature Laboratory of the University of Minnesota. There, results have been obtained by a wide variety of diagnostic techniques (LDA, emission spectroscopy, enthalpy probe, spectral analysis and numerical modeling) and by combining results from individual techniques. New knowledge for understanding of plasma plumes and their interaction with external air environment [74-75] was gained, thereby.

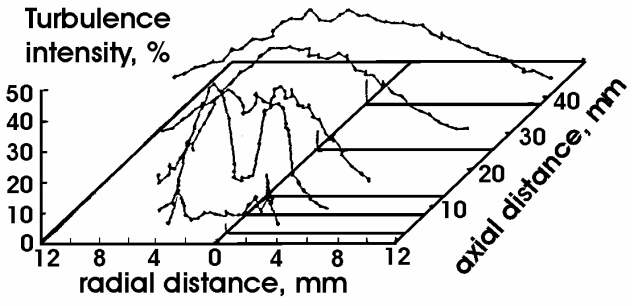

Figure 1.18 Evaluation of the turbulence intensity along the plasma jet [74].

The development of mean plasma velocities typical for thermal plasma jets reveals that a plasma jet is qualitatively similar to isothermal jets (Fig. 1.17). The steep mean velocity gradients were obtained at the edge of the nozzle exit. This is where the turbulence energy is generated and

thus the whole entrainment process initiates. The velocity profiles further downstream show the obvious spreading of the jet and the leveling-off of the velocity.

The amount of turbulence not only dictates the quantity of air entrained into the jet and thus the volume of useful plasma, but it also affects heat transfer rates to particles traveling through the jet. Turbulence in this case is defined as the ratio of the standard deviation of the individual velocity measurements for a given data point (also known as fluctuation velocity) divided by the maximum centerline mean velocity for a given axial distance downstream. The development of turbulence reveals a rapid increase in axial velocity fluctuations at the edge of the jet due to the mixing and entrainment of external air (Fig. 1.18). The initial rise of turbulence at the edge of the jet and the progression of the maximum turbulence towards the centerline are likewise characteristics of both combustion and isothermal jets.

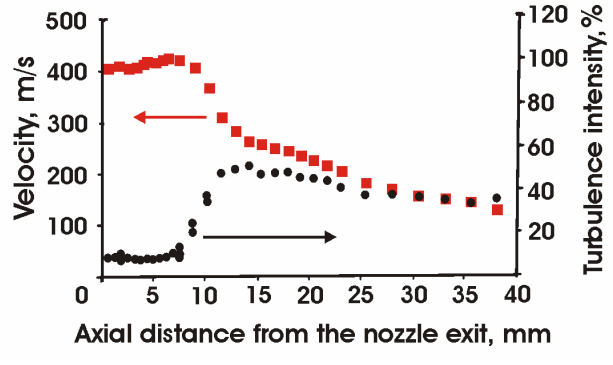

Figure 1.19 Axial velocity and turbulence intensity along the plasma jet [74].

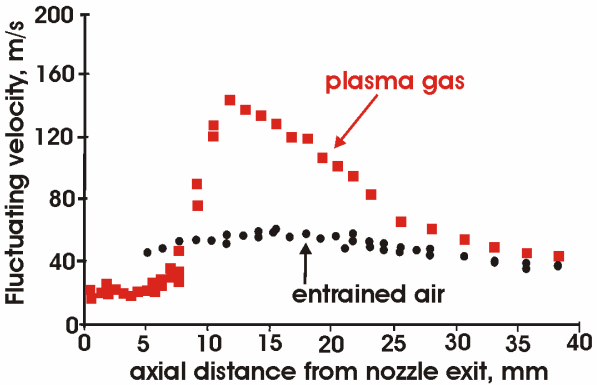

Figure 1.20 Fluctuating velocities of plasma gas and entrained air [74].

Centerline mean velocity and turbulence intensity is plotted together in Figure 1.19. The sharp increase in turbulence and the dramatic drop in axial velocity starting at the axial distance equal to near one exit nozzle diameter corresponds to the point where eddies of entrained air from the surrounding fluid have finally reached the centerline of the jet. The stretching of the plasma gas eddies as they flow over the slower cold eddies, is thought to be the main reason for the large increase in axial velocity fluctuations in the transition region of the jet. The low turbulence level in the exiting plasma jet exists because the central portion is still in the potential core region of the jet and the increased viscosity, due to high temperature, relaminarizes the flow. The plasma jet exit conditions were measured by Spores [76] at a lower *Re* of approximately 400 and were found with a fairly parabolic velocity profiles with a centerline turbulence intensity near 5% in the upstream and up to 34% in the downstream part of the plasma jet. Lesinsky et al. [77] reported peak turbulences in such jets in the range of 30-40%.

The plotting of the fluctuating axial velocity of plasma gas and of entrained air confirmed that the mixing of the two flows is not completed until quite big distances downstream where both flows finally show similar values (Fig. 1.20). The fluctuations of

both flows, of the plasma gas and of the entrained air, deviate greatly. While entrained air fluctuations remain relatively constant over the entire jet, the plasma gas fluctuation velocities experience a sharp local increase as the mean velocity rapidly decreases in this region. The entrained air continuously slows down the plasma while the plasma does not seem to be able to significantly accelerate the entrained air.

Based on all statements reported above the turbulence model in thermal plasma jets was described in [74]. As the plasma jet exits the nozzle, there are strong velocity and density gradients at the outer edge of the jet (Fig. 1.21). These gradients cause rolling up of the flow around the nozzle exit into a ring vortex which is pulled downstream by the flow, allowing the process to repeat itself again at the nozzle exit. Adjacently forming vortex rings at the outer edge of the jet have the tendency to coalesce, forming large vortices. Perturbations to these vortices then lead to wave instabilities growing around the entire ring. Next, the distorted vortex rings start entangling themselves with adjacent rings finally resulting in totally breakdown of the vortex structure into large-scale eddies and the onset of turbulent flow. This entanglement process of adjacent unstable vortices results in the first large-scale engulfment of external air, although some entrainment also takes place during the roll up processes on the jet shear layer. These large eddies of cold gas entrained in the jet have a much higher density and thus greater inertia than their high-temperature counterparts. The eddies of cold gas travel in the axial direction at much lower velocity, while the hot plasma gas essentially accelerates around and stagnates on the cold gas eddies with little initial mixing. All eddies in the flow are continually breaking down into smaller and smaller eddies, while diffusion is taking place on the molecular level at all eddy boundaries. The mixing and diffusion process eventually reaches the centerline of the jet, defining the end of the laminar core. The jet now undergoes transition and eventually becomes fully turbulent while eddies of external gas continue to be engulfed and absorbed into the main jet along its entire length, further reducing both the mean temperature and velocity.

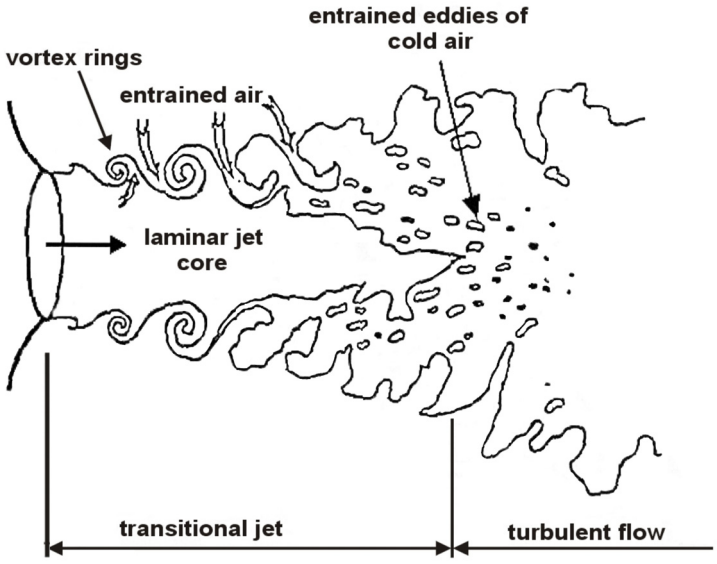

Figure 1.21 Model of entrainment into a thermal plasma jet [74].

In plasma spraying applications, large slow-moving particles injected into the plasma jet will first see the laminar high-temperature potential core of the jet, then in the transition region they will experience eddies of both types of fluid, and finally in the fully turbulent region homogeneous eddies of mixed fluid will carry them downstream. As large plasma spray particles traverse from the plasma into an entrained air eddy, they will experience large temperature fluctuations and temporary atmospheric oxygen concentrations, causing rapid oxidation of any susceptible powders. The heat and momentum transferred to these particles is the integrated time history of all eddies encountered.

The previously mentioned fluid dynamic of the plasma jet and the jet fluctuations may lead to the situation shown in Figure 1.22, where the plasma jet contains a big amount of cold gas and misses the hot plasma. Actually, the model of the plasma jet takes into account large scale entrainment of ambient gas and thus the not-mixing phenomenon of the dense cold gas bubbles with the hot plasma. The model treats the plasma jet as a two fluid mixture consisting of hot, out-moving fragments and cold, in-moving fragments [78].

Complimentary measurements obtained by seeding only the ambient air revealed that the air was transported to the jet center as soon as one exit diameter downstream of the jet exit. Enthalpy probe measurements of Brossa and Pfender [79] suggested that the air was entrained to the jet centerline before three exit diameters. This entrainment of external air cools the plasma jet and reduces the hot zone available for plasma processes.

The interaction of the thermal plasma jet with surrounding air puts restrictions onto its applications. The main problem is connected with plasma spraying of metallic powders. Unavoidable entrainment of the surrounding cold air into the plasma jet can alter the characteristics and quality of the coating produced. When spraying fully melted metallic particle, in most cases heated to their melting temperature in the plasma jet, fast chemical reactions may occur even if their residence time in the reacting zone is a few milliseconds at the maximum. In-flight oxidation of the metal particles occurs. It is, therefore, common to find oxide phases in metal coating [80-82]. Oxides in coatings are considered to influence the structure and properties of the deposits [21]. For these reasons, mastering

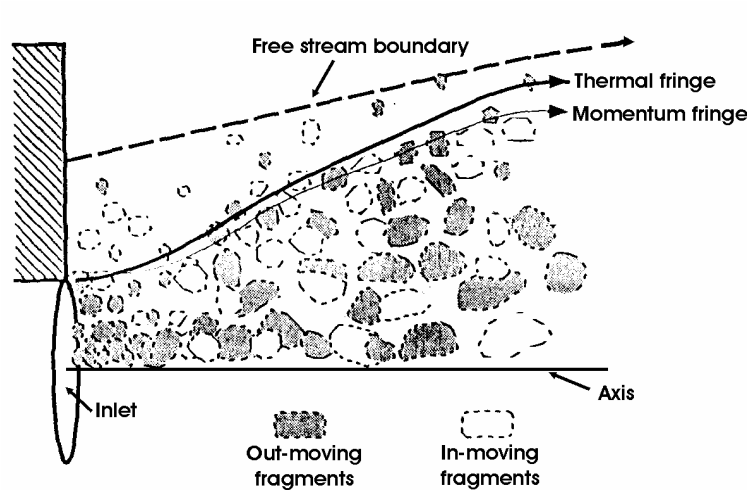

Figure 1.22 Two fluid model of the thermal plasma jet [78].

methods of controlling the entrainment into the plasma jet is highly desirable. Efforts are continually being made to develop practical methods for flow control not only in the core region but in the turbulent region as well. Numerous methods for altering the potential core length, the turbulence intensity varying from inflow adjustments to different types of forcing and the surrounding atmosphere content, have been discovered and are further described.

1.4.3 Control of the entrainment process

The control of the air entrainment is very important for efficient plasma processing especially for certain applications which require an oxygen-free plasma flow. In some applications, raising the arc power and plasma flow rate can lessen the entrainment [83-84]. A more direct and efficient approach is to improve the flow of the jet. In principle, it can be achieved by limiting the entrainment of air or by decreasing the turbulence intensity.

Several methods can be suggested to avoid this intrusion of air. One method is the operation of the torch in a surrounding gas environment of the same species as the primary arc gas. The second one is the generation of the plasma jet in a low-pressure environment of considerably lower density. Another possible candidate is the torch operation with shroud gas injection around the plasma jet blocking or delaying the ambient air entrance into the plasma jet.

Mash et al. [85] and Stetson and Hauck [86] seem to be the first who reported plasma spraying into a chamber with an inert gas. This spraying technique is called controlled atmosphere plasma spraying (CAPS). The spray gun is operated in a chamber and the conditions within that chamber are completely controlled. CAPS systems are extremely flexible with respect to the atmospheres which can be used and the internal chamber pressures that can be selected for spray conditions. Inert, protective atmospheres can be used for ensuring the purity of reactive spray materials or the protection of the work piece substrates which have the tendency to oxidize or to contaminate easily. The entrained gas does not contain oxygen any longer but the inert gas which is usually the same as the plasma forming gas. This arrangement yields coatings exhibiting unique properties not possible in standard atmospheric environment.

The second method how to avoid oxidation or contamination of the powder and the sprayed deposit is low pressure plasma spraying (LPPS), which makes use of plasma torches operated inside the chamber under reduced pressures. Only about a decade after the appearance of DC plasma spray torches, LPPS was introduced in industry. The pressure can be in the range from near atmospheric down to pressures as low as about 130 Pa. Within the pressure range of 1 kPa to 40 kPa the plasma jets expand to supersonic velocities and are characterized by Mach numbers higher than 1. Supersonic jets differ in their behaviour from subsonic jets. The major difference is that the jet can exit a nozzle at a pressure that is different from the ambient pressure. This can occur because information on the chamber pressure is carried through the flow by pressure waves that travel at the speed

of sound with respect to the fluid. When the fluid at the exit plane of the nozzle reaches the speed of sound or higher speed, the pressure waves carrying the chamber pressure information are unable to reach the flow inside the nozzle. Therefore, the chamber pressure is not felt by the flow and the geometry of the nozzle governs the pressure distribution inside the nozzle along with the torch operation conditions, namely the power [87]. In that case, the jet exit pressure differs from the chamber pressure. Figure 1.23 a) shows the structure of the supersonic jet in aerodynamic non-equilibrium situation. In the shown case, the static pressure of the jet is lower than the chamber pressure. It is an overexpanded jet. Native mechanisms develop to bring the jet pressure back to the chamber pressure. It is shown that oblique shock waves originating from the edge of the nozzle are formed. This mechanism increases the jet static pressure to the level of the pressure of the chamber by turning the flow (from zone a to b). However, these shock waves are reflected on the jet axis. Further down they meet the jet boundary where they are reflected in the shear layer in the form of series of expansion waves. This decreases the flow pressure back to the chamber pressure (from zone c to d). These expansion waves are also reflected on the jet axis so that the flow will go through another series of expansion waves (zones d-e) reducing again the flow pressure below the chamber pressure while turning the flow parallel to the jet axis. This is followed by the reflection of the expansion waves into compression waves at the jet boundary, as the pressure of the ambient gas at the boundary pushes the jet gas back toward the axis. These compression waves may coalesce into an oblique shock wave. This is once again forming a second compression/expansion cell, and will be followed by the third, and so on. The pressure change through each cell is weakened from cell to cell by the viscous effects, which also thickens the shear layer. Eventually the pressure is brought back to the chamber pressure [88]. The plasma gas in the jet interior expands and cools as it flows through the expansion zone and is compressed and heated as it passes through the shock diamonds. The increase of pressure and temperature after the oblique shock waves can be observed by the increased luminosity of the plasma, if the shock is strong enough. The position of greatest jet compression does not coincide with the position of minimum jet diameter. The streamlines in the figure indicate the flow path of the gas [89]. The expansions correspond to the regions where thermal energy transfers into kinetic energy, while in the compression regions kinetic energy

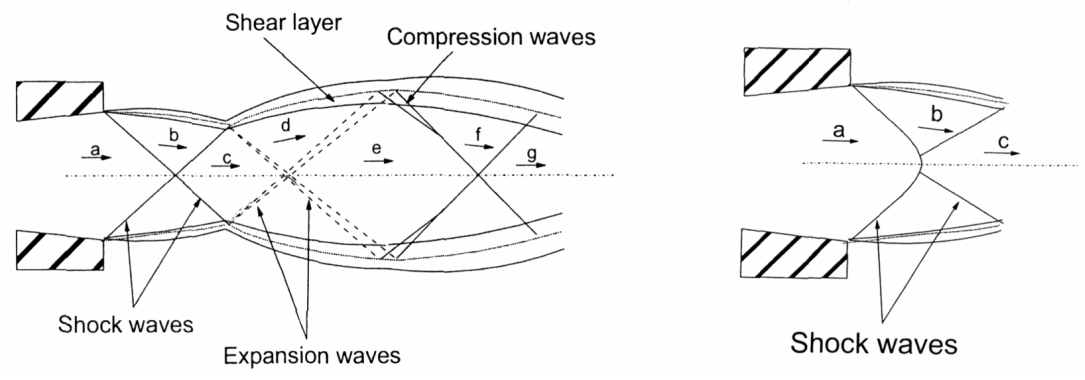

a) b)

Figure 1.23 Compression/expansion mechanisms in an over-expanded jet (a) and Mach reflection (b) [87].

transfers into thermal energy.

If the pressure of the gas at the nozzle exit is greater than the chamber pressure the jet has underexpanded character. In this case, the jet expands as soon as it leaves the nozzle. The geometry of the nozzle, the torch operating conditions and the chamber pressure determine the character of the jet [89-90].

As the chamber pressure is reduced, the compression-expansion cells are stretched, and build up farther down from the nozzle. This is mainly because of the absolute pressure reduction: the jet needs more distance to equilibrate pressure [91].

If the pressure difference between the jet and chamber is large, a striking change in the flow structure occurs. In that case, a Mach reflection appears as shown in Figure 1.23 b). It consists of an oblique shock and a normal shock, the latter one being located near the jet axis. The type of the reflection, either Mach type or regular type one, explained above, is determined by the angle between the shock wave and the jet axis: small angles of regular reflections (Fig. 1.23 a)) and large angles of Mach reflections (Fig. 1.23 b)). When gas passes through a shock, its velocity component normal to the shock is greatly reduced but parallel component remains unchanged. Thus, the shocks with large angles relative to the flow axis are much more effective at slowing down the flow than shocks with small angles. A prominent feature of Mach reflections is the existence of a slip discontinuity from the shock triple point, there the oblique shock, reflected shock and Mach disc meet. The flow velocity, density, and temperature are discontinuous across this contact surface. This discontinuity arises because the thermodynamic pathway through the oblique and reflected shocks does not equal the pathway through the Mach disc [89]. The Mach disc can be followed by a subsonic region, after which the jet again becomes supersonic [92].

The jet structures shown above are idealizations and entrainment of the surrounded air takes place in spite of reduced density gradients. The real supersonic jets do not have sharp, stable boundaries but turbulent boundaries where jet and ambient gases mix. Figure 1.24 shows a more realistic steady-state structure for an overexpanded jet. Near the exit nozzle, where the pressure difference is large, Mach reflection occurs, but farther downstream the reflections are regular. The mixing layer, which grows as a result of Kelvin-Helmholtz instabilities, progressively eats its way into the supersonic core of the jet. When the mixing layer reaches the axis of the jet, the flow is subsonic and fully

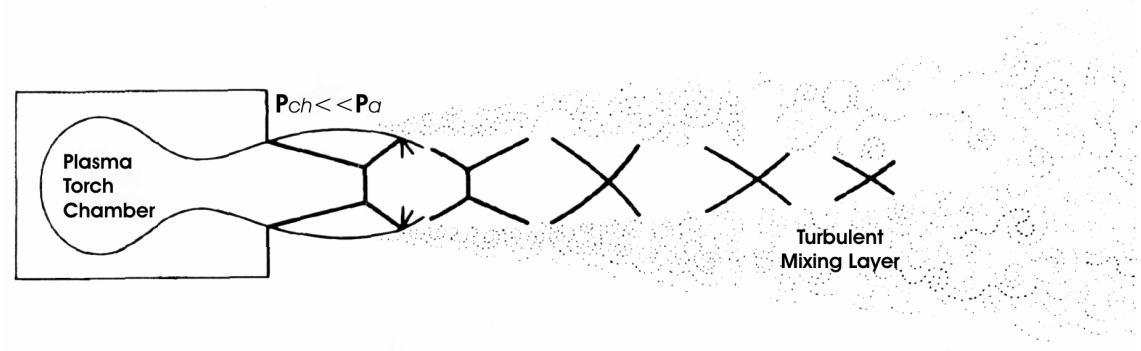

Figure 1.24 Realistic steady-state structure of an overexpanded supersonic jet, showing the presents of both Mach and regular reflections.

turbulent. The wave structures within the supersonic core are not steady since they are surrounded by the turbulent boundary layer. However, their average positions are well defined.

The main components of a low pressure plasma spraying (LPPS) system are shown in Figure 1.25. Two main constituents are the vacuum chamber inside which the plasma spraying process is carried out and the pumping system allowing the reduction of the pressure in the chamber to desired values. The plasma jet generated under low pressure conditions exhibits lower entrainment rates and high-quality coatings with low porosity and oxygen content can be produced. The constricted anode attachment, typical for the atmospheric pressure conditions, becomes diffuse providing reduced arc fluctuations [93]. The strongly increasing plasma velocity results also in an increase of the velocity of sprayed particles, and consequently, allowing the production of very dense coatings [94]. The growth rate for diamond deposition in a supersonically expanded DC plasma jet in low pressure chamber (less than 10 Pa) increased [95-96]. It has to be noted that plasma torches under vacuum conditions are often equipped with a Laval anode nozzle, which can determine the behavior of supersonic plasma jets not only depending on the chamber pressure but on the inner geometry of the nozzle as well [97-98].

The main disadvantages of both CAPS and LPPS systems are the requirements of a large chamber inside which the plasma torch is operated and the presence of a gas pumping system, which makes the system more complicated and the whole process quite expensive. Moreover, the chamber also limits the size of work-pieces.

Another solution involves adding a gas shroud attachment onto an atmospheric plasma spraying torch [99-103]. The theoretical basis for spraying with a gas shroud has its origins in compound jets, or jets in co-flowing or counter-flowing streams. This problem has been investigated by a number of authors in the past and is still of keen interest in a number of applied fluid mechanics problems [100]. Gas-shrouded nozzles for atmospheric plasma spraying were first mentioned in U.S. patents in 1969 [101].

In the past, two methods have been used: a solid shield and a gas shroud. The solid shield is a hollow metal or ceramic cylinder which is coaxial with the plasma jet and effectively extends the nozzle. The shield acts as a physical barrier preventing the air being entrained in the plasma jet. As a result, there is much less energy dissipation and the temperature and velocity of the plasma jet remains at higher levels downstream of the nozzle. However, the solid shield makes practical difficulties. Firstly, it is usually manufactured from metal and requires cooling to maintain it at tolerable low temperature what reduces the energy efficiency. Secondly, there is a tendency for the molten droplets to stick on the internal wall of the shield. If this occurs, it would narrow the internal bore, necessitating regular cleaning and reduce the efficiency of the technique.

Gas shrouding is a developing technique, which involves replacing the solid shield with inert, high-velocity gas streams coaxial with the plasma jet [102]. Shrouding attachments are used to inject a secondary gas, e.g. cold argon with argon plasma jets, around the plasma. The purpose of the injection of this secondary gas is to reduce the mixing of the plasma flow with the surrounding atmosphere and to extend the hot core of the jet by rearranging the gas flow to increase the dwell time of particles in the plasma. A

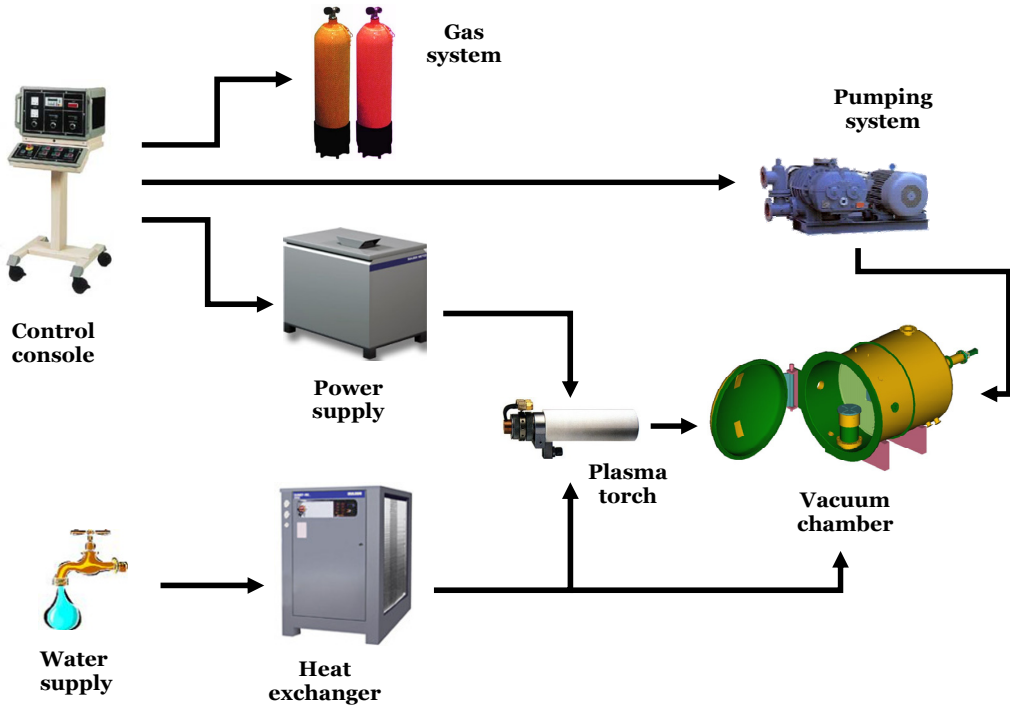

Figure 1.25 Components of the low pressure plasma spraying system.

more important objective of gas shrouds is to minimize the entrainment of oxygen into the plasma flow.

In designing shrouding attachment nozzles, certain limitations exist. Thermal spray powders are normally injected at the outlet cross-section of the spray torch. When spraying with gas-shrouded nozzle, the internal injection mode is generally used, with the particle injection point located inside the nozzle. Thus, the particles have a longer time available to heat up and to be accelerated towards the substrate. Since powder particles tend to disperse radially as they travel along the jet, divergent nozzles are required for the internal injection mode. The length of the nozzle is also of important influence, as the shroud must be selected in such a way that the energy losses to the cold walls are reduced. Moreover, the requirements for proper cooling of the nozzle, as well as for proper injection of the secondary gas, impose some limitations in choosing the nozzle length. Finally, the nozzle should be relatively easy to manufacture, to install and to replace.

Jankovic et al. [100] made numerical analysis on the flow field inside the shrouded nozzle, which showed that the angle of the nozzle, as well as the flow rate of the plasma gas, played significant roles in determining the flow pattern. The shroud nozzle, used in their experiments was a conical diffuser with sixteen shroud injection ports located concentrically around the jet. When shrouding gas was introduced, uniformly spaced jets surrounded the main plasma flow and formed a shroud around it. All results indicated the benefits of a gas shroud as the gas shroud improved the flow parameters in the free jet region. Delayed mixing with the surrounding air resulted in a higher plasma velocity and temperature, together with the lower concentration of entrained air in the free jet region. Even better results were obtained by injection of the shrouding gas through a continuous (ring shape) slot as in the case of several ports the continuous shrouding envelope around

the jet was formed only at the distance of approximately 10 mm from the nozzle exit. Air was entrained right at the nozzle exit before the formation of fully protecting envelope.

In the numerical study of Kang et al. [103] there is an indication that the cold shroud gas might affect the plasma flow fields in the downstream region of the plasma jet. Although a rather high amount of shroud gas injection results in less air entrainment into the plasma jet, it may cause cooling and/or instability of the plasma jet flow as well as additional costs for shroud gas. Therefore, the optimum flow rate of shroud gas has to be determined by considering not only its favourable shielding effect but also its unwanted cooling or destabilizing effect of the plasma jet.

On the one hand, the gas shroud avoids the problems associated with the solid shield regarding the possibility of particle sticking and the need for a cooling system. On the other hand, the gas shroud is expected to be a less stable barrier than the solid shield as it will dissipate and become more defuse as it travels downstream. Its efficiency will gradually diminish with distance from the nozzle. That is why the shroud assembly very often includes both the wall shroud and means for forming the gas shroud [104-105].

1.5 Plasma jet diagnostics

1.5.1 Methods for plasma flow diagnostics

The measurement of temperature, velocity, enthalpy and species concentration in high-temperature gases, including weakly ionized plasma, has considerable importance in many applications. In plasma spraying applications velocity and temperature measurements have arisen out of a need for more fundamental knowledge of particle behavior in a plasma flame to allow optimization of the plasma spraying process rather than rely on a method of "trials and errors". The energy transfer between the plasma and the injected material is dependent on the dynamics of flow and its chemical state. That is why the flow characterization implies knowledge of its velocity and temperature distribution as well as its composition. In the literature these measurements are included under the term of "plasma diagnostics"

Diagnostics of the thermal plasma jets are complex and difficult due to extremely high emitted light fluxes (up to 10^{11} W/m^3), very high temperature gradients (up to 4000 K/mm), very high thermal fluxes (over 10^{10} W/m^2), and also, typically for DC arc plasmas, high fluctuations of dissipated power (often more than 50%) [18]. The main diagnostic techniques, available to measure characteristics of the plasma jet close to the exit nozzle of the plasma torch, are emission spectroscopy and laser scattering. At the downstream part probe methods are widely used.

The main methods used for diagnostics of the plasma flow are described here.

Emission spectroscopy

It is now a well-established technique which gives the populations of excited levels from which temperatures can be deduced. During the last 20 years, the automation of signal treatment and the use of photodiode arrays or optical multi channel analyzers have

allowed routine measurements, especially with molecular spectra. However, in spite of the relatively fast on-line measurements, one has to be extremely careful in interpreting the following results. LTE assumption is often used to derive the temperature from excited level population. It implies that the collisions are the predominant mechanism and that temperature and concentration gradients are low, which is not the case in arc fringes or close to electrodes, where diffusion plays an important role, especially for electrons, and temperatures deduced from atomic lines are generally overestimated. The important requirement is cylindrical symmetry which is a prerequisite for Abel's inversion allowing evaluation of the radial profiles of the plasma jet characteristics. Moreover, when measuring DC torches plasma jet temperatures, the fluctuations introduce another problem [18].

Laser scattering

The scattering of electromagnetic radiation by plasma particles is a commonly used diagnostic technique as it generally non-perturbating and requires only line-of-sight access to the plasma.

Coherent Anti-Stokes Raman Scattering (CARS). In Raman spectroscopy, the energy levels of molecules are explored by examining the frequencies present in the radiation scattered by molecules. Some incident photons from a monochromatic incident beam may collect energy from the excited molecules and emerge as high-frequency anti-Stokes radiation [8]. This nonintrusive technique is applicable to the measurement of the concentration of any Raman active species, including O_2, N_2, CO, etc. Rotationally resolved spectra allow determining heavy species temperature T_h without any assumption of LTE. This technique has been very powerful to study the air entrainment in the jets (to demonstrate that the entrained bubbles are mixed only when they are heated enough) [18].

Rayleigh and Coherent Thomson Scattering. Rayleigh scattering is a scattering of the incident photons by atoms while in Thomson scattering the incident photons are scattered by free electrons. High-resolution line shape analysis of elastically scattered light allows measurement of the plasma velocity (shift of the Rayleigh peak), heavy species temperature (Rayleigh peak intensity), and electron density. No LTE assumption is required.

Similar as spectroscopy, laser techniques are practically non-intrusive, providing a wide range of information on plasma properties (particle densities, including ground state populations, particle temperatures and velocities). Unfortunately, its high conversion efficiency, high collection efficiency, excellent fluorescence and luminosity discrimination, as well as high spatial and temporal resolution are counterbalanced by the equipment price and the necessity of highly trained operators [18].

Probes

Electric probes are widely used in measurements of properties of non-thermal plasmas, but their application in thermal high pressure plasmas as classical Langmuir probe is complicated by the interaction of the probe with the plasma and by a variety of mechanisms influencing the probe current. Nevertheless electric probes are commonly

used for measurement of the plasma potential [106-107]. Information about the structure and shape of thermal plasma jets can be obtained from the probe measurements as well [108].

Enthalpy probes allow the simultaneous measurement of plasma jet temperature, velocity and, connected to the mass spectrometer, gas composition as well. These probes can be used in *Ar* or *Ar-He* plasmas at $T < 12000\ K$ and in *Ar-H2* (25% of vol.) at $T < 9000\ K$, i.e. in zones where the thermal flux is below 10^8 W/m^2 [109-112]. This technique will be discussed in detail in section (1.5.2).

Miscellaneous techniques

Video cameras. Computerized video-image processing and process-control software make it possible to automatically extract information from video images. The system can provide real-time pictorial information of the dynamic behavior of the plasma jets or particles in the solid or molten state moving at high speed within plasma jets. Plasma jet fluctuations can be studied with video cameras operating at exposure time up to 10^{-6} s [113].

Spectral analysis of fluctuations. This is a nonintrusive diagnostics technique capable of providing a great amount of information about the operation conditions of a plasma torch. Analysis of pressure fluctuations, for example, through acoustical spectral measurements, provides information about the flow structure due to the arc root motion. Furthermore, by spectral analyzing the signals from a photomultiplier or a photodiode focused on the axis of the plasma jet at a given location, one can gain insight into the temperature fluctuations of the jet and how they correlate with the arc root motion. Coupling with the power source, response can be deduced from the simultaneous study of arc current fluctuations. However, an appropriate signal treatment with adapted filters must be performed to find correlations.

Shadow and Schlieren visualization. Shadow-graphs of DC plasma jets reveal the abrupt development of turbulence from a well-behaved laminar flow near the nozzle exit. They reveal typical shear-layer instabilities close to the nozzle exit, characterized by the formation of the vortex rings around the jet. Schlieren imaging is used for visualization of the plasma jet structure. This method allows only the observation of the plasma jet fringes, where the interaction of the plasma flow with stagnant surrounding air takes place. Normally an observer is not able to see the contour of the jet itself but the jet boundaries. Nevertheless, the method gives information about the plasma jet spreading and the turbulence formation. [114-116].

Turbulence intensity measurements. These measurements have been performed by using Laser Doppler Anemometry (LDA) [77]. A laser Doppler anemometer measures the velocity of the seeded particles in a flow using light beams. It is important that these particles must be small enough to accurately follow all the movements of the flow. By measuring the velocity of the particles the velocity of the flow is known. Mostly alumina particles ($d < 3\ \mu m$) are used as such tracers. These techniques have several advantages: LDA does not disturb the flow being measured, it can be used in flows of unknown

direction and it can give accurate measurements in unsteady and turbulent flows where the velocity is fluctuating with time. Among the disadvantages are high costs.

1.5.2 Enthalpy probe diagnostics

The measurement of gas properties at atmospheric pressure and temperatures above 5000 K had long been a serious problem. The temperatures are too high for the application of the traditional techniques, which depend on solid-state properties, e.g. thermocouples or thermometers of any type, would be beyond their melting point. Simple optical techniques such as pyrometry are limited by source brightness temperature [117]. However, many sophisticated laser techniques have been developed and applied to these types of flow fields, they are expensive and require delicate, complicated equipment. In many situations the application of thermodynamic probes to measure local gas characteristics, especially enthalpy, represents a robust, low cost alternative.

The determination of enthalpy using different devices started at the end of the 50s when work was carried out in many countries to develop high-temperature processes and equipment. The largest number of development activities of measuring devices was reported in the 60s and 70s. Measurement methods were proposed and substantiated, appropriate sensors were developed and subjected to successful tests in measuring the enthalpy of different high-temperature media: inert, hot, plasma. In later stages, the development of the measurement procedures continued along the path of optimization and improvement of the existing devices and development of automated systems. It should be noted that the enthalpy of low-temperature flows is measured by conventional methods, for example, using thermocouples, thermal resistors and other heat sensitive elements.

In the ensemble of methods to measure enthalpy there are usually three most important groups: 1) sound flow, 2) direct determination of the enthalpy by taking gas samples and 3) determination of the enthalpy from the heat exchange between the gas flow and a solid. The first of the methods was not used widely because of the complicated design of the probe. The other two methods are used extensively, but the second method based on gas samples has been used more widely [118].

A device introduced into the gas flow in order to measure flow enthalpy is named an enthalpy probe. Used in thermal plasma research since the early 60's, the enthalpy probe has been the object of many studies to determine its ability to provide correct measurements in a variety of flow patterns and geometry, and it is generally considered to be a reliable diagnostic tool in the range from 2000 to 12000 K [109].

Detailed analysis of the design solutions and procedure of determining the enthalpy makes it possible to classify the enthalpy probes in two large groups – *stationary* and *non stationary*. Both methods provide the determination of the enthalpy by calorimetric measurement of gas samples. Historically, the stationary method was the first one to be developed. The founder of the method is seemed to be Jerry Grey, who founded its own company in the USA. The method was then used as a basis for developing various devises – enthalpy probes, sensors, etc.

Non stationary enthalpy probes have been described only seldom in the literature as they are not yet used widely. The high-speed enthalpy probe, representing this group of enthalpy sensors, consists of three tubes one inside another. The enthalpy of the gas is determined by measuring the electrical resistance of the central tube. The enthalpy probe is inserted into the high-temperature flow for a short period of time. The water jacket protects it against overheating. The sampled gas flows through the measuring pipe at a constant rate. The measuring pipe is used in such a manner that the entire energy of the gas flow is sucked away by the pump and absorbed in the tube. The temperature of the tube continuously increases when taking a gas sample. The resistance of the internal pipe of the probe is measured as a function of time at a constant flow through the pipe.

They are used far less frequently than their stationary analogues due to a complicated design, the need to use high-speed apparatus and an insufficient stability in the high temperature flow. Erosion, cavitations and surface damage greatly shorten the service life of the probes. Moreover, it is difficult to analyze the measurement error in these probes. But these probes provide high operating speed (measurement time is several milliseconds, what is especially important when long-term keeping of the probe in the flow is not possible), have small size and enthalpy is measured within a single cycle during taking gas sample, thus the accuracy of measurements increases.

Stationary enthalpy probes. According to the application, these probes are divided into probes for subsonic and supersonic flows. They have many similar features, especially in the procedural part, but also some design differences. According to the position of the measuring part of the probe in the flow, there are probes with longitudinal and transverse flow-around.

As mentioned before, the first probe of the stationary type was developed by J. Grey and it is called the longitudinal enthalpy probe (Fig. 1.26 a)). It consists of three coaxial tubes; two of these tubes, the inner and outer, are connected together at the inlet part and form the hemispherical head with a measuring orifice at the inlet. The intermediate tube is positioned between the outer and the measuring tubes and is used to divide the cooling flow and direct it into the inlet part of the probe. In the outlet part of the probe the tubes are connected in such a manner that they ensure the inlet and outlet of the cooling liquid, positioning of the temperature gauges in the inlet and outlet areas (for example, thermocouples), and connection of the sensor to the systems for gas sampling and pressure measurement. The calorimetric method is used to determine gas enthalpy values. The measurement consists of two main steps: a ‘tare’ mode without sucking the gas through the probe, when the amount of heat received by the probe per unit time is only the result of heat transfer through the outer surface of the probe and the ‘sample’ mode when the hot gas flows through the inner tube of the probe and the probe is in contact with a high-temperature flow on both outer and inner surfaces. The detailed description of the method will be given later. Other types of the stationary probes are based on the longitudinal enthalpy probe.

The two-tube enthalpy probe is similar to Grey’s probe. The only difference is the cooling system. The design of the internal measuring tube together with the outer tube

ensures the required cooling rate and defines the direction of movement of the cooling liquid. Therefore, the intermediate tube is not required.

In the enthalpy probe with internal heat insulation the insulator is placed on the intermediate tube. The presence of heat insulation reduces the intensity of the heat exchange between the counter flows of the cooling liquid, increases probe sensitivity and reduces the measurement error. However, these probes are not used in practice because of production problems and problems in developing methods of decreasing the intensity of this heat exchange.

In enthalpy probes with divided flow of the cooling liquid an additional intermediate tube is used. Three outer tubes form the cooling system. The cooling liquid is

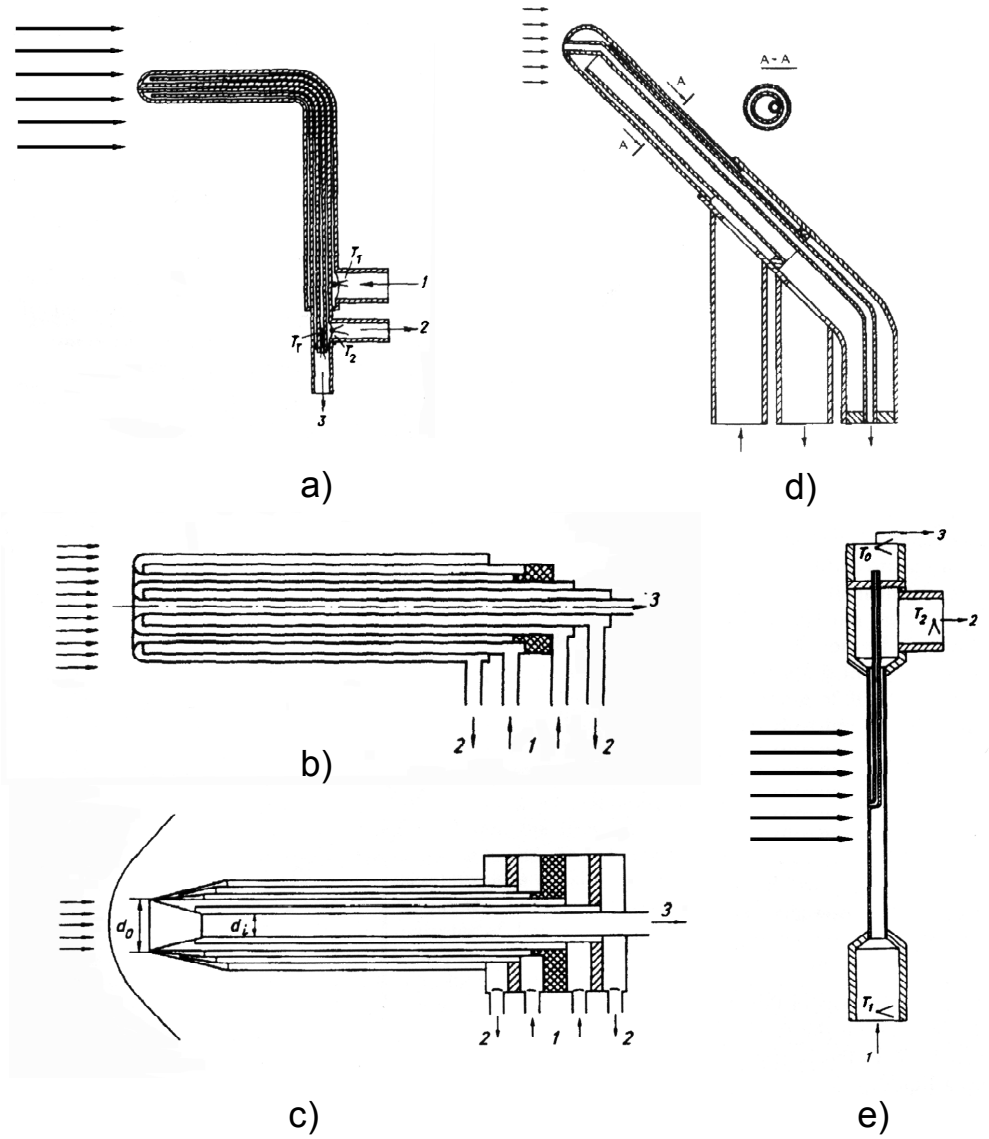

Figure 1.26 Enthalpy probe designs [118]:

a) Longitudinal enthalpy probe;
b) Probe with a cooled screen;
c) Probe for supersonic flow;
d) 'Angular' enthalpy probe;
e) Transverse enthalpy probe.

supplied between two intermediate tubes and, consequently, is directed to the inlet part of the probe – the part with the highest thermal stresses. Here the liquid is divided into two parts: one part cools from the outside, protecting it against the high-temperature medium, and the other part of the liquid passes in the gap between the intermediate and the measuring tube, receiving mainly the heat flow from the measuring tube. Thus, the slightly more complicated design of the probe and its larger dimensions are compensated by improved sensitivity of the measurement.

There are two types of the enthalpy probe with a screen – with a cooled and uncooled screen. The uncooled screen is positioned on the outer side of the probe. It is made of a heat-insulating material, for example graphite, and repeats the shape of the probe. The screen not only protects the probe against overheating but also increases the sensitivity of calorimetric measurements of the gas sample if these measurements are carried out on the background of a small total heat flow on the probe. This type of the probes is used on a limited scale because the presence of the screen increases the dimensions and amplifies the perturbation effect of the probe. In the enthalpy probe with a cooled screen a screen of three coaxially positioned tubes is placed on the normal longitudinal enthalpy probe (Fig. 1.26 b)). A heat insulator, for example air, is placed between the measuring probe and the screen. The cooling liquid is supplied into the probe in such a manner that the internal tube of the screen and the outer tube of the measuring part are cooled by a liquid of same temperature, ensuring equal temperatures of the walls of the measuring part of the screen in the absence of the heat overflow. The accuracy of the measurements is sufficiently high because the parasitic heat flow to the measuring part of the probe rapidly decreases. But due to the big dimensions of the probe they can be used efficiently only for diagnostics of flows with large transverse dimensions.

The enthalpy probes for measurements in supersonic flow are usually equipped with a screen (Fig. 1.26 c)). The nature of the gas flow in the top part of the probe in the regime with and without gas sampling can differ as a result of changes in the position of the shock wave so that the speed of gas sampling should be minimal. To ensure that the amount of gas is sufficient from the viewpoint of ensuring required sensitivity, the size of the measuring orifice must be increased what has to be taken into account in the design of the probe.

The ‘angular’ enthalpy probe was designed as a result of improvement of longitudinal one by minimizing the part of the probe introduced into the flow (Fig. 1.26 d)). The internal measuring tube in the inlet part is bent so that it is possible to place the initial part of this tube along the flow and the external under an angle to the flow, which is usually around 45˚. The intermediate tube is placed in the same position as in the longitudinal probes and is used as a guide for the cooling liquid. This probe is efficient in operation and retains the advantages of the longitudinal enthalpy sensor.

In contrast to the longitudinal probes, the measuring part of the transverse probe is normal to the flow and the relatively short initial section of the measuring tube of the probe is positioned in the direction along the flow (Fig. 126 e)). The probe consists only of two tubes: an internal for measuring, and an external used for transport of the cooling liquid.

The most suitable probes ensuring both reduced dimension and high flow rates of the cooling liquid are those with an external diameter of 2-3 mm.

The main advantages of these probes are the possibility of decreasing their transverse dimensions and their suitability for measuring the flow characteristics in closed channels.

Disadvantages of the transverse enthalpy probe include, firstly a high level of the caused perturbations of the high temperature flow by the body of the probe. Secondly, as a result of the small length of the initial section of the measuring tube, positioned along the flow, the probability of the appearance of distortions in the results of the measurements as a consequence of the distortion of the gas flow lines in front of the flow increases.

The most widely used probe seems to be the longitudinal enthalpy probe made by Grey and co-workers. They demonstrated the potential and limitations of the technique for measurement of the plasma specific enthalpy: temperatures as high as 12000 K were measured by their probe. Grey stated a number of limitations in this probe technique [117]:

1. Equilibrium must exist in the gas when the temperature is to be measured, since the probe measures only a total gas enthalpy;
2. Transients cannot be measured;
3. Spatial resolution is limited by the finite sampling tube diameter;
4. Calibration of the probe requires approximately axisymmetric flow.

The technique was used to study the laminar and turbulent arc jet mixing and heat transfer phenomena. It was believed that the probe technique was superior to other methods for high temperature measurements in multi component fields, with strong property gradients.

Even though the results of these studies showed a promising future for enthalpy probes, the technique was rarely used during the period between 1965 and 1988 but has since reemerged over the past several years, when the enthalpy probe has been rediscovered and is enjoying now wide application to a variety of thermal plasma processing problems [109,111].

Expanded application to plasmas with complicated gas mixtures and to high-velocity oxy-fuel thermal spray systems consisting of combustion products along with entrainment of the surrounding atmosphere requires that the gas composition has to be accurately known. Once composition is known the mass flow rate through the probe can be accurately determined and subsequently the enthalpy and other thermodynamic properties may be deduced [109]. Rahmane *et al*. [112] have shown that a mass spectrometer, linked to a water-cooled probe (similar to the enthalpy probe), is capable of providing the plasma composition in real time. Swank *et al.* [110] have combined the technique of mass spectrometry to the enthalpy probe system so that the plasma composition is simultaneously measured along with its temperature and velocity.

The enthalpy probe is now considered as a standard, robust tool that has been used successfully in thermal plasma diagnostics, whether for DC plasma or radio-frequency plasma jets. It represents a water-jacketed gas sampling and stagnation pressure probe from which the enthalpy, temperature and velocity of a hot flowing gas can be derived once the composition is known.

Principle of the stationary enthalpy probe

The enthalpy change can be measured calorimetrically by monitoring the temperature change that accompanies a physical or chemical change occurring at constant pressure. The change in temperature of the calorimeter is proportional to the heat which the process releases or absorbs [119].

The stationary enthalpy probe allows measuring simultaneously plasma jet enthalpy, temperature, velocity and composition (Fig. 1.27).

The calorimetric method used to measure the gas enthalpy depends heavily on a 'tare' measurement, which effectively eliminates errors in cooling water temperature measurements. In the 'tare' mode observations of the coolant temperature rises while no gas flows through the probe. Thus, measurement of the heat load on the probe from the hot surrounding is being measured. Gas is then allowed to flow and the same coolant measurements are repeated, together with measurements of the gas flow rate and the gas temperature at the probe exit. The difference between the heat loads on the probe cooling circuit in these two cases represents the energy associated with the extracted gas sample. The rate of heat removal from this gas sample is then given by the difference between the measured delta of cooling water inlet and outlet temperatures:

$$\dot{m}_g \left(h_{in} - h_{out}\right) = \dot{m}_w C_{p_w} \left[\Delta T_{sample} - \Delta T_{tare}\right], \tag{1.9}$$

where m_g – gas sample mass flow rate, m_w – cooling water mass flow rate, h_{in} – unknown gas enthalpy at the probe entrance, h_{out} – gas enthalpy at the probe exit thermocouple, C_{pw} – cooling water specific heat, ΔT – cooling water temperature rise. The unknown gas enthalpy h_{in} at the probe tip is now uniquely determined, provided that the gas sampling flow rate and the gas enthalpy at the probe exit are known. The exit gas enthalpy is determined from the measured gas temperature at the probe exit and the gas sample flow rate is measured via a sonic orifice. The enthalpy of the gas at the exit nozzle usually is very low and can be neglected. Thus, the specific enthalpy of the gas at the sample point can be calculated using the following equation:

$$h = \frac{\left(Q_w \rho_w C_{p_w} \Delta T\right)_{sample} - \left(Q_w \rho_w C_{p_w} \Delta T\right)_{tare}}{Q_g \rho_g}, \tag{1.10}$$

where Q_w – cooling water flow rate, Q_g – sampling gas flow rate, ρ_w and ρ_g – density of water and gas respectively at STP[2]. The gas density at STP can be calculated as:

$$\rho_g = \sum_{i=1}^{n} x_i \rho_i \,, \tag{1.11}$$

[2] STP – standard temperature and pressure

where n – number of the gases in the gas mixture, x_i – mass fraction of gas i, ρ_i – density of the gas i. These equations require a prior knowledge of the composition of the sampled gas for the proper calculation of the sampled gas mass flow rate, its specific enthalpy and density. Knowledge of the composition is also needed for the calculation of the corresponding gas temperature from the measured specific enthalpy values, using standard tabulated data of the thermodynamic properties. The composition of the sampled gas can be measured using an on-line mass spectrometer, which is inserted into the gas sample line of the probe. Under these conditions, the corresponding specific enthalpy table, as a function of temperature and composition, could be compiled, using the following mixing rule:

$$h_{mix}(T) = \sum_{i=1}^{n} x_i h_i(T) \,, \tag{1.12}$$

where h_i – specific enthalpy of gas i at the absolute temperature T. The enthalpy of a substance increases as its temperature is raised. The relation between the increase in enthalpy and the increase in temperature depends on the conditions and substance itself (Fig. 1.3). The corresponding gas temperature can then be calculated for the measured gas composition and its specific enthalpy.

Although the primary objective of the enthalpy probe is the measurement of the enthalpy it can be used for the determination of the local gas velocity at the sampling point. If the velocity of the flowing gas has to be measured at the local position, a Pitot tube should be used. The Pitot tube represents an L-formed tube, which orifice is located against the direction of the flow. A pressure gauge connected to the Pitot tube measures the total pressure p_t of the flowing gas. The static pressure p_s of the gas has to be measured as well. The Bernoulli equation for the present case is

$$p_s + p_d = const = p_t \,, \tag{1.13}$$

where p_d is dynamic pressure. In the case of the incompressible flow the dynamic pressure is equal to the kinetic pressure, expressed as $\frac{V^2}{2}\rho$, where V is the flow velocity and ρ represents the gas density. So the total pressure is equal to the sum of the static pressure and kinetic pressure [120].

From the dynamic pressure, which is given by the difference of the total p_t and static p_s pressures, the velocity can be calculated:

$$V = \sqrt{\frac{2p_d}{\rho}} \,. \tag{1.14}$$

As it is shown in Figure 1.27 the enthalpy probe represents the L-formed tube. At low Mach numbers, the flow may be considered to be incompressible and the velocity can

be determined from equation 1.14. The total or stagnation pressure is measured in the 'tare' mode, while the chamber pressure can be determined in the 'sample' mode. Assuming that the static pressure is constant and uniform across the chamber, the dynamic pressure can be defined as:

$$p_d = p_s - p_c, \tag{1.15}$$

where p_s – stagnation pressure, p_c- chamber pressure.

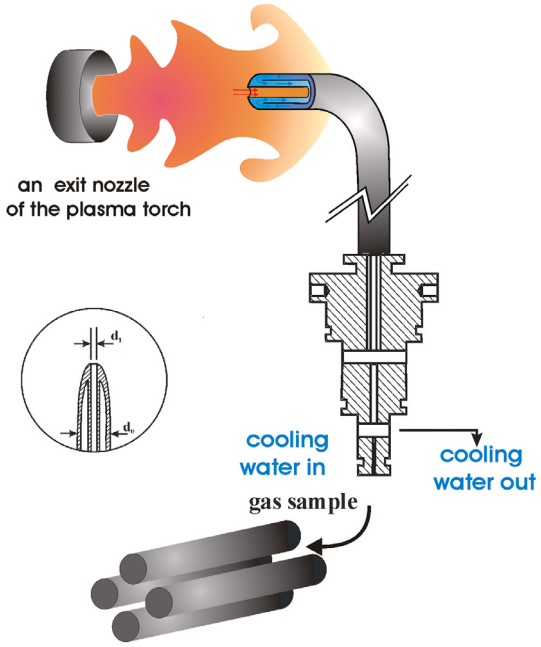

Figure 1.27 Stationary enthalpy probe with mass spectrometer in the jet.

2. Objectives of the present research

As it follows from the survey above, the study of the fundamental phenomena of the plasma jet behavior is a key for process control for industrial applications. Thermodynamic and transport properties of the plasma play governing roles in momentum and heat transfer to the material to be treated. The process of the plasma jet interaction with cold ambient atmosphere determines the plasma jet behavior. It results in the strong entrainment of the ambient gas into the plasma jet leading not only to a reduction of plasma jet temperature and velocity but also causing a plasma jet spreading and a change of the plasma gas composition as well. The entrainment process is still not fully understood. The general idea of this work is a more detailed study of the entrainment process itself as well as an examination of methods how to affect it.

The plasma jets have been generated with the help of two different types of DC arc plasma torches – a torch with gas and a torch with hybrid gas-water stabilization of the arcs. The choice of the plasma sources allows generation of plasma jets in a wide range of parameters and thus makes it possible to analyze the entrainment process with respect to plasma generation conditions.

The properties of the plasma jet have been measured through whole the jet starting from the regions very close to the nozzle exit of the torch to the regions far from the plasma generator. Measurements in the upstream part of the plasma jets have been done by means of emission spectroscopy. The enthalpy probe diagnostic method has been applied to obtain plasma jet characteristics at the downstream parts of the torch, where material processing usually takes place. One of the main aims of the work was to develop a method of applying the enthalpy probe diagnostic in plasma containing water steam. The problem of the diagnostic is condensation of water in the diagnostic system, which distorts measurements of the plasma jet composition. The thesis discusses how to determine the real plasma gas composition and evaluate true plasma jet characteristics.

The work is aimed to link plasma generation conditions to the plasma jet behavior and its interaction with the surrounding atmosphere. Both parameters of the plasma torches and conditions in the surrounding have been changed. The thesis discusses:

- Development of the plasma characteristics along the jet;
- Influence of the arc current;
- Influence of the plasma gas composition;
- Generation of the plasma jet under low pressure conditions;
- Application shroud systems with different shroud gases;
- Effect of the carrier gas injection.

3 Experimental arrangement, diagnostic tools and their analysis

During the course of this work two different torches were applied – the hybrid torch with water-argon stabilization of the arc and the torch with gas stabilization. The plasma torch with gas stabilization was a part of a VPS system and all experiments took place inside the plasma reactor. Most of the experiments with hybrid gas-liquid stabilized torch were made on open atmosphere, but the torch was also operated within a vacuum chamber to study pressure effects on the properties of the generated plasma. The main diagnostic tool, used in present experiments, was an enthalpy probe. Schlieren installation was applied for visualization of the plasma flow.

The plasma torch designs, the low pressure chambers, the enthalpy probe system connected to the mass spectrometer and the Schlieren imaging installation are described in detail in this chapter. The suitability of the enthalpy probe technique for the performed experiments is discussed.

3.1 Design of the plasma systems

3.1.1 Plasma torch with gas stabilization of arc and plasma reactor

The applied plasma torch for plasma spraying was designed by DLR-Stuttgart based on a F4 plasma gun from Sulzer Metco (Plasmatechnik), Switzerland. The schematic drawing and the photo of the torch are shown in Figure 3.1. It represents a quick exchangeable plasma gun with gas stabilization of the arc. The arc is formed between a thoriated tungsten cathode and a copper anode. A standard F4 nozzle with a cylindrical inner contour with 6 mm diameter was applied in the experiments. Both, the cathode and the anode have an internal cooling by pressurized water. These components are replaceable and all seals incorporated in the design must be completely water tight since a leak within the cooling circuit will lead to rapid erosion of anode and cathode. Plasma gas is injected through an injector with holes tilted in tangential direction creating a gas swirl around the cathode. This leads to an increase of the arc voltage due to increased arc cooling and arc elongation, and thus, to an increase of the arc power. The plasma torch can work with arc currents from 200 to about 1000 A for argon as plasma forming gas and to 800 A for a mixture of argon with helium and/or hydrogen. The torch efficiency, which is defined as the fraction of power contributed to the gas, is calculated by considering the heat loss to cathode and anode. Depending on arc current and plasma gas it varies from 35% to 50%. The arc is always started with an arc current of 150 A and with a gas flow rate of 50 slm of argon supplied as plasma forming gas.

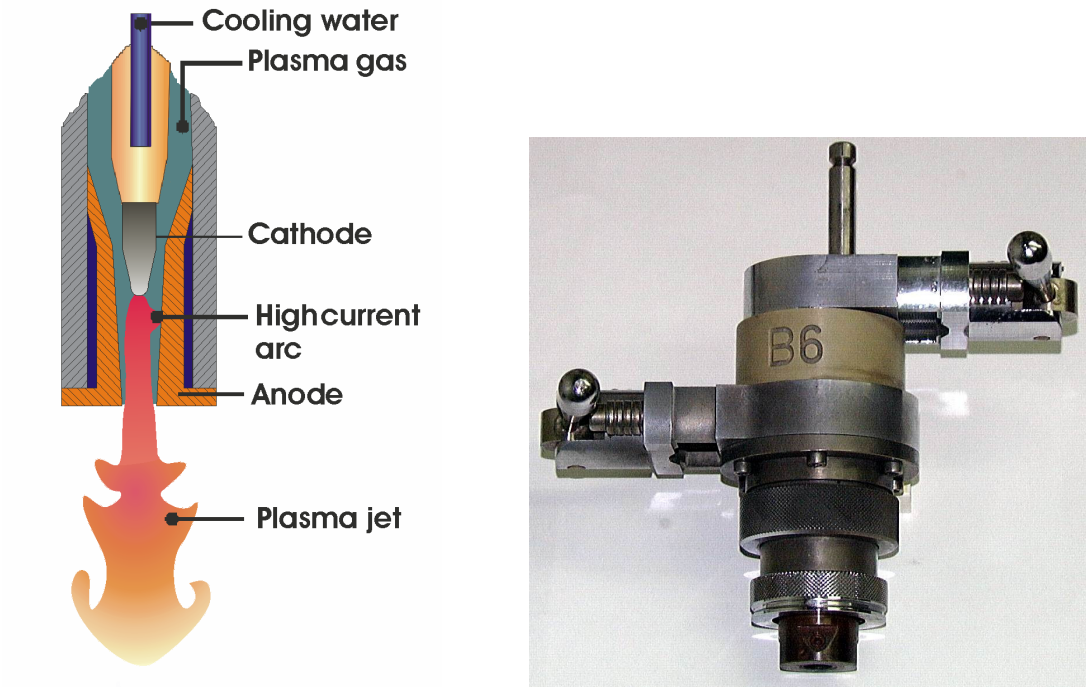

Figure 3.1 The schematic diagram of the plasma torch with gas stabilization of arc and photo of the quick connectable plasma torch.

It has to be emphasized that the arc behavior strongly depends on the operating parameters, mainly on arc current, plasma gas nature, mass flow rate, nozzle diameter and design. In the experiments described here argon was used as a primary plasma forming gas. Argon is the easiest of commonly used gases to form a plasma and tends to be less aggressive towards electrodes. Furthermore, hydrogen and/or helium were added as secondary gases to form more powerful plasma gas mixtures. At a given temperature hydrogen possesses a higher energy content compared to argon because of the dissociation energy of its molecules. Helium imparts good heat transfer properties and provides better sensitivity to control the plasma energy.

Volt-ampere characteristics of the torch for pure argon plasma gas and for mixtures of argon with hydrogen and helium are shown in Figure 3.2. An increase of the arc current leads to an increase of the mean electric arc diameter, unless the anode nozzle prevents the arc column from expanding. The V-A characteristics of the plasma gas are rising with increasing current when pure argon is applied as well as when helium is used as a secondary gas. In these cases the walls inside the torch prevent a widening of the arc and the increase of the arc current is accompanied by an increase of the power

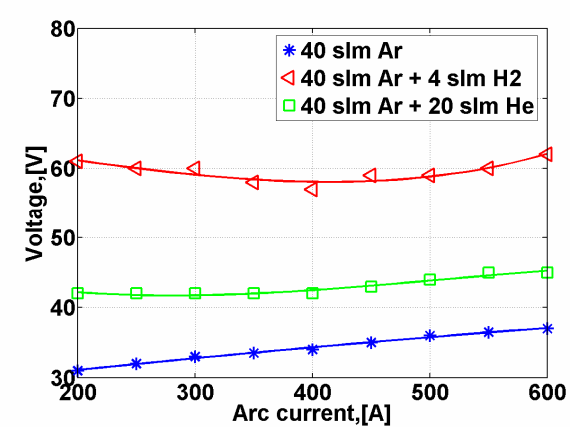

Figure 3.2 Volt-ampere characteristics of the quick connectable plasma torch for different gas mixtures.

losses. The characteristic changes its curve progression if hydrogen is used as secondary gas. Between 200 and 400 A the characteristics first drop with increasing current while for arc currents more than 400 A it is arising. This can be explained by the important role which hydrogen plays with the increase of the mean integrated thermal conductivity in the plasma column. The high thermal conductivity of hydrogen at temperatures higher than 4000 K results in a severe constriction of the arc column reducing the conductive thermal losses. Furthermore, for geometrical reasons the arc is able to expand at lower current values with increasing arc current. In contrast, the conductive thermal losses to the walls start playing an important role for arc currents higher than 400 A.

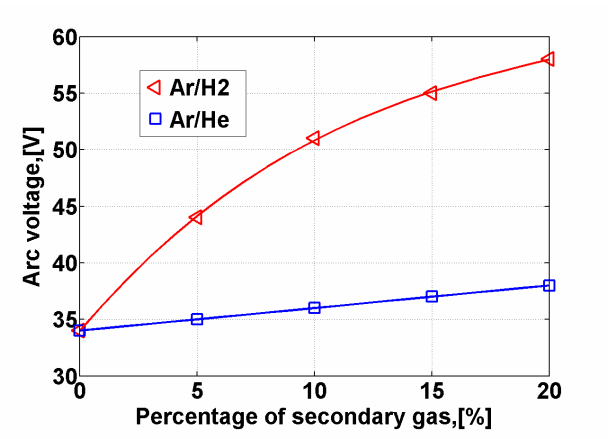

Figure 3.3 Effect of percentage of the secondary gas added to the argon plasma forming gas (I = 400 A, total gas flow rate - 50 slm).

Rising of the plasma enthalpy and thermal conductivity also explains the drastic increase of the arc voltage by addition of hydrogen – about 10 V for only 5% of hydrogen added to the mixture (Figure 3.3). The constriction of the arc column results in an increase of the electric field strength, and thus, of the arc voltage. Moreover, hydrogen as secondary gas provokes the restrike mode of the arc root oscillations while for pure argon the arc is running in "take over mode" with lower level of voltage fluctuations.

Adding of helium has a quite different influence. Not only the thermal conductivity of the mixture is increased compared to that of pure argon, especially for temperatures higher than 9000 K, but moreover, the viscosity of the Ar-He mixture is higher than that of pure argon, limiting the turbulences in the jet fringes and thus the convective cooling. Such conditions induce a low voltage increase with cumulative helium percentage. A small difference to pure argon plasma is also due to the fact that in the presence of many helium atoms inefficient collisions for ionization are more numerous, which has to be compensated by a higher field strength when the helium content increases. Consequently, higher electric power levels can be achieved with Ar-H_2 plasma mixtures than with Ar-He ones, and thus, higher specific enthalpies.

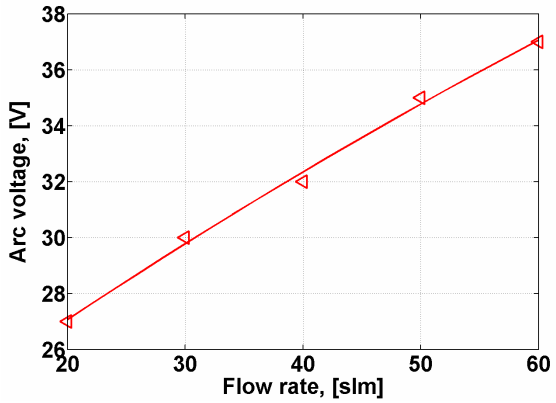

Figure 3.4 Effect of plasma gas flow rate on arc voltage (I = 400 A, argon plasma gas).

The effect of the plasma gas flow rate is shown in Figure 3.4. An increase of the arc voltage with plasma gas flow rate results from two effects – the requirement of more

energy for heating the higher amount of gas as well as a constriction of the cathodic part of the plasma giving an extension of the arc as it was explained in the section 1.3.2.

The plasma torch is positioned vertically inside the plasma reactor and can be moved up and down (Figure 3.5). The used reactor has double walls, which are water-cooled. The reactor not only functions as a vacuum chamber but also provides protection against noise and NO_x gases. The reactor is connected to a heat exchanger for hot gases coming from the reactor and a particle filter to protect the pumping unit. It consists of two pumps with filters. An oil pump is applied as a fore pump to provide rarefaction of the gas at the exit of the Roots pump. The Roots pump is brought in operation as soon as a pressure of less than 10 kPa is reached in the chamber. The pressure in the reactor can be varied between 1 to 100 kPa.

A DC power supply provides constant current operation of the torch. A universal control system (MF-VPS-F6, GTVmbH, Luckenbach, Germany) is applied to control the plasma spraying conditions, i.e. plasma current, gases and their flow rates as well as the flow rate of the carrier gases. The heart of the control system is a microprocessor, which monitors the process and adjusts the regarded values. The system was mostly driven in the mode of constant current maintenance. A gas controlling cabinet of GTV is used to vary the plasma gas flow and to mix different gases. It contains mass flow controllers suitable to keep gas mass flows constant independently of environmental influences such as pressure and temperature.

An enthalpy probe tip is introduced into the reactor through a special aperture, which allows horizontal moving of the probe providing radial scanning of the plasma jet. Both vertical movement of the plasma torch and horizontal movement of the enthalpy

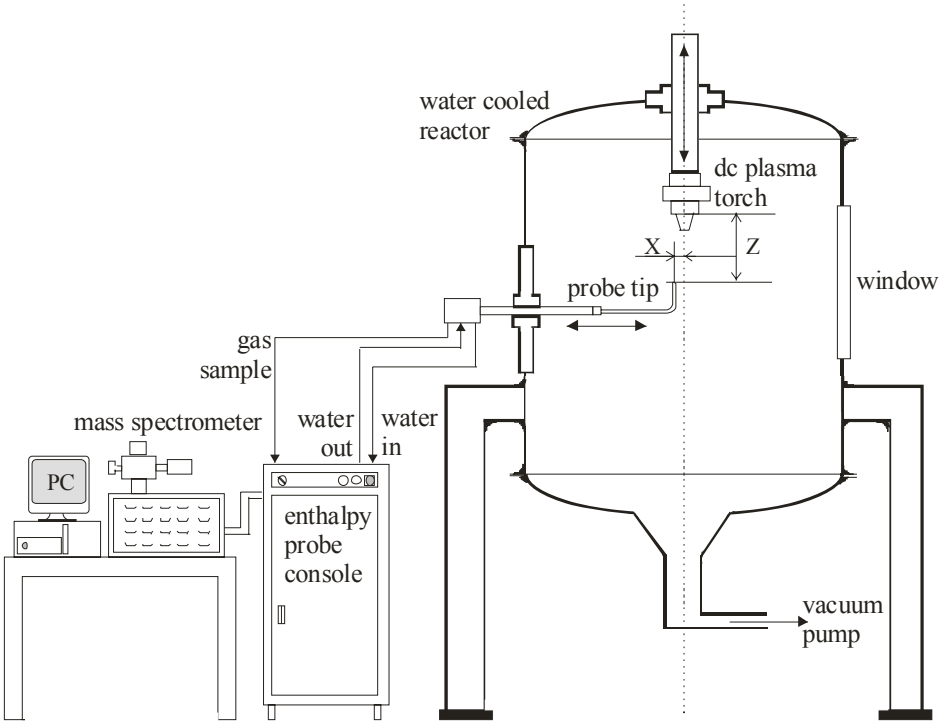

Figure 3.5 Plasma reactor with enthalpy probe system and mass spectrometer.

probe are controlled with the help of a SM Electronic positioner (SM 300), allowing 0.1 mm steps.

3.1.2 Torch with hybrid gas-liquid arc stabilization and low pressure chamber

Description of the main constructive features of the plasma torch with hybrid gas-liquid stabilization of the arc was given in section 1.3.4. The photograph of the torch is shown in Figure 3.6. The schematic diagram of the experimental setup with the plasma torch is shown in Figure 3.7. Argon was supplied along the cathode tip made of thoriated tungsten. A vortex component of the argon flow, which was injected tangentially, assured a proper stabilization of the arc in the cathode nozzle. From the cathode region the argon plasma flows to the water vortex stabilized part, where it passed through the water channel with an inner diameter of 7 mm. The length of the argon stabilized arc column was about 6 mm, while the length of the arc column stabilized by water vortex was 50 mm. The diameter of the cylindrical exit nozzle was 5.7 mm. The anode of the torch was represented by a rotating cooper disc 180 mm in diameter and 15 mm thick. It was located outside of the arc chamber about 4 mm downstream the exit nozzle and was rotated with the frequency of 50 Hz. The length of arc column part outside the chamber between exit nozzle and the anode varied between 4 and 20 mm as the anode attachment moved along the anode surface. Both the anode and the cathode had internal water cooling.

Both the electrode cooling and water stabilization were provided by the water system. The water circuit was divided into two main lines. The first line served for the cathode and anode cooling. The second line was utilized for supplying and regulation of water flow into the stabilizing channels of the plasma torch. Pressurized water was supplied into the torch chamber, where the water vortex was created. Surplus water was exhausted from the stabilizing torch chamber with the help of the underpressure being

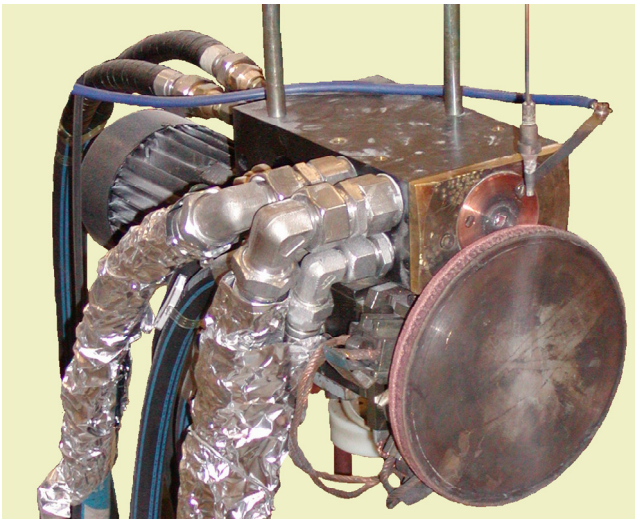

Figure 3.6 Plasma torch with hybrid gas-water stabilization of arc.

made in the main water tank. The water flow rates through the system had to be exactly adjusted and kept constant to ensure stable operation of the torch. The flow rates and temperatures of water were measured both at the inputs and at the outputs of arc chamber and electrodes.

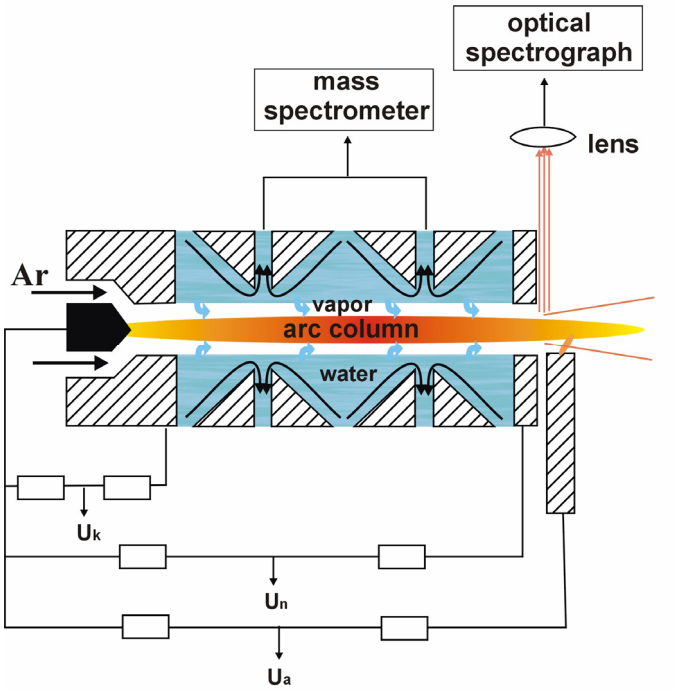

Figure 3.7 Hybrid gas-water plasma torch with arc diagnostics.

The plasma torch was operated with the help of special control software, which allowed monitoring of the ignition process, controlling the cooling and stabilizing water flow rates and varying of the arc current. The flow rate of the secondary argon gas was controlled with the help of a gas system of Brooks instrument (Brooks Instrument, Hatfield, USA) based on a system of mass flow controllers.

The ignition of the arc is a quite difficult process. High voltage impulse (~ 12 kV) is applied to the cathode nozzle to initialize the arc between the cathode and the cathode nozzle. The argon flow blows ionized gas toward the exit nozzle causing the arc column to be formed between the cathode at an applied voltage of 600 V and the grounded anode. The whole process of the arc column development took usually about 3 ms.

Potentials of the electrodes, the cathode nozzle and the exit nozzle were measured by the high resistance voltage dividers. If the resistance of voltage divider was much higher than the resistance of the sheath between the arc column and the nozzle wall, the potential of the nozzle was equal to the potential of the arc column. The total arc voltage included also the potential drop of the section of the arc in the free jet region downstream of the exit nozzle. Volt-ampere characteristics of the whole arc and of the stabilized section of the arc inside the arc chamber are presented in Figure 3.8.

The voltage drop on the cathode gas stabilized part of the arc column, determined from measurements of the potential of the cathode nozzle, was in the range of 7 to 15 V,

thus the power dissipated in this part of arc column was 2.1 to 4.5 kW, what is substantially lower than the total arc power. High values of arc voltage and arc power are typical for water-stabilized arcs [121]. The influence of the argon flow rate on arc voltage is shown in Figure 3.9. The argon flow rate was varied between 12.5 and 24 slm. Small changes of arc voltage existed when argon flow rate increased.

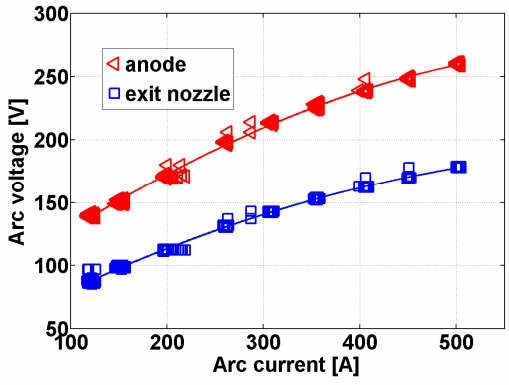

Figure 3.8 Volt-ampere characteristics of the hybrid argon-water plasma torch (argon flow rate – 17.5 slm).

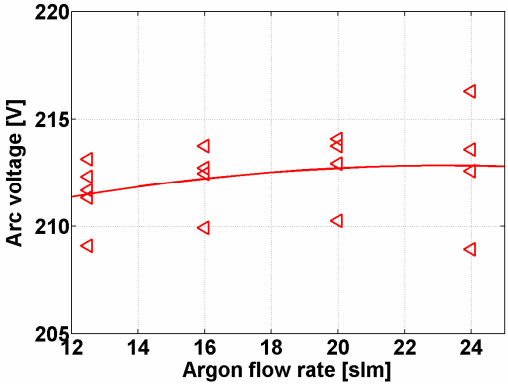

Figure 3.9 Dependence of arc voltage on argon flow rate (arc current = 300 A).

From calorimetric measurements on cooling loops of the electrodes and of the water stabilizing system the power losses were determined. It has to be noted that in the case of water stabilized arcs power losses included not only losses to the electrodes, but to the stabilizing water vortex as well. The power loss of the arc column downstream the nozzle in the free jet region could not be measured. The efficiency of the torch was defined as a ratio of the total enthalpy flux to the power input and it varied between 40 and 60 % depending on arc current and argon flow rate. The efficiency increased with increasing both the arc current and the argon flow rate.

For evaluation of the plasma arc characteristics a mass flow rate of plasma had to be known. In case of the hybrid plasma torch the mass flow rate is given by the sum of argon flow rate and evaporation rate of water. A direct measurement of the water evaporation rate was impossible. An amount of water vapor in the gas mixture had to be derived from the measurements of the arc properties close to the exit nozzle by means of the emission spectroscopy and from analyzing the composition and flow rate of the exhausted gases. As argon plasma mixed with heated and ionized steam a part of this mixture was exhausted together with stabilized water from the plasma torch chamber. A rotameter together with a mass spectrometer were introduced at the exit of the exhaust to analyze exhausted gases.

Temperature and composition of the plasma jet close to the exit nozzle were measured by means of emission spectroscopy using the monochromator Jobin Yvon HR-320 (Horiba Jobin Yvon Inc., NJ, USA) equipped with a linear photodiode array detector [122]. The electron number density was obtained from Stark broadened H_β line independently of the assumption of LTE. The temperature was calculated from the ratio of various argon atomic and ionic lines assuming Saha equilibrium. In colder parts, where

there were no ionic lines detected, the temperature was estimated from approximate LTE composition and measured electron number density. The plasma composition was determined from ratios of emission coefficients of argon, oxygen and hydrogen atomic lines using LTE equations.

Table 3.1 The water evaporation rate and plasma composition

Arc current, A	Argon flow rate, slm	Argon-steam ratio	Evaporation rate, g/s
300	17.5	45% - 55%	0.27
150	17.5	55% - 45%	0.184
150	22.5	75% - 25%	0.09
150	26	80% - 20%	0.086

As far as the total flow rate of Ar supplied to the torch chamber was known, the Ar flow rate at the exhaust could be calculated knowing exhausted gases composition and flow rate. The amount of argon remaining in the chamber mixed with water steam and the composition of the mixture was measured at the exit nozzle. Assuming homogeneous mixture inside the torch chamber the water vapor flow rate at the exit nozzle as well as at the exhaust could be calculated and the evaporation rate of the water then was derived. The results of the calculations are shown in Table 3.1.

The calculations showed that the evaporation rate of water depends not only on the arc current but on argon flow rate as well. Increasing of the arc current resulted in an increasing of the water evaporation rate, while increasing of the argon flow rate had opposite effects. Increasing of the arc current led to the increasing of the arc temperature as it will be shown later and, thus, radiation intensity, what in turn led to an increase of the water evaporation rate. In the contrary, argon impeded water to be vaporized and its higher flow rates caused decreasing of the evaporation rate of water inside the arc chamber. As a result, the composition at the exit nozzle of the torch strongly depended on arc current and argon flow rate.

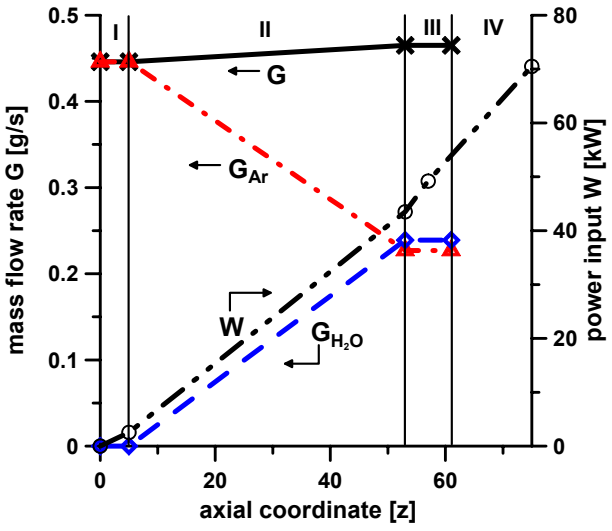

Figure 3.10 Distribution of mass flow rate and power input inside arc chamber (I = 300 A, Ar = 15 slm).

The composition and flow rate of the plasma gas changed along the arc chamber. Mass balance inside the arc chamber together with distribution of the power input is shown in

Figure Figure 3.10. While argon, which was supplied in the upstream part of the arc chamber (I), was continuously exhausted (G_{Ar}) together with stabilizing water, the amount of water steam carried on increasing as water evaporated along the stabilizing part (II) despite being exhausted together with argon (G_{H_2O}). Thus, the total mass flow rate (G) along the arc chamber remained almost constant.

The hybrid plasma torch was attached horizontally to a double-walled water-cooled reaction chamber (Figure 3.11), which was evacuated by a rotary vacuum pump to enable variation of the plasma jet surrounded pressure. The pressure in the reactor was varied from atmospheric down to 4 kPa and was controlled by the throttle valve. The pressure was monitored with the help of a manometer. The atmosphere inside the reactor was a mixture of the plasma forming gas with air. The enthalpy probe was positioned inside the plasma reactor at the fixed distance z = 100 mm from the plasma torch nozzle exit. A special moving system allowed horizontal and vertical scanning of the plasma jet (*x* and *y* axis in Figure 3.11) with the step of 1 mm.

The enthalpy probe system requires that no water vapor is entering. Water vapor might damage some system components, so elimination of water in a gas sample line is a question of great importance. Moreover, water vapor condensates on the surface of tubes and components (like filters) in the gas sample line hampering proper measurement of the stagnation pressure and making difficulties for gas sucking. A freezer was inserted into the gas sample line to avoid water vapor entrance into the system. The temperature in the freezer was maintained at the constant value of -5 °C. Water vapor been sucked into the freezer condensed and was frozen there.

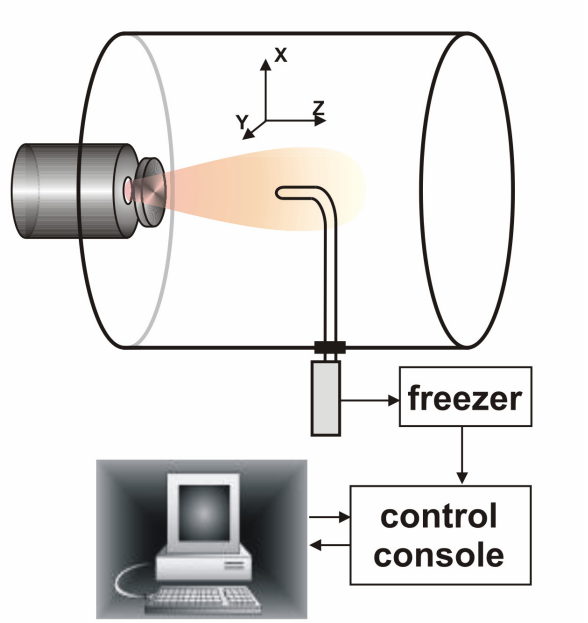

Figure 3.11 Low pressure chamber.

3.2 Enthalpy probe diagnostic system

3.2.1 Description of the enthalpy probe system

The enthalpy probe system used in the experiments was supplied by Tekna Plasma Systems Inc. Sherbrooke, Quebec, Canada. (Fig. 3.12) The probe itself is principally the same as the longitudinal Grey's probe. The measurements applied the stationary method.

Tekna's enthalpy probes are made of thin walled 316 stainless steel tubing. They consist of a probe stem and a standard insert with O-ring seals, which fits into the bulkhead. The bulkhead is designed to receive Tekna's enthalpy probes providing connection for the cooling water circuit and the gas sampling line. The bulkhead incorporates two RTDs and one thermocouple for the measurement of the cooling water temperature in and out and the sampled gas temperature. The cooling water temperature is measured with a resolution of 0.1 °C and a precision of 0.3 °C. The gas temperature coming out the probe tip is measured with a thermocouple. The plasma temperature calculation neglects this energy contribution.

Figure 3.12 The enthalpy probe system of Tekna Plasma Systems Inc.

The gas sampling system consists of a high capacity vacuum pump which draws a sample of gas through the inner tube of the probe tip. The gas sampling rate is controlled by a mass flow controller, which allows adjusting and measuring the flow rates up to 5 slm. This instrument does not measure a volume flow rate but rather a mass flow rate. These flow rates are controlled with a pump in order to maintain a partial vacuum in the sampling line. It has to be noted that the mass flow rate controller has been calibrated by the manufacturer for nitrogen, that is why a Gas Correction Factor (GCF), depending on the density of the gas considered, its specific heat, and its molecular structure, has been introduced to convert its output Q_{out} to a volume flow rate:

$$Q_g = Q_{out} \times GCF_{mix}, \tag{3.1}$$

$$GCF_{mix} = \frac{1.2996 \cdot S_{mix}}{\rho_{mix} \cdot C_{p\,mix}}, \tag{3.2}$$

where S_{mix} is the molecular structure correction factor of the mixture, $C_{p\ mix}$ means the specific heat of the gas mixture and ρ_{mix} is the density of the mixture. All these properties depend on the properties of the individual components of the mixture and are calculated, using the following rule:

$$P_{mix} = \sum_{i=1}^{n} x_i P_i, \tag{3.3}$$

where P is a corresponding characteristic (density, molecular structure factor or specific heat), x_i - mass fraction of the gas component, n – number of gas components present in the mixture.

A differential pressure gauge is provided for direct measurement of the dynamic pressure under no flow tare conditions. The unit is supplied with a gauge with a full range of 2.49 kPa.

An absolute pressure gauge (0-135 kPa) with a precision of +/- 3% is used as an indicator of the pressure in the chamber (sample mode) and the stagnation pressure at the probe tip under no flow conditions (tare mode).

The cooling water circuit during measurements operates under close loop conditions when the pressure intensifier brings the pressure in the circuit to 1000 psig in order to bring the boiling point of water to 275° C. A device for water treatment is used to demineralise the water during the filling of the tank and to filter it. A variable speed pump allows ensuring a water circulation until a maximum flow rate of 1 slm.

It can be observed that the inlet diameter of the probe has a strong influence on the measurements. Flow perturbation in the measurement zone can also be minimized by proper choice of the size of the probe tip used. For example, a small inlet diameter should less affect the plasma jet flow, resulting in a high spatial sensitivity. However, for low pressure conditions, a larger inlet diameter is required in order to increase the amount of the sampled gas. As a result, Tekna Plasma Systems Inc. proposes three probe dimensions with an inlet diameter of 2.67 mm (ENT 635), 1.27 mm (ENT 476) and 0.66 mm (ENT 317).

In the present experiments the enthalpy probe ENT 476 was chosen as it allowed much higher gas sampling rate at the expense of a perturbation of the flow caused by its larger diameter.

3.2.2 Mass spectrometer unit

The mass spectrometer is used to determine the composition of the sampled gas. The gas composition is then used to evaluate, when operating under plasma of more then one gas, the proper enthalpy tables and the Gas Correction Factor for the mass flow meter.

The enthalpy tables can vary considerably when different gases are mixed together. Similarly, the reading of the mass flow meter will be affected by the gas composition.

A mass spectrometer always contains the following elements: a devise to introduce the substance to be analyzed, an ionizer, one or several analyzers to separate the various produced ions, a detector to 'count' the ions, and finally a data processing system that produces the mass spectrum in a suitable form [123]. Its basic design is illustrated in Figure 3.13.

The first step in mass spectrometric analysis is the production of gas-phase ions by the electron impact. The ions are produced in the ionizer. The number of ions formed grows rapidly with increasing energy, reaching a maximum at 50-150 eV and then, as the energy continues to increase, slowly decreases again. Apart from the ions with single charge at higher energies ions with multiple charges also occur. Since the ion yield and thus the sensitivity should be as high as possible, electron energies of the order of 100 eV are employed [124]. Ions provide information concerning the nature and the structure of their precursor molecule.

The separation of the different kinds of ions with respect to space or according to their mass/charge ratio is effected by magnetic and/or electric fields. The high-frequency quadrupole mass spectrometer is used almost universally. Quadrupoles are dynamic mass analyzers, which are very simple in their geometry and very complex in behaviour [125]. In a high-frequency quadrupole electric field, which in the ideal case is generated by four hyperbolic rod electrodes a distance of $2r_o$ apart at the tips, it is possible to separate ions according to their mass/charge ratio (m/e). The voltage between these electrodes is composed of a high-frequency alternating component $V\cos\omega t$ and a superposed direct voltage U. If ions in the direction of the axis of the field are injected into the separating system, the influence of the high-frequency electric field causes them to oscillate at right-angles to the axis of the field. Some ions would pass through the mass analyzer, while others would strike the rods, be neutralized and pumped away as gas. The ion beam passes through the mass analyzer and is then detected electrically and transformed into a usable

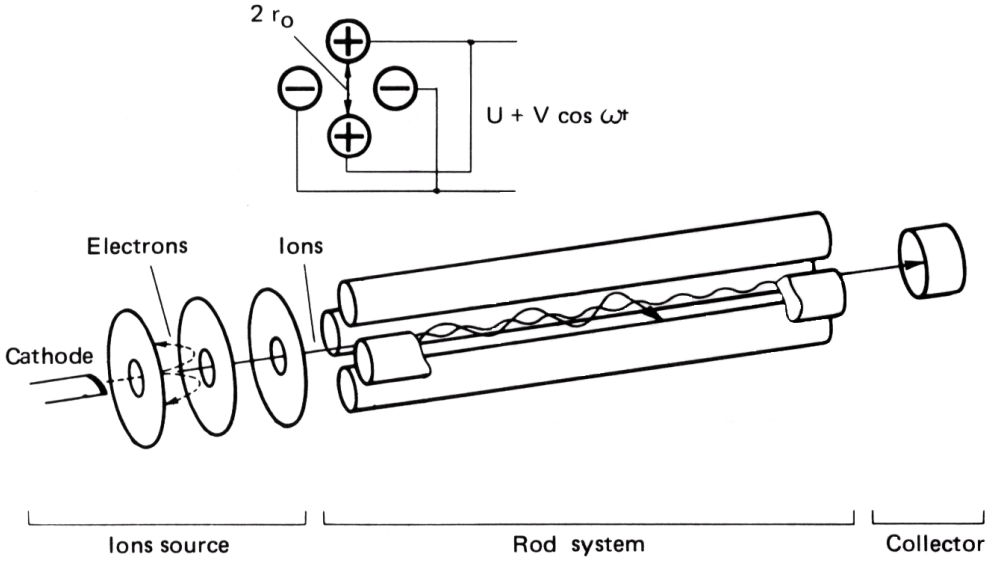

Figure 3.13 Quadrupole mass spectrometer [123].

signal by a detector. The mass scan can be affected by varying the voltage and a linear mass scale is obtained.

The *Quadrupole analyzer QMS 200* (Pfeiffer, Wiesbaden, Germany) was used in the present experiments. It consists of an ion source, a quadrupole mass filter and a Faraday detector. The molecules are ionized by the filament, filtered by the quadrupole mass filter and then sensed by the Faraday detector. All this operations takes place at high vacuum, in the present application at a pressure 4E - 6 mbar. The *ion source* of the analyzer incorporates two thoriated tungsten filaments which generate the ions. The second filament can be used in the circumstance that the primary one becomes defective. Ions generated by the ion source are transmitted to the quadrupole mass filter, where they are separated with respect to their m/e ratio. The Faraday detector serves as a collector for the ions reaching the detector. It consists of an electrode placed on-axis at the end of the mass filter. Ions reach the inside of the detector where they give up their charge, causing a current flow. A sensitive electrometer amplifier is connected to the Faraday collector, enabling the signal current to be amplified and measured. The sensitivity of this detector is limited by the noise of the amplifier. Nevertheless, this detector is very precise because it is independent of the mass and energy of the detected ions.

Table 3.2 Sensitivity for QMS 200

gas	mass number of base peak	sensitivity for base peak, $\times 10^{-5}$ [a/mbar]
He	4	6.4
Ar	40	24
H_2	2	13
N_2	28	20
O_2	32	14

The three main characteristics of an analyzer are the upper mass limit, the sensitivity (or the transmission) and the resolution. The mass limit determines the highest value of the m/e ratio that can be measured. The QMS 200 covers the range from 1 to 200. In the investigations carried out the range up to 50 was sufficient as all fragment ions of the gas components to be analyzed were found in this range.

The sensitivity is the ratio between the number of ions reaching the detector and of the ions produced in the source. The sensitivity differs for different types of the ions. The sensitivity for the base peak of the gases appeared in the examined plasma jets are shown on the Table 3.2.

The resolving power is the ability to yield distinct signals for two ions with a small mass difference. Two peaks are considered to be resolved if the value between the two peaks is equal to 50% of the weaker peak intensity when using quadrupoles. A resolution is a variable. In the Figure 3.14 a detail of the spectra, when different resolutions were set,

are shown. The spectrum shows the ion current of double-charged oxygen (16) and nitrogen (14) and the main peak of water vapor (18). In the present experiments resolution was adjusted to the value of 50. This resolution provides good ion current intensity and is high enough to distinguish neighbor peaks.

Normally a mass spectrometer is operated in such a manner that a definite part of the measuring range is scanned periodically at suitable speed, the data thereby acquired being collected. Therefore, operation in this manner is not desired and there is a way one obtains information, which, though limited with respect to mass range, is faster or more accurate. The largest amount of specific information is acquired when the peaks of interest only are periodically scanned. In this way a maximum of true measuring time and statistical accuracy are obtained. Primarily, mass spectra provide nothing but intensities associated with defined mass numbers. With the QMS software equipped with Quantitative Analysis Module – Multiple Concentration Detection (MCD) it is possible to adapt all parameter individually for each peak and provide concentration measurements of the individual components. The measured ion currents are transferred to a solution matrix and the individual concentrations of the components in the gas are determined via calibration factors in the MCD. The incoming measurements could be stored and further processed.

The mass spectrometer is linked to the pump of the enthalpy probe system through the sampling line. The gas sample is analyzed at a controlled pressure of 4.10^{-6} *Pa*. The control valve is used with a control unit for controlling gas streams and thus for maintaining the desired pressure.

Mass spectrometer calibration.

Mass spectra only provide intensities of definite mass numbers. The derivation of partial pressures and concentrations from such data requires calibration. Many of the cases occurring in our applications, however, are so simple that the kind of gas can be identified directly on the basis of discrete characteristic masses without having to allow for mutual interferences. These are (characteristic masses in parenthesis): H_2 (2), He (4), N_2 (28), O_2 (32), Ar (40). The interpretation of mass spectra is essentially the solution of systems of linear equations, which can be performed by a computer, provided the individual fragment spectra and calibration factors are known. Reliable calculation of concentrations necessitates prior knowledge what kinds of gas are involved. The measurement accuracy depends mainly on the calibration, the user has to know not only the components really

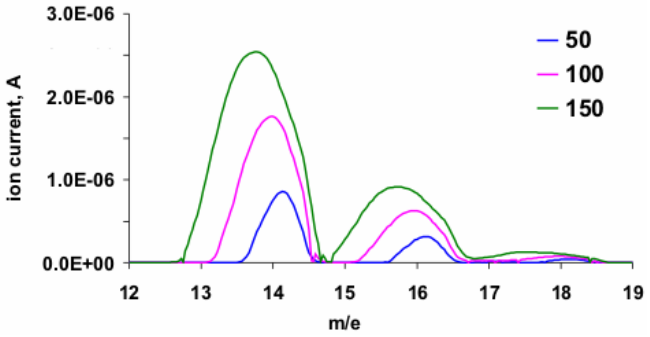

Figure 3.14 Detail of the spectra for different MS resolutions.

present in the plasma but their approximate concentration (%vol.) as well. No computer program can allow for unforeseen admixtures. The manufacturer recommends operating within a range of 20 % of the real gas composition to maintain an accuracy of 1 %.

The calibration procedure consists in determining calibration factors, used to calculate the concentrations from the knowledge of current intensities (Concentration = Intensity / Calibration factor). The mass spectrometer can be calibrated with the help of a calibration mixture. There are different methods how to get the calibration mixture. One of the most attractive methods is obtaining the calibration mixture by mixing various gases on-line and controlling their flow rates with high precision mass flow controllers calibrated for the respective gases. This calibration method is very versatile since the calibration mix can be modified easily and rapidly. The precision of this technique depends on the precision of the mass flow controller and their own calibration which usually range between 1 - 2% of full scale.

For the present measurements the mass spectrometer was calibrated by this method. First the gas mixture was let flow for some time until the gases were well mixed and the ion currents for the base peaks were stable. Then, the spectrum of the gases was obtained and analyzed by the method explained below. The volumetric ratio of the gas components obtained from the spectrum was verified with the composition of the calibration gas. The percentage of the gas components were inserted into the calibration tables and calibration of the mass spectrometer was carried out.

The evaluation of the mass spectra was done according to the relationship:

$$C_n = \frac{I^+{}_n}{S_n}, \tag{3.4}$$

where C_n – the partial pressure of the component n, I_n – ion current as measured for the component n and S_n – the sensitivity for a corresponding gas (see Table 3.2).

For example, the spectrum from the Figure 3.15 represents the mixture of the air

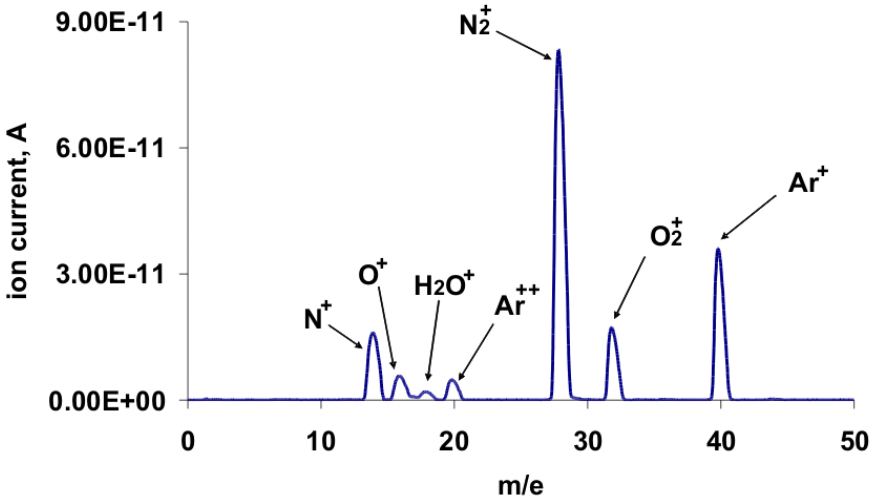

Figure 3.15 Example of the measured spectrum.

with argon. The partial pressure of the gas components are:

$$p_{N_2(28)} = \frac{8.3 \cdot 10^{-11}}{2 \cdot 10^{-4}} = 4.15 \cdot 10^{-7}\, mbar\,;\; p_{O_2(32)} = \frac{1.71 \cdot 10^{-11}}{1.4 \cdot 10^{-4}} = 1.22 \cdot 10^{-7}\, mbar\,;$$

$$p_{Ar(40)} = \frac{3.57 \cdot 10^{-11}}{2.4 \cdot 10^{-4}} = 1.49 \cdot 10^{-7}\, mbar\,.$$

Only base peaks are taken into account. The total pressure amounted to:

$$p_{total} = p_{N_2} + p_{O_2} + p_{Ar} = 6.86 \cdot 10^{-7}\, mbar\,.$$

And thus the percentage ratios of the different gases in the mixture were:

$$\%N_2 = \frac{4.15 \cdot 10^{-7}}{6.86 \cdot 10^{-7}} \times 100 = 60.5\ \%; \quad \%O_2 = \frac{1.22 \cdot 10^{-7}}{6.86 \cdot 10^{-7}} \times 100 = 17.8\ \%;$$

$$\%Ar = \frac{1.49 \cdot 10^{-7}}{6.86 \cdot 10^{-7}} \times 100 = 21.7\ \%.$$

Different calibration mixtures were obtained as different gases were used in the experiments. For the measurements of the plasma jets generated by the hybrid water-argon torch atmospheric air (78.1% of N2, 20.9% of O2 and 0.93% of Ar) was used as a calibration gas as it was found out, that the plasma jet in the measured locations contained mostly air and water vapor condensed before the gas sample reached the mass spectrometer. For the measurements of the plasma jets generated by the gas stabilized torch three mixtures were prepared: air with argon (22% Ar, 18% O2, 60% N2), air with argon and hydrogen (26% Ar, 13% O_2, 58.5% N_2, 2.5% H_2), and air with argon and helium (19% Ar, 12% O_2, 42% N_2, 27% He) were prepared. All percentages are expressed in volume.

3.2.3 Analysis of the enthalpy probe techniques

Enthalpy probe measurements have often been compared with those from emission spectroscopy technique. Incropera and Lippert have shown that the enthalpy probe technique is slightly less accurate than emission spectroscopic methods for temperatures above 10000 K, but it is still applicable in this temperature range [141]. Below 10000 K, enthalpy probes generally provide better accuracy. More recently, in a study of the entrainment of cold gas into the plasma jet, Pfender *et al*. [74] and Chen et. al. [111] have demonstrated that emission spectroscopy tends to systematically indicate higher temperatures than enthalpy probes, especially in the jet fringe regions. These discrepancies were explained by the intermittent flow of a mixture of hot and cold gases in the fringes of the plasma jet. Emission spectroscopy is sensitive only to the high temperature species,

while the enthalpy probe measures an average temperature of the hot plasma gas and the entrained cold gas. It has been shown by Fincke and co-workers that enthalpy probe performance in both subsonic and supersonic compressible flows agree very well with laser scattering results and also with the results of mathematical modelling studies [71, 129, 142].

Much less attention has been given to the question of the probe sensitivity and accuracy. In enthalpy probe measurements, the major sources of error are the determination of the mass flow rate through the probe and the density of the gas mixture. The uncertainty on plasma enthalpy method is estimated to 7.4 % for enthalpy, and around 8 % for temperature, whereas this error is around 7 % for velocity [112].

The Bernoulli equation was derived on the basis of the following assumptions: a) ideal fluids (zero viscosity); b) laminar flow; c) constant density; d) incompressible flow; e) steady-state flow. It may be noted that an incompressible flow is not necessarily a constant density flow. Atmospheric pressure plasma flow is an example of an incompressible, variable-density flow. So for the thermal plasma jets assumption c) is not valid.

First measurements of the error due to a temperature gradient were reported by Hare [126]. In order to examine this effect, he set up an experiment where the stagnation pressure of a cold nitrogen jet was measured by a graphite probe with its tip heated inductively. Stagnation pressure was measured for different probe temperatures, while the free-stream temperature remained constant. An increase in temperature difference caused an almost exponential increase in the difference between the isothermal stagnation pressure and the non isothermal one. In Hare's experiments, the relative error varied from 10 to 50%. But Hare's results cannot be used directly in plasma flows, where the gas temperature is higher than the probe temperature.

The more recent experimental work of Fincke et al. [127] demonstrates in contrast with Hare that the enthalpy probe measurements are accurate.

M. Jankovic et al. [128] examined the effect of rapid changes in flow density on the measured stagnation pressure. They found the trend of the systematic error of measurement. This is a consequence of two opposite influences. An increase in velocity tends to suppress the thermal boundary layer and to minimize the error. At the same time, an increase in temperature means an increase in temperature gradient within the boundary layer, resulting in an increase in the error. They found, that the error in stagnation pressure could reach 10%, which translates into a maximum error of 3% in the calculated velocities which seems to be acceptable.

In the low pressure environment the assumption of an incompressible flow is not valid and the formation of a normal shock wave in front of the probe must be accounted for. First, the Pitot tube techniques commonly used for the determination of the flow velocity cannot be directly applied because these jets are usually not in aerodynamic equilibrium with the surrounding atmosphere [88]. This means that the free stream local static pressure can differ strongly from the chamber pressure because of the shock wave formation (see above). Erroneous results are obtained if the latter is used to approximate the static pressure, which is not directly accessible by measurements. A second

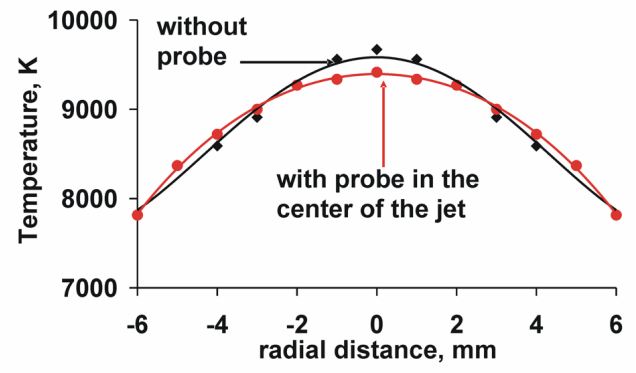

Figure 3.16 Effect of enthalpy probe presence in the jet [112].

complication comes from the required assumptions about the stagnation process that have been made in order to deduce the free-stream jet properties from the quantities measured downstream of the shock [129]. Third, the low collision rate and the high velocity of these flows can lead to deviation from LTE. Selezneva et al. [92] demonstrated that along the jet core the deviation from LTE is more pronounced in the expansion regions, where the pressure drops and the velocity rises. In the compression zones, where the pressure rises and velocity decreases, the electron temperature is closer to the temperature of the heavy particles and the deviation from LTE is less pronounced. In the shock region, where the energy of the heavy particles transfers from kinetic to thermal, zones with a higher heavy particle temperature than electron temperature can occur.

The present chapter describes the enthalpy probe techniques from the point of view of its sensitivity, affecting of the flow field and reliability of the probe measurements under difference conditions.

Effect of the probe presence on the plasma flow

As the probes are intrusive they may disturb the plasma at the same location at which measurements are being taken. The small probe size may minimize disturbances but not entirely eliminates them. But too small dimensions of the sampling probe orifice offer restriction for sufficient gas sampling, which can affect the accuracy of the measurement. The smallest available probe tip is 3.17 mm outer diameter (ENT 317) particularly suited for sampling gases or plasmas at atmospheric pressure. At low pressure, a large probe tip has to be used either ENT 476 or ENT 635 which has respectively a 4.76 mm and 6.35 mm outer diameter. These probes allow much higher gas sampling rates at the expense of a slightly more serious perturbation of the flow caused by their larger diameters.

M. Rahmane *et al.* checked experimentally possible disturbances associated with the use of enthalpy probes in the DC torch plasma jet [112]. For that purposes two radial profiles of the temperature of a subsonic plasma jet, using the emission spectroscopy method were measured with the same plasma torch operating conditions and axial location (35 mm from the anode exit). One of these profiles was observed with the probe ENT 476 located 1 to 2 mm below the level where the spectroscopic measurements were done, and the other with the probe removed from the jet. Results are presented in Figure 3.16. It was observed that with the probe located in the jet jet, the plasma was cooled by less than 3% on the centerline, a result which is within the experimental error associated with emission spectroscopy technique. Thus, the disturbance of the plasma by the probe is not significant.

It must be emphasized that the accuracy of measurements depends on the amount of sampled gas. To provide a good accuracy of measurements, following requirements have to be fulfilled. First, the temperature difference in both modes has to be high enough – typically more than 10 °C and less than 50 °C. Of cause, this temperature difference is limited by the maximum heat load that the probe can accept without any damage (the ENT 476 probe cannot absorb more than 1500 W). Second, to perform a useful measurement, a temperature difference of several Kelvin has to be maintained between ΔT_{tare} and $\Delta T_{sampling}$, otherwise erroneous plasma temperatures can be obtained. Third, the flow around the probe tip should be as close as possible to isokinetic conditions in order not to cause locally flow perturbations. This is satisfied when the gas velocity at the probe entrance is equal to the free stream velocity. This condition is considered to be the most critical condition for an effective enthalpy probe technique.

Isokinetic sampling

The ratio, which describes local flow perturbation over sampling of the flowing plasma gas, is called isokinetic ratio. The isokinetic ratio shows if the velocity of the sampled gas at the probe entrance is equal to the free stream velocity and the ratio is defined as follows:

$$\kappa_{iso} = \frac{Q_g \rho_g}{\frac{\pi d_i^2}{4} v_0 \rho_0}, \tag{3.5}$$

where Q_g, ρ_g, d_i, v_0 and ρ_0 are respectively the sampling gas flow rate, the gas density in STP conditions, the inlet probe diameter, the free stream velocity and the density. It is seen from the ratio that Q_g should be set with attention to the flow conditions around the probe. The dependence of K_{iso} on amount of sampled gas is shown in Figure 3.17. Increasing of the sampling gas flow rate resulted in increasing of the isokinetic ratio.. In ideal case, the velocity at the probe tip approaches the free stream velocity, the isokinetic ratio is equal to one and the perturbation of the flow pattern by the probe is the least (Figure 3.18). Further increasing of the sample gas flow rate leads to a deviation from isokinetic conditions and to a disturbance of the flow field.

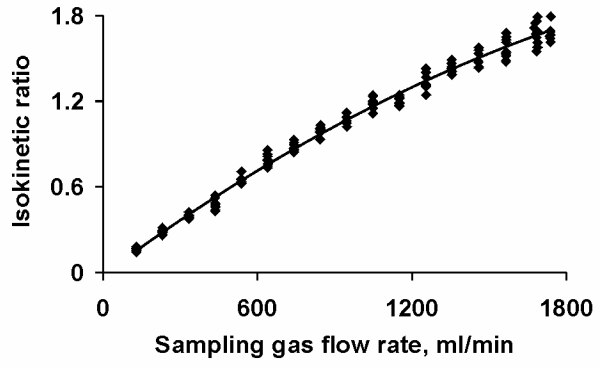

Figure 3.17 Dependence of isokinetic ratio on sampling gas flow rate.

In a number of cases, however, isokinetic sampling is not possible. If the gas enthalpy is relatively low at the point of measurement, sampling rates above the isokinetic levels will be

required to insure a significant difference in the heat load to the probe for accurate measurement of the specific enthalpy of the sampled gas. This will imply drawing of gas sample from regions beyond the probe tip ($K_{iso} > 1$) At very high gas enthalpy levels it is also possible to obtain subisokinetic sampling, which will result in a distortion of the flow pattern around the probe tip ($K_{iso} < 1$). Such phenomenon has to be taken into account in the final analysis and interpretation of the results. In addition, there is also a technical limitation concerning the amount of gas that can be withdrawn, especially for plasma jets operating under low pressure conditions.

Maintaining the probe at the same location in the centerline of the plasma jet, plasma jet characteristics were measured several times at different mass flow rates of the intake gas sample. Figure 3.19 illustrates the effect of the isokinetic ratio on the measured temperature and, in turn, on the calculated gas velocity. When the isokinetic ratio increases, the reproducibility of the measurements improves. For $K_{iso} = 0.2$ the error of the temperature measurements could reach 30% while for conditions with K_{iso} higher than 0.6 temperature measurement errors are within 3%. For K_{iso} higher than 1.2, the measured values of plasma temperature and calculated values of gas velocity are lower than in reality because of the sucking of gas from the regions beyond the probe tip, where the plasma gas temperature is lower compared to the center of the jet.

Thus, the isokinetic ratio has to be set in the range of 0.6 to 1.2 not to disturb the plasma jet and to provide accurate measurements of the plasma jet characteristics.

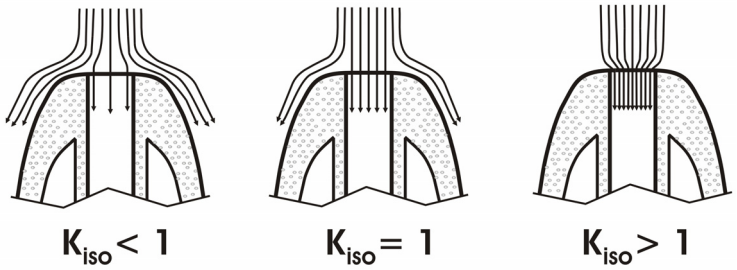

Figure 3.18 Sampling conditions for different K_{iso}.

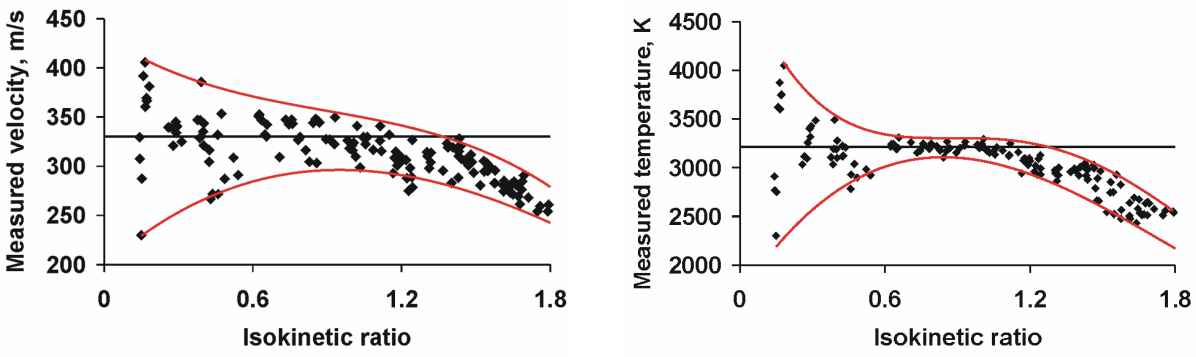

Figure 3.19 Measured temperature and velocity as a function of isokinetic ration.

Moreover, the plasma jets are not fully homogeneously mixed. This means that hot and cold gas volumes of a jet with entrained cold gas are sampled which raises certain problems to deduce the true mean temperature value. Cox et al. studied the behavior of enthalpy probes in fluctuating temperature environments [130]. He found that results obtained from enthalpy probes did not represent the true mean temperature of a gas in which temperature inhomogeneities occur. In the case he studied temperature fluctuations were high as he approximated to a rotating arc jet the 'spiral staircase' geometry. The effect of the plasma jet fluctuations due to its pulsation and improper mixing with the air bubbles on the enthalpy probe measurements could be neglected. This effect becomes apparent at the jet fringes and it has to be paid attention during measurements in the zone of the jet fringes.

To avoid erroneous measurement of the plasma jet characteristics, the probe should be inserted into the flow at least for 20 seconds before recording the results. Figure 3.20 shows the dependence of the outflow water temperature behavior after change-over from tare to sample mode and back. It takes about 20 seconds till the water temperature value, increasing or decreasing, depending on if the probe is sucking or not. Too fast measurements of the outflow water temperature value in the tare mode could lead to underestimated values of plasma enthalpy. In the sample mode early measurements could result in incorrect low enthalpy values as well.

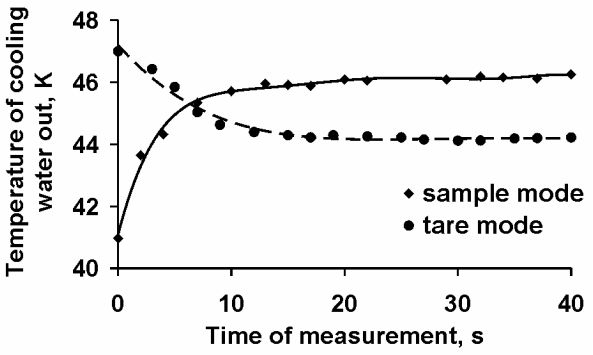

Figure 3.20 Adjustment of the time in each measuring mode.

Sensitivity of the enthalpy probe

The probe performance depends very much on its sensitivity factor which represents the contribution of the gas sample to the overall heat load on the probe cooling water circuit. Since the probe sensitivity factor is proportional to the amount of the sampled gas, there is a tendency to increase the gas mass flow rate to achieve a better accuracy. On the other hand, increasing gas sample mass flow rate could result in increasing departure from the isokinetic sampling conditions as it was shown above.

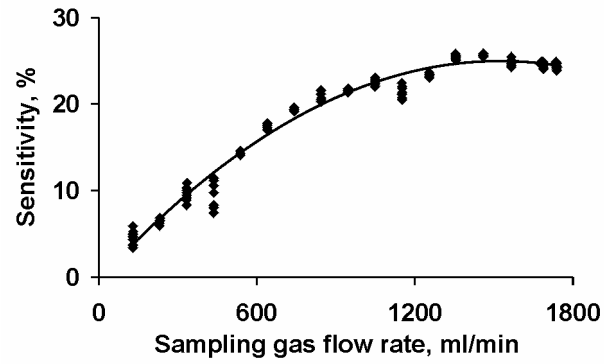

Figure 3.21 Sensitivity of the enthalpy probe as a function of sampling gas flow rate.

The sensitivity of the probe, as it was defined by Grey, is determined as the ratio of the heat flow, received by the probe from the gas sample in the measuring tube to the total heat flow to the probe as a whole from the examined flow:

$$\sigma = \frac{Q_s - Q_t}{Q_s} \times 100 = \frac{\Delta T_s - \Delta T_t}{\Delta T_s} \times 100 \qquad (3.6)$$

Thus, the sensitivity of the enthalpy probe is the fraction of the heat flow resulting from taking gas samples on the general background of the heat flow received by the probe. This factor is represented by in the Figure 3.21. It is seen that σ increases from 4% at gas sampling rate of 100 ml/min to above 25% at 1800 ml/min. But as it was shown above excessive increases in the sampling gas flow rate results in deviation from the isokinetic conditions.

Another way to increase the sensitivity is the reduction of the cooling water flow. But the effect of the cooling water flow rate is not as significant as of the sampling of the gas flow rate (Figure 3.22). Reduction of the water flow rate from 550 to 350 lm/min resulted in an increase in sensitivity by 1%. A big variation of the sensitivity could be explained by fluctuations of the plasma jet during measurements. Moreover, care should be taken in choosing the water flow rate values during the tare and sampling steps of the measurement. A too large value of water flow while it will insure proper thermal protection of the probe will result in a too low value of ΔT with a corresponding loss of jet accuracy. A too low value of water flow should on the other hand, compromise the probe life under high heat flux conditions. The highest level of the water flow rate is also limited by the mechanical resistance of the probe (the maximal cooling water flow rate for the ENT – 476 probe is around 0,8 slm).

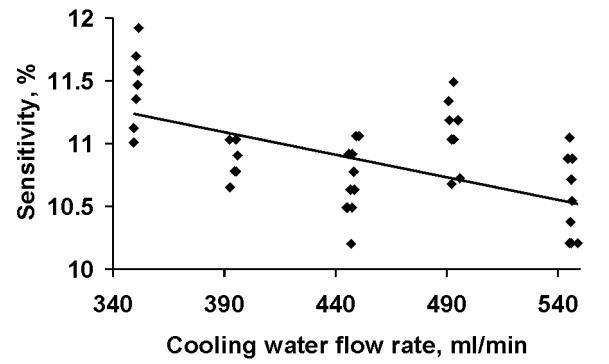

Figure 3.22 Sensitivity of the enthalpy probe as a function of sampling gas flow rate.

A further way of increasing the probe sensitivity is to reduce the amount of heat incident on the probe surface which originates from the surrounding hot gas, by protecting the probe tip with a thermal barrier coating. This could also solve a problem connected with a too large total heat flux received from the plasma by the exposed probe surface. In the presence of this large heat flux background, the accurate measurement of much smaller amount of heat, carried by the intake gas sample is a complex problem. For that reason the probe tip is coated with a ceramic coating, which serves as a thermal barrier. Consequently, the tare heat flux onto the coated probe tip can be significantly reduced, the result being a safe, sensitive probe which can also be used for the diagnostic of plasma jets operating under low pressure conditions, even with small mass flow rate of the intake gas sample.

Figure 3.23 represents the radial profile of the tare plasma heat for a probe without a thermal barrier coating (TBC) and with TBC's of about 80 and 150 μm thicknesses [112]. There is a significant reduction of the heat flux towards the probe with its tip coated. Thus,

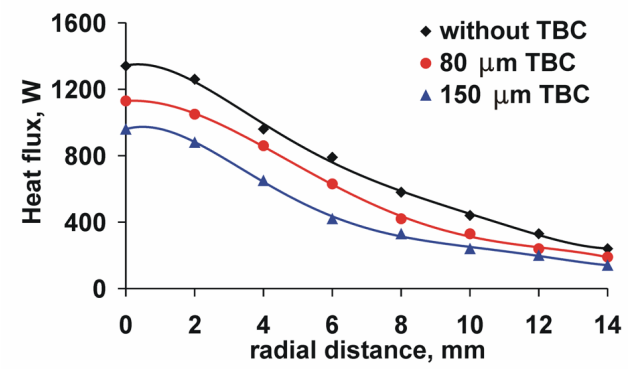

Figure 3.23 Effect of thermal barrier coating on heat flux onto the enthalpy probe [112].

the heat flux in tare mode is considerably reduced while the heat flux associated to the gas sampling is maintained. This will increase the sensitivity of the probe since the proportion of the heat flux coming from the gas will be greater.

In general case, the sensitivity also depends on the accuracy of the determination of the flow rate of cooling water and sucked-away gas and the stability of the parameters, determining the intensity of the heat flow to the sensor [118].

Water correction

As it was mentioned above the freezer is inserted into the gas sample line of the enthalpy probe system. Such arrangement could lead to erroneous interpretation of measured data because of water condensation and freezing. The plasma jet contains water vapor but it is frozen while the sampling process takes place. The sampled gas, which comes to the mass spectrometer chamber to be analyzed, does not contain any vapor causing the incorrect determination of the plasma jet composition. Thus, in following calculations incorrectly determined plasma jet composition can lead to improper treatment of the results because the plasma jet temperature and velocity are calculated basing on determined gas composition. A result mistake can be appreciated.

In fact the first mistake could appear in the measurements of the sampled gas flow. Heat contained in the water vapor is taken into account in calorimetrical measurements, but water condensed while the sampled gas is flowing towards the flow controller. Thus, the flow rate measured and regulated by the mass flow controller could differ from the real

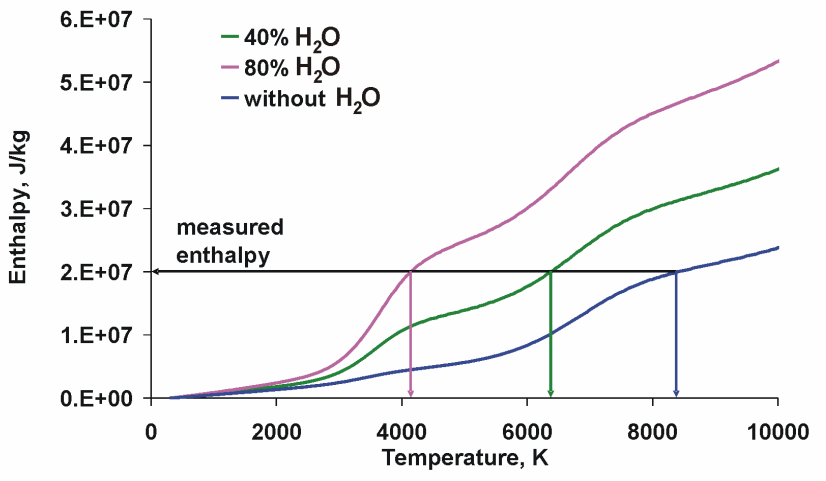

Figure 3.24 Enthalpy as a function of temperature for different amount of water steam.

flow rate at the probe entrance.

The next problem corresponds to the determination of the temperature from the measured enthalpy. The enthalpy is a function of temperature and gas composition. In Figure 3.24 there is the dependence of enthalpy on temperature for several gas mixtures. The enthalpy was calculated for a mixture of plasma gas with air (50% plasma gas and 50% air). As water vapor has a high enthalpy, the addition of the same amount of it into the gas mixture results in strong changes of the total enthalpy of the mixture. The greater the amount of water vapor is contained in the mixture the higher is the enthalpy of the mixture. Consequently, the error in determining of the gas temperature is bigger for higher percentages of water vapor in the measured mixture. Corresponding to Figure 3.24 for the given measured enthalpy the calculated temperature could be twice higher than the real value (for 80% of water in the plasma gas). Incorrect evaluation of the temperature leads to wrong values of the plasma density and so to erroneous determination of the plasma velocity (Eq. 1.14).

The algorithm of the recalculation of the plasma jet properties has been worked out to avoid the errors mentioned above. The algorithm of recalculation consists of two main parts: the first is the determination of the real plasma gas composition and the second is the recalculation of the measured values to the real.

The composition of the plasma gas at the position of 2 mm from the nozzle exit was measured by means of optical emission spectroscopy [122].At the exit form the nozzle

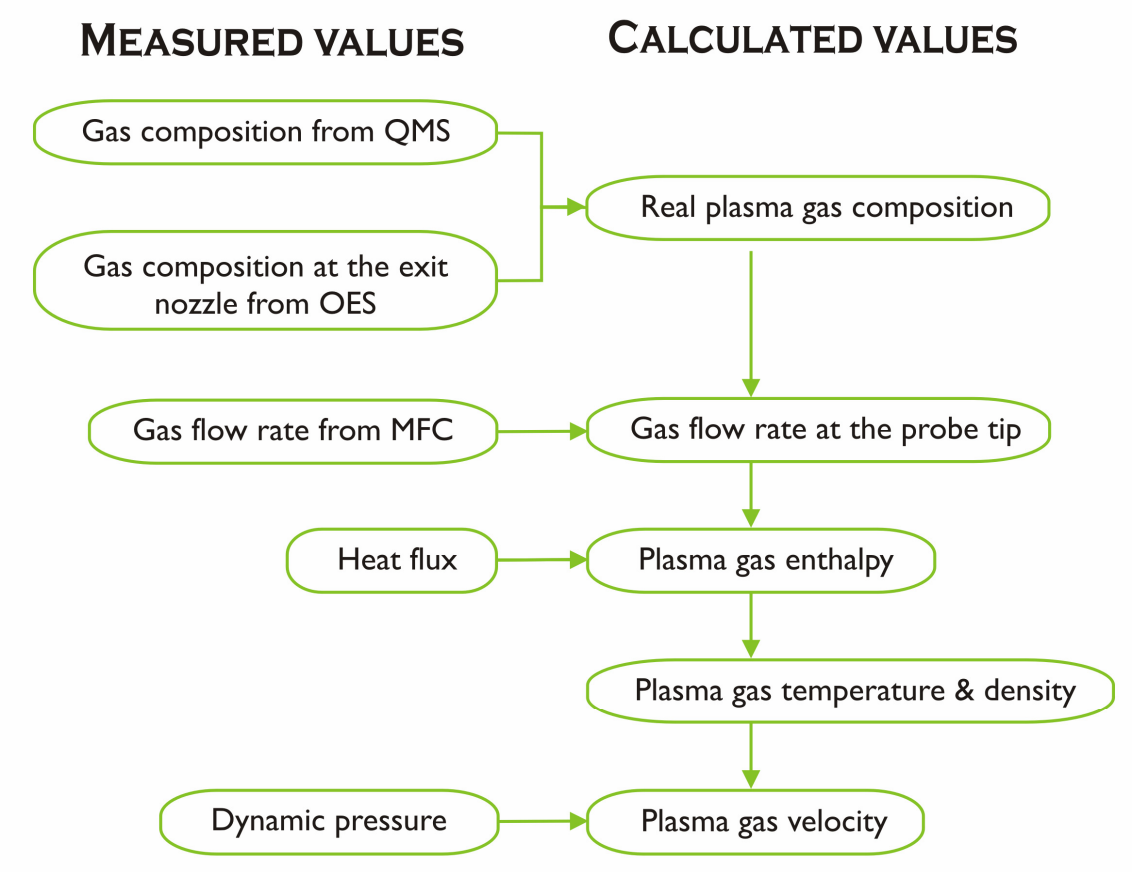

Figure 3.25 Algorithm of the plasma jet properties calculation.

there was no evidence of the air in the plasma. The plasma composition was determined from ratios of emission coefficients of argon, oxygen and hydrogen atomic lines using LTE equations. It was assumed that there was no demixing in the plasma jet at the regions close to the exit nozzle and that the plasma gas was mixing with entrained air homogeneously along the jet. The demixing process could appear inside the torch where very large temperature gradients and concentration gradients of both the neutral and charged particles exist resulting in thermal diffusion, normal mass diffusion and ambipolar diffusion. Since diffusion rates depend on the characteristics of the constituents (mass, ionization potential, etc.) the result could be diffusive demixing of the gaseous species. Nevertheless, the spectroscopic measurements showed nearly homogeneous mixing of argon and hydrogen. However, oxygen did not seem to be well mixed in the core of the plasma jet. These demixing effects could persist for some distance downstream in the jet flow and were being mixed out by jet turbulence. But both assumptions are valid for the interpretation of the enthalpy probe measurements as treated measurements have been done in the region, where the plasma jet represented a fully turbulent flow.

The real composition of the plasma in each point in the jet can be derived from the mass spectrometer measurements if amount of water vapor at the plasma torch exit is taken into account. As the plasma jet represents a mixture of plasma gases with ambient air and there is only about 1% of argon in the atmosphere, the ratio of argon to water vapor in each measured point is the same as at the exit nozzle.

The further evaluation of the plasma jet properties is shown in Figure 3.25. First, the gas flow rate at the probe tip is determined from the value obtained with the help of the mass flow controller. Then the enthalpy of the flow is calculated. It is known that the exit gas in the probe has a negligible energy compared to the plasma, so it is assumed that the calculated enthalpy value equals to the enthalpy of the gas at the probe tip. The plasma temperature is evaluated from the tables of thermodynamic properties by interpolation of the temperature for the known enthalpy. The plasma density is interpolated for the known temperature from the table located together with the enthalpy. The last step is the calculation of the plasma velocity from the measured dynamic pressure.

3.3 Schlieren imaging

Schlieren imaging is a simple technique of flow visualization. The German word 'Schliere' designates in a transparent medium a local inhomogeneity, which causes an irregular light deflection. The principle of the method was developed almost a century and a half ago and is attributed to Foucault [131]. Toepler was the first scientist to develop the technique for observation of liquid or gaseous flow [132]. He recognized and described the wide applicability of 'knife-edge' method. Today this method is the most frequently applied optical visualization system in aerodynamic and thermodynamic laboratories, since it combines a relatively simple optical arrangement with a high degree of resolution. It has been extensively used in the study of shock waves generated by flames, pulsed laser ablation or glow discharges [133-137]. However, papers about visualization of flow generated by DC arcs with Schlieren method are rare [114-116].

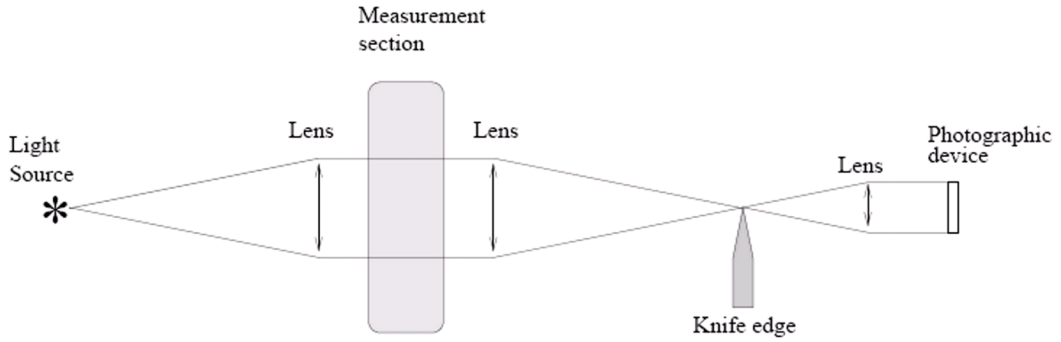

Figure 3.26 'Knife-edge method of the flow visualization.

The description of the principle of the Schlieren imaging is following (Figure 3.26): a parallel light beam passes through the measurement section, where rays are deviated because of local inhomogeneity. The deviation angle θ is given by [138]:

$$\theta = \frac{d}{dy}\int n d\ell , \tag{3.7}$$

where ℓ is the distance along the ray path, y is a direction perpendicular to the optical axis and n the refractive index. As it follows from the equation, the regions with refractive index variations will cause variations of the angle θ. The deflected rays will superimpose on the rays passing through the plasma without deflection and will cause increase or decrease of light intensity on the image plane depending on the sign of θ. An image of the light source is formed in the plane of the knife edge, which is placed in the focal plane of the second lens. A decrease of the light intensity is observed if deflected rays are obstructed by the knife edge. The sensitivity of the Schlieren instrument is inversely proportional to the slit width of the knife edge. It would follow that the sensitivity could be

increased without limit by reducing the width of the open part of the slit image. This is not so in practise as the most severe restriction on reducing the width of the slit of the knife edge results from the influence of diffraction. According to the diffraction theory, $\delta^2/\lambda f > 1$ is the condition to neglect diffraction perturbations, where δ is the size of the source image, λ is the wave length and f is focal length of the second lens in Figure 3.26 [139]. Thus, an experimental compromise has to be found between contrast of the image and diffraction disturbance since a decrease of the width of the slit at the knife edge does not allow obtaining a highly contrasted image in the screen plane because diffraction perturbations increase.

The Schlieren optic installation is shown in Figure 3.27.

One has to take care about proper choice of the light source as waves with frequency below the plasma frequency given by $\omega_p^2 = n_e e^2/\varepsilon_0 m_e$, where n_e, e, ε_0 and m_e is respectively the electron number density, the elementary charge, the vacuum permittivity and the electron mass cannot propagate into plasma. The refractive index of plasma depends on the electron number density with the well-known relationship regarding the propagation of electromagnetic waves in plasmas:

$$n = 1 - \left(\frac{\omega_p}{\omega}\right)^2, \tag{3.8}$$

where ω is the frequency of the illuminating light [140]. For example, considering an

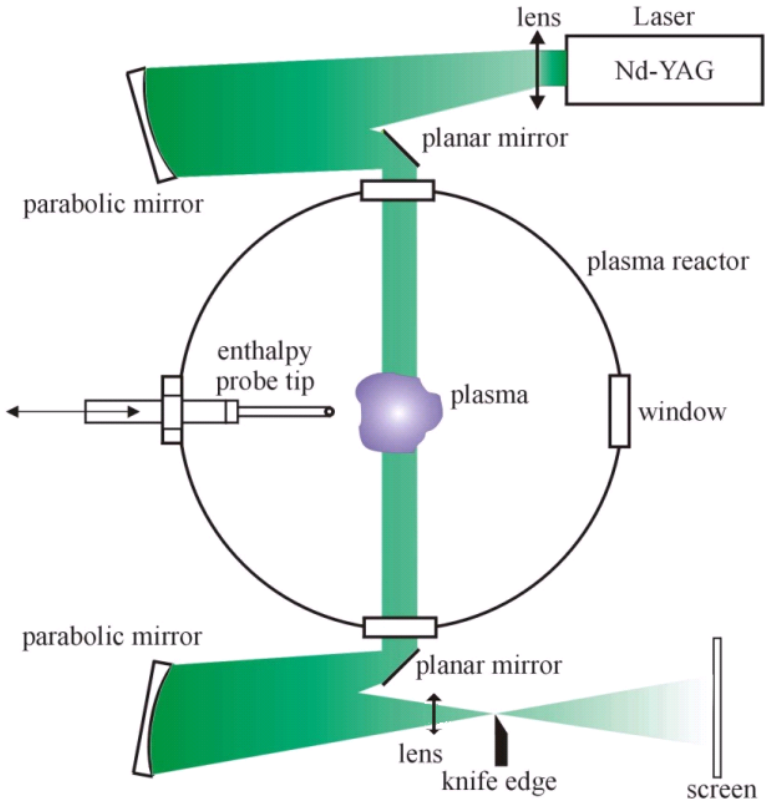

Figure 3.27 Schlieren optic arrangement.

argon-hydrogen plasma at 10,000 K, the electron number density is around 10^{22} m^{-3}, and the plasma frequency is about 10^{7} Hz.

Thus, a pulsed Xe-pumped Nd-YAG laser with $\lambda = 532\,nm$ (Minilase I, New Wave Research Inc., Sunnyvale, CA, USA) was applied as the light source, which corresponds to a wave frequency of about 10^{14} Hz. The length of the laser pulse was 5-7 ns and laser power more than 12 mJ. The laser beam passes through the diverging lens to the parabolic mirror and then to the planar mirror, which directs the beam towards the plasma jet. Two quartz windows were arranged on the plasma reactor walls face to face to allow passing of the light. On the opposite side the converging lens, which is usually used to focus the laser beam on the knife edge, was replaced by a convergent spherical mirror with the focal length of 294 cm. A convergent lens (focal length is 50 cm) has been added in order to make diverging the light beam that comes from the second mirror to provide a satisfying resolution of the Schlieren images under insufficient available place in laboratory. The image is projected on a screen and pictures are taken by a digital camera (Minolta Digital Camera RD-175), which is synchronised by a pulse from laser. The time exposure of the digital camera used for experiments was 8.10^{-3} s. Shorter time exposures (up to 5.10^{-4} s) were available, however the illumination is too weak to obtain a high resolution for pictures.

4. Results of the experimental investigation of the plasma jet behavior

The experimental section of the present work describes results obtained from the measurements of the plasma jets properties and their analysis. The plasma jets were studied under a wide range of parameters. Development of the plasma jet was studied from its exit from the torch nozzle to the distances where a substrate could be placed. The plasma jets generated by two DC arc plasma torches – gas and gas-water torch - were investigated. The influence of the plasma generation conditions and of the surrounding on the plasma jet properties is shown. The plasma jets were generated under atmospheric and low pressure conditions. The plasma gas composition as well as the arc current was varied. The application of the shroud nozzles and different shroud gases were studied.

The results of the investigations are described in the present chapter.

4.1 Development of plasma jet characteristics along the jet

4.1.1 Plasma jet generated by gas stabilized torch

The study of the plasma jet characteristics was started from the regions close to the nozzle exit of the plasma torch, where the plasma jet exiting from the nozzle enters the stagnant surrounding atmosphere. Indeed, in this part of the jet the process of air entrainment starts.

There was no any diagnostics technique available to measure the properties of the plasma jet at the gas torch exit nozzle. Thus, plasma jet properties at this region were calculated from the measured net power of the torch. The net power was determined from the measured power of the torch and power losses, which were calculated from the calorimetric measurements in the torch cooling system. In the case of a cylindrical free jet the pressure variation is small and we can consider the pressure at the exit nozzle to be equal to the ambient pressure. Due to this assumption the equation of ideal gas is valid. All net power of the torch is delivering from the torch chamber by the supplied plasma gas. Thus, the enthalpy of the jet at the nozzle exit of the torch is:

$$\overline{H_0} = \frac{F_e}{\dot{M}_0}, \tag{4.1}$$

where F_e means the net power of the torch and $\dot{M}_0$ the plasma gas flow rate. As the plasma gas composition is known, the calculated value of the enthalpy corresponds to the temperature to be defined. The temperature was evaluated using tables of the thermodynamic and transport properties for the different gas compositions performed with

the help of the computer code ADEP [143]. The plasma jet velocity was evaluated from the equation for thermal energy flux:

$$H_0 = C_p \overline{T}_0 \dot{M}_0 , \tag{4.2}$$

where C_p – the specific heat at constant pressure, $\overline{T}_0$ - average flow temperature at the nozzle exit of the torch. The mass flow rate is:

$$\dot{M}_0 = A \overline{\rho}_0 \overline{V}_0 , \tag{4.3}$$

where $\overline{\rho}_0$ is the average density of the plasma flow. The plasma jet density is derived from the perfect gas law:

$$\overline{\rho}_0 = \frac{pM}{R\overline{T}_0} , \tag{4.4}$$

where p – pressure in the jet, M – molecular mass of the plasma gas and R – gas constant). Thus, the average plasma jet velocity can be calculated from:

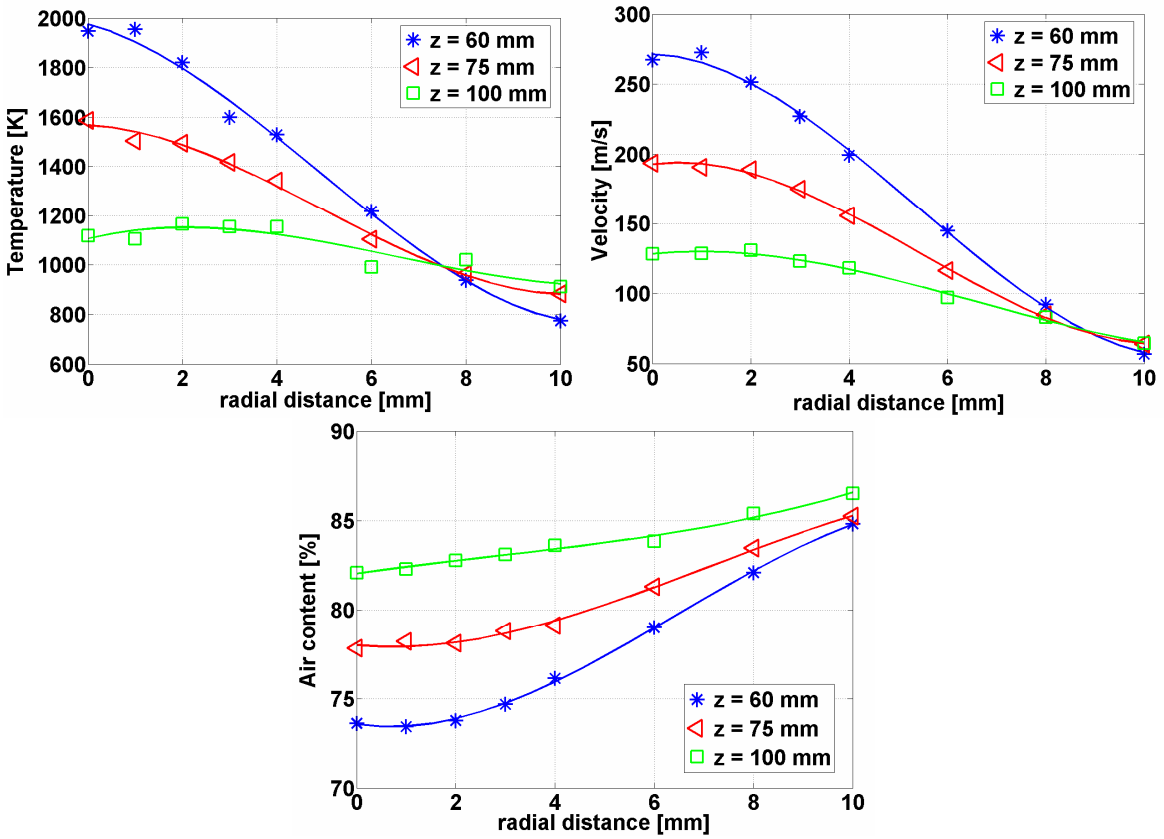

Figure 4.1 Radial profiles of the plasma jet characteristics at several distances from the exit nozzle of the torch (plasma gas – Ar + 10% H_2, plasma gas flow rate – 44 slm, arc power – 20 kW).

$$\overline{V_0} = \frac{\overline{H}_0 R}{A C_p p M}. \tag{4.5}$$

Plasma jet temperature and velocity at the distances farther from the nozzle exit were measured by means of the enthalpy probe.

The radial profiles of the plasma jet at several distances are shown in Figure 4.1. The measurements were done under atmospheric pressure. The plasma gas flow rate was 44 slm containing 40 slm of argon and 4 slm of hydrogen; the arc current was 380 A, which corresponded to 20 kW of arc power. The results show that both plasma jet temperature and velocity decreased with increasing distances from the nozzle exit. The situation started to change at the jet fringes at radial distances near 8 mm, where values of temperature and velocity were getting higher for longer distances from the nozzle exit. This demonstrated a plasma jet spreading, while the centerline velocity and temperature dropped. In these regions the plasma jet was no longer laminar and represented a fully turbulent flow. The amount of air increased with distance evidencing a mixing of the plasma gas with the surrounding air. The surrounding air continued penetrating into the plasma jet center, while its amount in the jet fringes remained almost unchanged.

The evaluation of the plasma jet properties at the plasma jet center is shown in Figure 4.2. Plasma jet temperature and velocity at the exit nozzle were calculated as it was

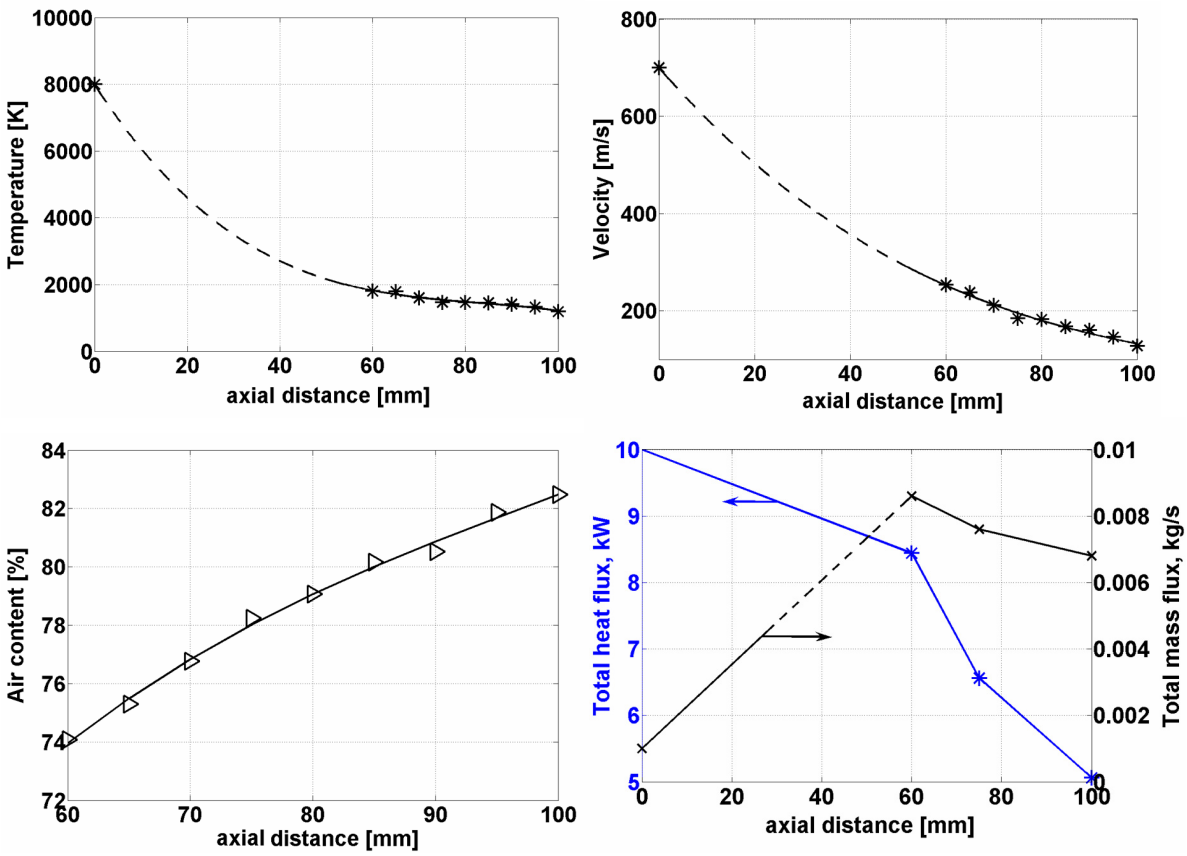

Figure 4.2 Axial development of the plasma jet properties along the plasma jet and at its centerline (plasma gas – Ar + 10% H_2, plasma gas flow rate – 44 slm, arc power – 20 kW).

explained above. The dashed line corresponds to the fitting values of the plasma jet characteristics. It was impossible to measure closer to the nozzle exit of the torch because of the high heat fluxes. The air content at the plasma jet centerline is shown only for the measured area. It was supposed that air was not contained in the plasma flow at the nozzle exit of the torch. As a result of the intensive ambient air entrainment process, plasma jet temperature and velocity intensively decreased with distance from the nozzle exit, while air content increased.

Under the assumption of jet symmetry the total mass, momentum and heat fluxes of the jet per unit time in the axial direction can be determined by integration of the axial component of the mass, momentum and heat flux densities at various radial distances. Thus, the total mass flux was calculated from the equation $G = \int 2\pi r \rho V dr$, the total momentum flux from $M = \int 2\pi r \rho V^2 dr$ and the total enthalpy flux from $H = \int 2\pi r \rho V h dr$. The total fluxes calculated from the measured profiles of plasma jet velocity V, enthalpy h and density ρ for several distances from the nozzle exit are shown in the Table 4.1.

Table 4.1 Total mass, momentum and heat fluxes at the different distances from the torch nozzle exit (plasma gas – Ar + 10% H_2, plasma gas flow rate – 44 slm, arc power – 20 kW).

Axial distance, mm	Total mass flux, kg/s	Total momentum flux, kg·m/s	Total heat flux, kW
60	0.0086	1.44	7.44
75	0.0076	1.0127	5.56
100	0.0068	0.7163	4.06

The law of momentum conservation does not work in the present calculation and the total momentum flux decreased with distance from the nozzle exit and at the distance of 100 mm it was two times less than in the distance of 60 mm. But the momentum flux of the jet has to be conserved. Plasma jet spreading means that momentum and mass are transferred perpendicular to the direction of the flow. Surely, when force acts in several directions, the momentum is not conserved in one direction. In the plasma jet boundaries turbulence stresses are present and momentum might not be conserved. But in the present case forcing in perpendicular direction is much smaller than along the main flow and momentum changes in supposed to be insignificant. Under these conditions the edges of the jet play an important role in the total momentum transfer. But they were not taken into account as measurements of the plasma jet velocity in the boundary layer were uncertain and the measurements of the plasma jet temperature were below probe sensitivity. That is why theoretical calculations were involved.

The fully developed regions of the turbulent jets are similar, and therefore radial distributions of velocity and temperature at some distance from the nozzle exit can be described relatively simply assuming Gaussian distribution:

$$V_z = V_m \exp\left(-\eta_V^2\right) \text{ and } T_z - T_\infty = (T_m - T_\infty)\exp\left(-\eta_T^2\right), \quad (4.6)$$

where

$$\eta_V = \frac{r}{\sqrt{2} tg\alpha_V z} \text{ and } \eta_T = \frac{r}{\sqrt{2} tg\alpha_T z} \tag{4.7}$$

are variables describing decay of the jet both in downstream direction z and radial direction r. T_m, V_m are centerline values of temperature and velocity at z, T_∞ the temperature of the ambient air, α_V and α_T represent spread angles of temperature and velocity reflecting plasma jet spreading [144].

Velocity profiles measured (Figure 4.1) and calculated from the relation 4.6 are displayed together in the Figure 4.3. The theoretical curve excellently fits together with measured values showing that Gaussian profiles are satisfied.

The Gaussian profiles fitted well also with measured temperature, but the temperature spread angles α_T differed for each distance from the α_V. The normalized velocity and temperature profiles show a different development of velocity and temperature (Figure 4.4). The heat transfers faster perpendicular to the main flow direction providing quicker temperature increase at the jet fringes. This effect could be caused by radiation heat transfer in the regions close to the nozzle exit.

The spread angles for plasma jet temperature and velocity are shown in the Table 4.2. The inappropriate mixing caused by plasma jet fluctuations led to a dependence of the temperature spread angle on the axial position. α_T increased with the axial distance z. The velocity spread angle α_V remained constant along the jet showing conical jet shape, which was also confirmed by the Schlieren images (section 4.7).

The mass and momentum fluxes were calculated from the evaluated profiles of plasma jet velocity and density. The plasma jet density profile could be expressed as Gaussian:

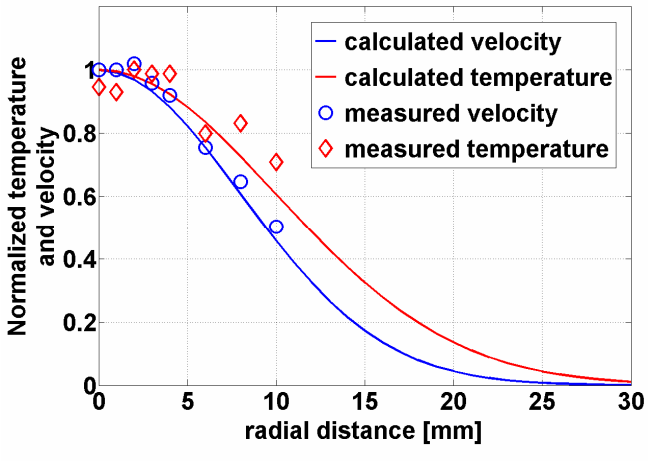

Figure 4.4 Dimensionless profiles of the plasma jet velocity and temperature.

Table 4.2 Spread angles of the corresponding plasma jet properties depending on distance from the nozzle exit (plasma gas – Ar + 10% H_2, plasma gas flow rate – 44 slm, arc power – 20 kW).

Z, [mm]	α_V	α_T
60	5°	10°
75	5°	10°
100	5°	14°

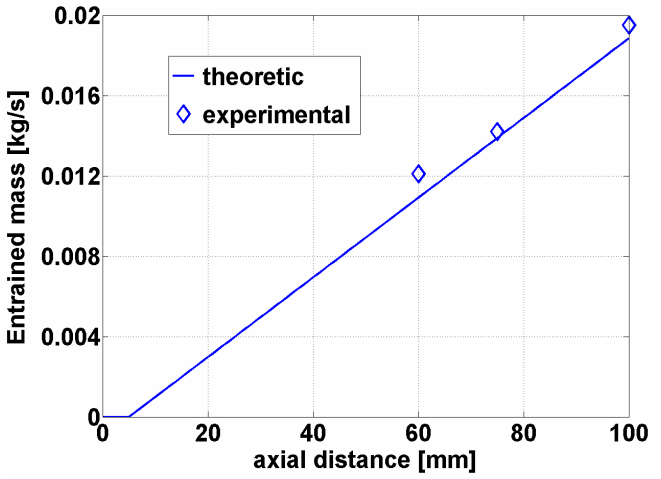

Figure 4.5 Mass flow rate of the ambient air entrained into the plasma jet (plasma gas – Ar + 10% H_2, plasma gas flow rate – 44 slm, arc power – 20 kW).

$$\rho_z - \rho_\infty = (\rho_m - \rho_\infty)\exp\left(-\eta_\rho{}^2\right), \tag{4.8}$$

where ρ_z, ρ_m, and ρ_∞ are densities of the plasma jet in the examined point, at the plasma jet centerline at the given distance z and of the ambient atmosphere respectively. The variable η_ρ describing mixing of the jet supposed to be equal to η_T as density is a function of temperature and the density spread angle coincides with the temperature spread angle α_T. The results of the calculations are shown in the Table 4.3. Here, the momentum in the axial direction changed relatively little along the jet. The total mass flux increased with distance from the nozzle exit because the amount of cold ambient air entrained into the jet increased providing a rising of the jet density.

Table 4.3 Calculated mass and momentum fluxes in the plasma jet (plasma gas – Ar + 10% H_2, plasma gas flow rate – 44 slm, arc power – 20 kW).

Axial distance, mm	Total mass flux, kg/s	Total momentum flux, kg·m/s
60	0.0131	1.51
75	0.0152	1.31
100	0.0205	1.33

The magnitude of entrainment can be illustrated by the fact that a turbulent jet entrains fluid equivalent to the jet mass flow rate at the nozzle exit for about every three nozzle diameters' distances along the jet axis. The general relation for non-constant density systems is [145]

$$\frac{\dot{m}_e}{\dot{m}_0} = 0.32\left(\frac{\rho_\infty}{\rho_0}\right)^{1/2}\frac{z}{d_0} - 1\,, \tag{4.9}$$

where ρ_0 is the plasma jet density at the nozzle exit of the torch and d_0 is the nozzle diameter (d_0 = 6 mm). The theoretical entrainment rate along the jet for the considered case is plotted in the Figure 4.5 together with experimental values marked as diamonds. The theoretical curve fits the experimental values well. Hence, it is possible to calculate the amount of the entrained air along the plasma jet using a very simple dependency. Corresponding to the relation 4.9 ambient air started entraining into the plasma jet already at the distance of 5 mm. Thus, the entrainment rate could be decreased either by decreasing of the mass flow rate of the fluid at the nozzle exit and increasing its density or by decreasing the density of the surrounding.

4.1.1 Plasma jet generated by hybrid argon-water torch

The behavior of the plasma jet generated by the hybrid argon-water torch differs from the jet described above. The main reason for this is the strong interaction of the main plasma flow with the anodic jet, which is formed at the position of the anode attachment. As a result of such an interaction deflection of the main plasma flow from the torch chamber axis occurs. Studies of the plasma jet by repeated photographing for the different working conditions have shown that the deflection angle depends on the applied arc current and on the flow rate of the secondary gas argon [146]. Increase of both arc current and argon flow rate led to straightening of the jet because of the increased momentum flux of the main plasma flow. The deflection angle of the plasma jet obtained from the enthalpy probe measurements for arc current 150 A and different argon flow rates are shown on Table 4.4.

Table 4.4 Deflection angle of the plasma jet (arc current – 150 A).

Argon flow rate, slm	12.5	17.5	27.5
Deflection angle	10°	4°	3°

Deflection of the plasma jet could lead to additional perturbations and cooling of the jet. The plasma jet temperature and velocity profiles deviate from the Gaussian curves. The deviation of the experimental results obtained at the distance 60 mm from the exit nozzle for an arc current of 150 A and an argon flow rate of 17.5 slm is depicted in Figure 4.6. In the upper part (positive values of the radial distance) the Gaussian profile fits the values of the plasma jet velocity well, while the experimental values are situated under the theoretical curve for the lower part of the plasma jet. This was a result of the interaction of the plasma jet with the anodic jet. The anodic jet pushed the main plasma jet upwards making it narrower.

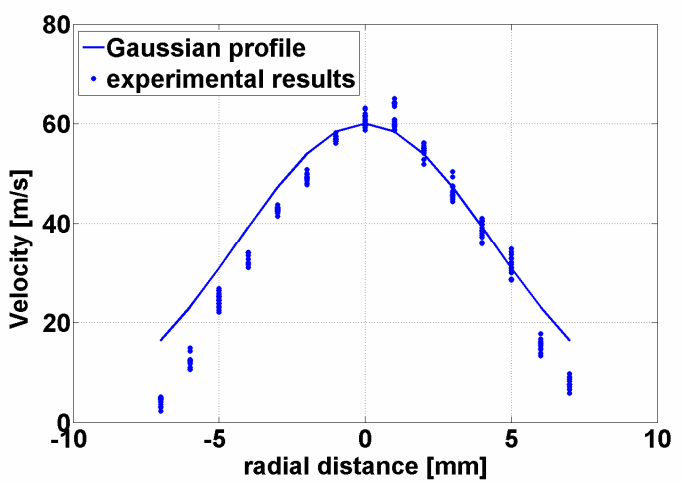

Figure 4.6 Experimental and Gaussian profiles of the plasma jet velocity.

Profiles of plasma jet temperature and composition in the regions close to the nozzle exit were evaluated from the optical emission spectroscopy measurements. The laminar part of the jet was too hot for the enthalpy probe. The turbulent part of the jet was too unstable for optical diagnostics and here the measurements were done by the enthalpy probe. The measurements were performed for an arc current of 150 A and for the argon flow rate 22.5 slm. The transition to the turbulent flow regime occurred approximately at the axial distance of about 50 mm in this case. The whole plasma jet was scanned including its heavily fluctuating fringes.

The results of the plasma jet investigations are shown in Figure 4.7. The highest values of the temperature were observed in the centerline of the plasma jet at the nozzle exit. The temperature at the edges was assumed to be equal to the temperature of the ambient air. The centerline plasma jet temperature was going down with distance from the torch and the jet spread.

The velocity profile at the nozzle exit of the torch was determined from the temperature profile and power balance of the torch assuming LTE. First, the Mach number M was obtained from the equation:

$$M = \frac{F_e}{\int_0^{R_E} 2\pi r \rho c h \, dr + (1 - f_{Ar}) \, [\lambda + C_w (T_B - T_0)] \int_0^{R_E} 2\pi r \rho c \, dr}, \tag{4.5}$$

where F_e is the total plasma enthalpy near the nozzle exit, ρ the plasma density, h the plasma enthalpy, c the sound velocity, f_{Ar} the molar fraction of argon, λ the specific latent heat of vaporization, C_w the specific heat capacity of water, T_B the boiling temperature and T_o the temperature of the water in the vortex and R_E the radius of the nozzle. Under the assumption that radial pressure gradients are negligible and radial velocities are small compared to the axial velocities, the Mach number can be assumed to be independent of radial coordinates at the nozzle exit. Knowing the value of Mach number, the velocity profile can be derived from the measured temperature profile using the relation:

$$V(r) = M \cdot c\{T(r)\}, \tag{4.6}$$

where sound velocity c is a function of temperature for equilibrium conditions in the plasma. The pressure at the nozzle exit was supposed to be equal to the atmospheric pressure. As the dependence of the sound velocity value on the pressure is weak, the possible erroneous estimation of the pressure has a negligible effect on the resulting values of velocity.

Similarly to the plasma jet temperature the plasma jet velocity was the highest at the torch nozzle exit. As the plasma jet moved away from the nozzle exit, it spread and at the position 75 mm the jet was twice wider than at the nozzle exit, which corresponded to a spread angle of 5°. Thus, plasma jets generated by the hybrid torch have similar spread angles α_V as with jets generated by the gas stabilized torch (in the previously discussed case the spread angle was about 5° as well).

The mass and enthalpy fluxes (flux densities[3]) were calculated from the measured profiles. The mass flux in the center of the jet at the nozzle exit was the lowest because of the very high temperature. Under such high temperatures the plasma density, which is a function of temperature, is very low. Thus, in spite of high jet velocities, the mass flow rate through the nozzle exit of the torch was very low. The mass flux increased towards the jet fringes because the plasma density increased reaching substantially higher values at the fringes. Farther downstream along the jet the profile of the mass flux changed and the maximum values were at the center of the jet. This was caused by entrainment of external

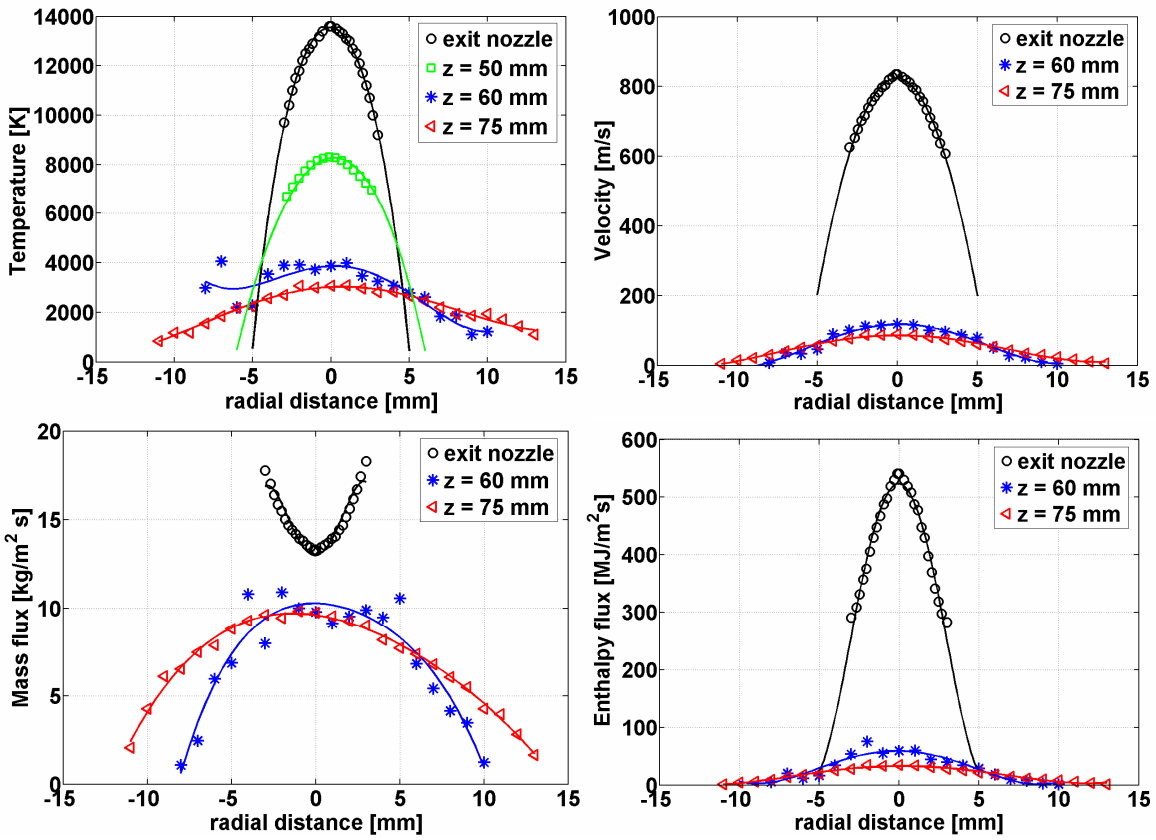

Figure 4.7 Development of the plasma jet generated by the hybrid gas-water torch (argon flow rate – 22.5 slm, arc current – 150 A).

air with high density. Appearance of air in the jet centerline was observed already just behind the anode. As a result the plasma jet density was much higher than at the nozzle exit accompanied by a still high plasma jet velocity. The total mass flux *M* increased with the distance from the nozzle exit (Table 4.5) because of cold ambient air being entrained along the whole jet.

Table 4.5 Total mass and heat fluxes at the different distances from the hybrid torch nozzle exit (argon flow rate – 22.5 slm, arc current – 150 A).

Axial distance, mm	Total mass flux, g/s	Total heat flux, kW
2	0.344	9
60	0.947	2.6
75	1.3	2.4

The profiles of the enthalpy flux in axial direction followed the temperature and velocity profiles. The enthalpy flux was the highest at the nozzle exit and then dropped at the jet centerline. The values of total heat flux strongly dropped between the nozzle exit and z = 60 mm demonstrating strong air entrainment even in comparison with the gas torch in which the heat flux drop was not so drastic. Probably this effect was caused by an intensive transition of kinetic energy of axial flow into energy of turbulent motion, which was not taken into account in the total heat flux calculations. However the heat flux changed only little between 60 and 75 mm because turbulence was already developed and transfer of kinetic energy of axial flow into turbulent energy was low.

The profiles of argon concentration in the jet evaluated from enthalpy probe measurements and decrease of concentration of the plasma gas components at the centerline position are represented in the Appendix A. At the positions farther from the nozzle exit the decrease of the plasma fraction due to air entrainment was substantial. The rapid decrease of plasma fraction up to 60 mm was slowed down at longer distances. This change can correspond to the transition of the plasma jet to fully turbulent flow.

Different dynamic of these two types of plasma jets results in different Reynolds numbers. Reynolds number for the gas stabilized torch Re = 854 was higher than for the hybrid torch Re = 470. It means that the plasma jet generated by the gas torch under present conditions was affected more by inertial force, which supposedly is producing random eddies, vortices and other flow fluctuations. But the rapid jet decay indicated a higher level of turbulence for the plasma jet generated by the hybrid torch. Fast transition of the plasma jet to turbulent behavior was caused by a large difference between density of the plasma jet, which was extremely low, and ambient air density as well as by strong interaction of the main flow with the anodic jet. The concerned case represents critical conditions of the hybrid plasma torch current and power. Under these conditions the anodic jet perturbed the jet a lot causing additional fluctuations leading to turbulence.

4.2 Influence of the arc current intensity

The increase of the arc current intensity leads to a rise of electrical power dissipated inside the torch chamber. Thus, it affects all processes not only in the arc column, but also in the plasma jet, which obtains and carries more energy.

Increase of the arc current in the plasma torch with hybrid argon-water stabilization of the arc leads to the change of the plasma gas composition. The higher arc current value leads to an increase of the evaporation rate of water in the water stabilized chamber and consequently the amount of water vapor increases. Thus, the fraction of the water components in the plasma gas mixture rises so that the water content in the plasma jet increased from 40 to 55 % caused by an arc current rise from 150 to 250 A for an argon flow rate of 15 slm. The total plasma gas flow rate increases as well.

The effect of arc current for the hybrid plasma torch is explained in Appendixes A and B. The obtained results showed that the plasma jet temperature and velocity at the nozzle exit increased for higher arc current. The temperature rise was connected with higher Joule heating being released by the arc. The increase of evaporation rate for higher arc currents resulted in increased mass flow rate at the nozzle exit of the torch and thus, according to the continuity equation, the plasma jet velocity had to increase as well.

In the experiments presented in Appendix B the plasma jet characteristic profiles for different arc currents were measured under the pressure 30 kPa in the downstream regions of the plasma jet. The temperature and velocity increased with arc current increase and thus the air entrainment was reduced.

For the plasma torch with gas stabilization of the arc the plasma jet temperature and velocity at the torch exit were calculated for two arc current intensities and for two plasma gases: pure argon and a mixture of argon with 10% of hydrogen. Similarly as in the case of the hybrid plasma torch, the increased arc current resulted in increasing both the plasma jet temperature and velocity for both plasma gases (Table 4.6). The dependence of the plasma jet characteristics on arc current was more pronounced for an argon-hydrogen plasma because of a higher Joule heating being dissipated inside the torch.

Table 4.6 Dependence of the plasma jet characteristics on arc current intensity.

Plasma gas	Arc current, A	Net power, kW	Average temperature, K	Specific heat C_p, J/kg·K	Average velocity, m/s
40 slm Ar	540	6	9300	567	778
	800	8.5	10700	698	895
40 slm Ar + 4 slm H_2	350	7	8000	773	692
	600	16.6	11900	1210	1048

Temperature and velocity increased not only at the nozzle exit of the torch but in the downstream regions as well. Measurements of the plasma jet characteristics downstream the jet were performed for the argon jet (gas flow rate - 40 slm). The arc

current increase from 550 to 650 A led to a rise of arc power from 19 to 24 kW. The resulting temperature and velocity profiles at the distance 60 mm from the torch nozzle exit are shown in Figure 4.8. The temperature rose from about 1600 K to almost 2000 K in the centre of the jet and the velocity from 260 to 340 m/s, which means an increase of about 25% for only 100 A difference in arc current. The higher arc current resulted in a prolongation of the laminar jet core as the viscosity of the plasma rose with temperature for evaluated temperatures at the nozzle exit under the studied conditions (Fig. 1.5).

Nevertheless, further development of the entrainment process was faster for higher arc current. The air content at the jet centerline was relatively high already at the distance 40 mm from the nozzle exit. It was lower for higher arc current values for the regions closer to the nozzle exit. However, the values of the air content became equal at the distance 90 mm and subsequently were higher than for lower current. Such a behavior of the plasma jet exhibits strong linking of the entrainment process to the velocity and density gradients, which are higher for higher arc currents. But the difference of the air content is not very significant. The strong difference in temperature and velocity was caused mainly by different initial conditions at the plasma torch exit.

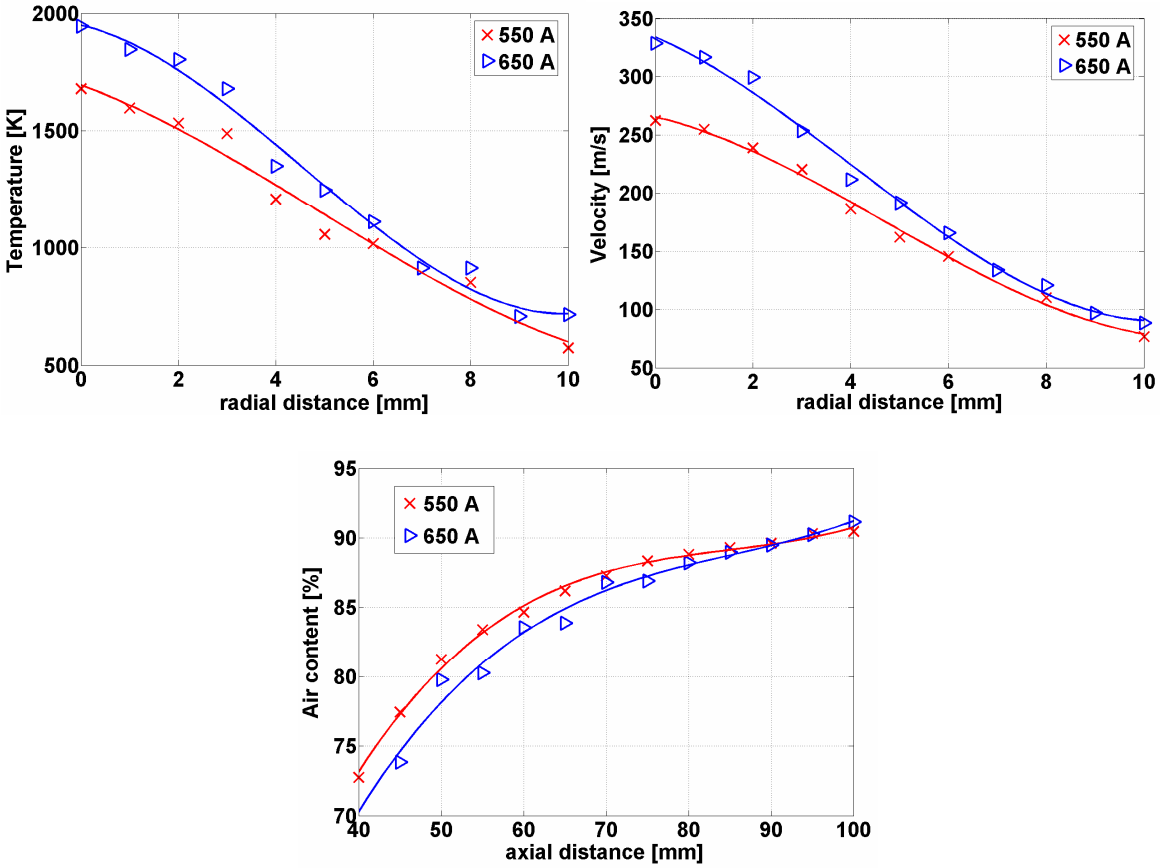

Figure 4.8 Dependence of the plasma jet characteristics on arc current in gas stabilized torch (plasma gas – argon, plasma gas flow rate – 40 slm , z = 60 mm).

4.3 Effect of gas nature

4.3.1 Effect of argon flow rate in the hybrid plasma torch

In the hybrid plasma torch the composition of the plasma gas can be varied by changing the flow rate of the secondary gas. Argon is usually used as a secondary gas. Increasing of the argon flow rate resulted in increasing of the argon fraction in the plasma gas mixture (Table 4.7). The argon-steam ratio was evaluated from the spectroscopic measurements of the lines of hydrogen and argon ions at the plasma torch exit assuming LTE.

Temperature and velocity profiles at the nozzle exit of the torch are shown in Figures 4.9 and 4.10. The temperature profiles were evaluated from the spectroscopic measurements and the velocity profiles were calculated from the temperature profiles from the equation 4.6 knowing the Mach number (eq. 4.5). It can be seen that the temperature profiles were not affected by the change of the argon flow rate from 17,5 to 28 slm. The absence of the argon influence is caused by the strong difference of the enthalpies of water steam and argon (Fig. 1.3). Addition of a quite high amount of argon with low enthalpy has little effect on the total energy balance of the arc and the temperature remained almost unchanged. In the contrary the plasma jet velocity was strongly affected by the argon flow rate. Adding of argon caused an increase of the plasma velocity mainly because the mass flux through the nozzle exit increased. The plasma density increased as well and thus the total momentum and enthalpy flux also increased with argon flow rate (Table 4.7).

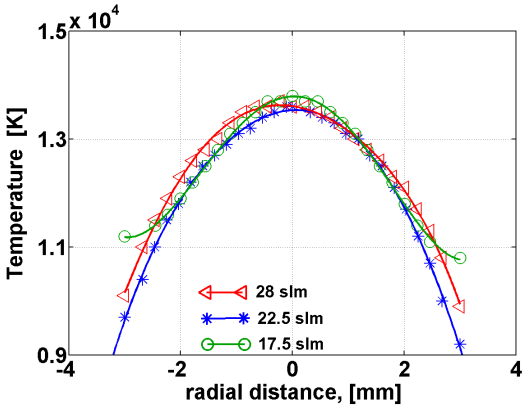

Figure 4.9 Profiles of plasma temperature at the position 2 mm downstream of the torch exit for various argon flow rates (arc current - 150 A).

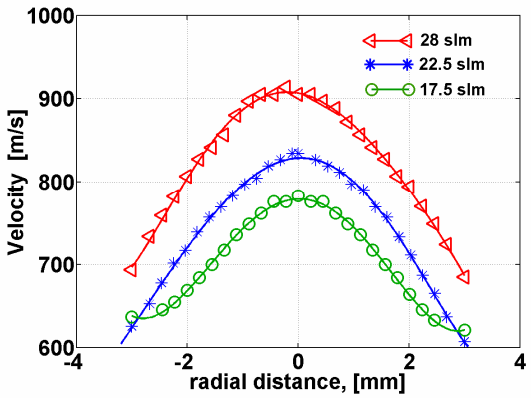

Figure 4.10 Profiles of plasma velocity at the position 2 mm downstream of the torch exit for various argon flow rates (arc current - 150 A).

Properties of the plasma jet in the downstream regions of the plasma jet were measured with the enthalpy probe. The main results are represented in Appendix A. The jet core was prolonged due to the increase of the argon flow rate. The spread angle of the jet evaluated from the profiles of mass flux density and the jet dimensions increased. The plasma jet velocity increased while the plasma jet temperature slightly decreased for higher argon flow rates.

The results showed a lowering of the heat losses in the plasma jet which is due to the reduction of the intensity of turbulence and hence of entrainment of cold gas. This

phenomenon occurred because of decreased density difference between plasma flow and surrounding. The increase of the argon content in the argon-steam plasma led to a substantial increase of the plasma density and subsequently the density ratio of plasma to ambient gas was reduced.

Table 4.7 Dependence of the plasma jet properties on argon flow rate at the torch nozzle exit for I = 150 A.

Argon flow rate	Argon-Steam ratio	Mach number	Total momentum flux, kg·m/s^2	Total enthalpy flux, kJ/s	Total mass flux, g/s
17.5 slm	55% - 45%	0.22	0.125	8	0.18
22.5 slm	75% - 25%	0.29	0.25	9	0.344
28 slm	80% - 20%	0.33	0.323	10	0.4

4.3.2. Effect of plasma gas composition and flow rate in the gas stabilized torch

Effect of plasma gas flow rate

Measurements were done under 40 kPa. Pure argon was chosen as the plasma forming gas because in general it is probably the most favored primary plasma gas. Argon flow rates were set to 20, 40 and 60 slm. The radial profiles of the plasma jet characteristics were measured at the distance 60 mm from the nozzle exit of the torch. First, the arc current was fixed at the value 550 A and only the plasma jet flow rate was varied. The arc voltage and consequently the arc power rose with argon flow rate increase as it is shown in Figure 3.4. Increasing the argon flow rate resulted in two opposite phenomena affecting the flow velocity at the nozzle exit. With increasing of the gas flow rate the plasma velocity has to rise according to the continuity equation as the plasma jet flows through the same area of the nozzle exit. But a higher gas flow rate reduces the temperature of the plasma. In turn a temperature decrease leads to a higher density of the gas resulting in a lower plasma jet velocity. Therefore, changing the gas flow rate of the plasma jet at the nozzle exit leads to a modification of the plasma plume itself.

The effect of the plasma gas flow rate on the plasma jet characteristics for a constant arc current of 550 A is shown in Figure 4.11 a). The plasma jet formed by 20 slm of argon was short and not very stable. Increasing the argon flow rate to 40 slm had a favorable effect on both plasma jet temperature and velocity. The centerline velocity was even doubled and the air content reduced along the jet cross section. However, further increasing of the argon flow rate resulted in a reduction of the plasma jet temperature, while the plasma jet velocity remained almost unchanged. According to measurements with an argon plasma jet performed by Fincke et al. [71-72] the engulfment process starts closer to the nozzle exit when the flow velocity increases. However, the air content reduction with increasing argon flow rate pointed out that a higher amount of plasma gas remained. A stronger ambient air entrainment because of higher plasma velocities at the nozzle exit can be controlled, thereby. Potentially higher velocity

gradients are responsible for this effect. Moreover, the plasma jet temperature might be smaller already at the exit of the torch.

Figure 4.11 b) represents the characteristics of the plasma jets with the same arc power for different plasma gas flow rates. In contrast to Figure 4.11 a) a same amount of energy to generate the plasma jets was dissipated by the arc as Joule heating. The development of the plasma jet characteristics with argon flow rate variation was similar to the case of constant arc

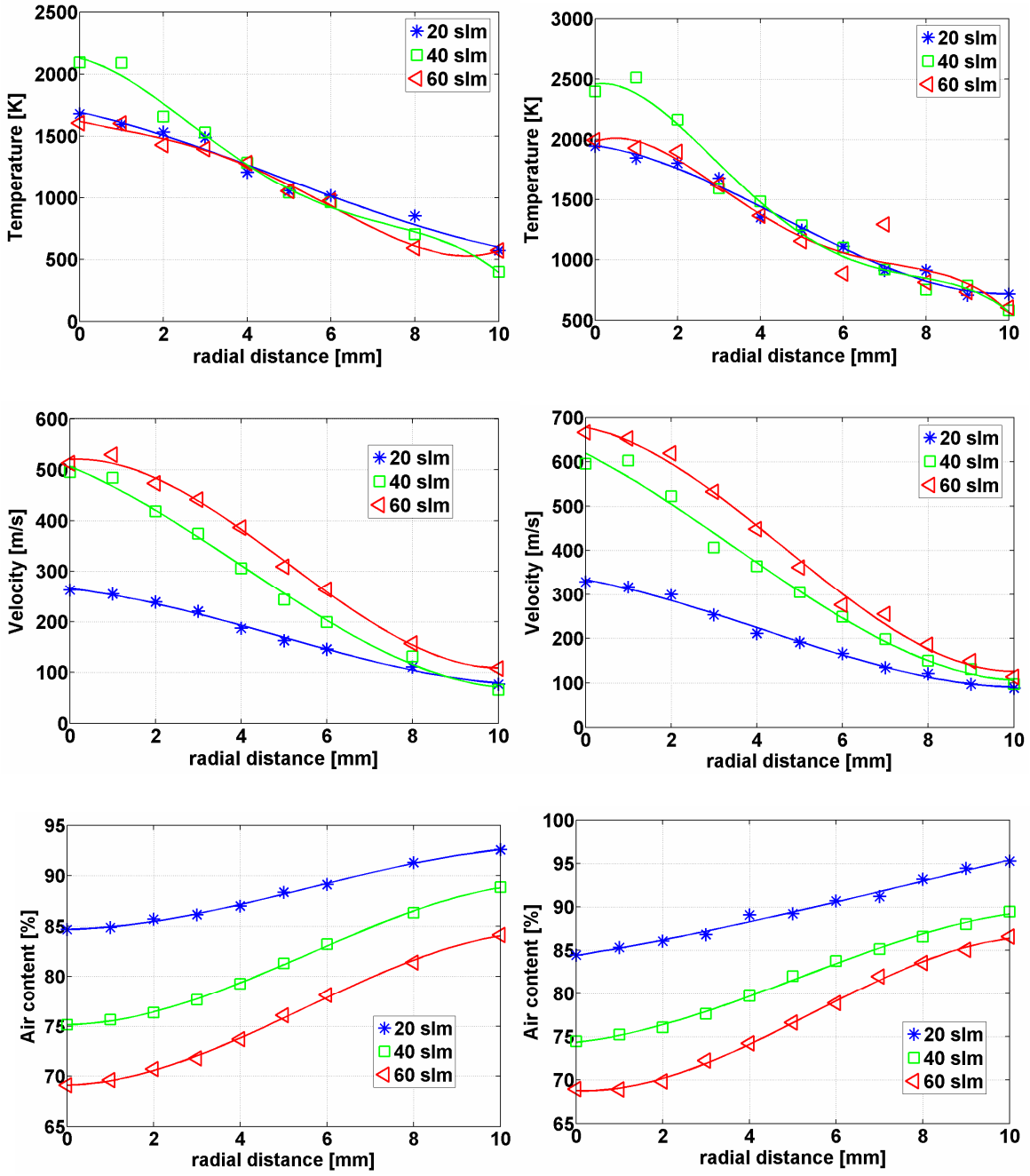

Figure 4.11 Plasma jet characteristics depending on plasma gas flow rate for argon plasma:
a) fixed arc current 550 A;
b) fixed arc power 20 kW.

current. This indicates that increasing the plasma jet velocity has a stronger influence on the process than temperature reduction. Higher mass flows at the exit nozzle provide a better plasma jet stability and prolongation.

Effect of plasma gas composition

The effect of plasma gas composition was studied by mixing of different plasma gases. Argon was used as primary plasma gas to which 20% of hydrogen or helium was added. Thus, three plasma gases were tested: pure argon, mixtures of argon with helium and with hydrogen as well. The total plasma gas flow rate was set to 50 slm. Plasma jets were generated under a reactor pressure of 40 kPa. In all experiments the arc power was kept constant to 20 kW, while the arc current was varied. Thus, the plasma gas got almost the same amount of heat. Differences observed in the behavior of the plasma jets were a result of different plasma gas nature. The profiles of the plasma jet characteristics were measured at a distance of 60 mm from the nozzle exit. The results of these measurements are shown in Figure 4.12. Visual observation of the argon plasma jet showed that the jet was stable at a short laminar region near the nozzle exit. Ambient air rapidly mixed into the jet and at z = 60 mm it reached about 70 % at the jet centerline.

Adding of helium had only a negligible effect on the plasma jet properties concerning temperature and velocity compared to the jet with pure argon. It is because both

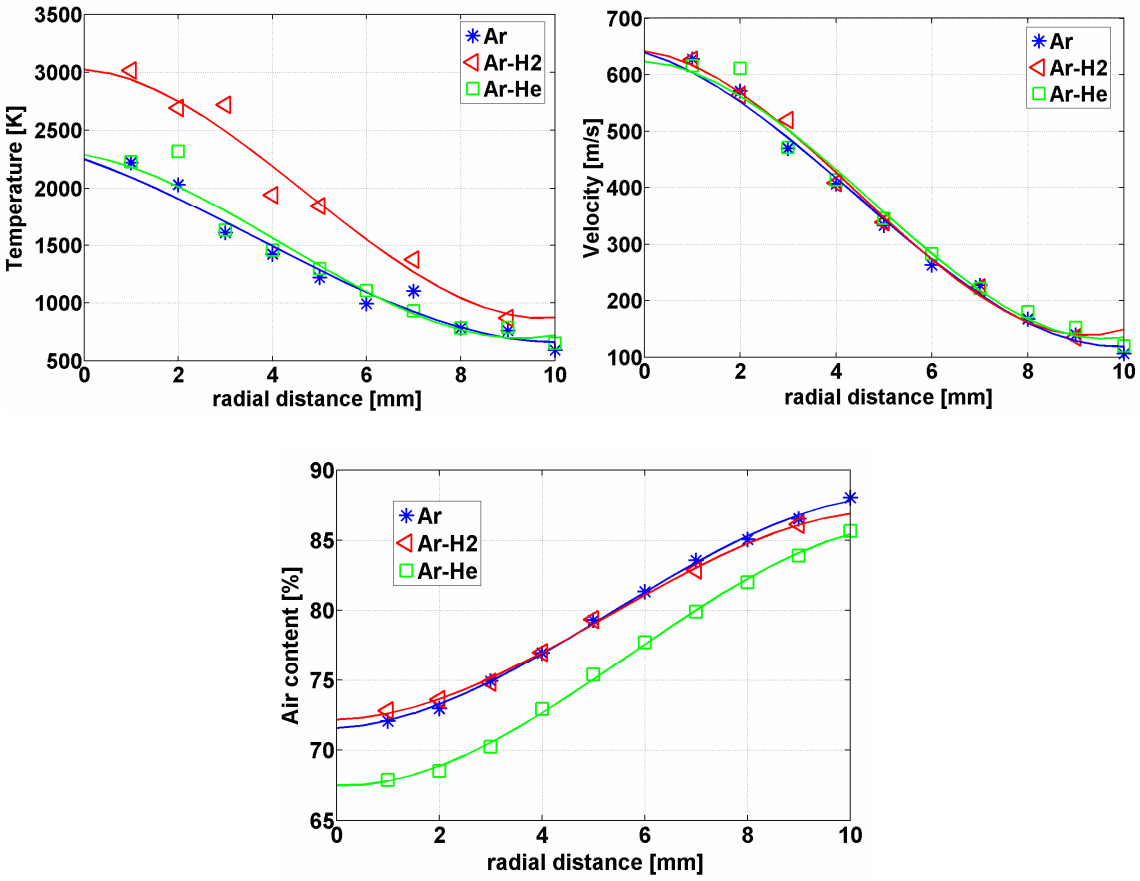

Figure 4.12 Dependence of the plasma jet characteristics on the plasma forming gas mixture (plasma gas flow rate – 50 slm, arc power – 20 kW).

gases have similar properties. Helium has a higher enthalpy and thus needs more heat to reach same temperature values as with argon plasma. Nevertheless, the air content was reduced mainly at the jet centerline. This indicates that the entrainment process was slowed down due to the higher viscosity of helium plasma.

Adding of hydrogen resulted in strong changes of the plasma jet and its properties. The high luminous part of the plasma flow became longer indicating prolongation of the laminar jet core and the plasma jet slightly expanded. In this case the plasma jet velocity depends almost only on the total flow rate of the plasma gas. The centerline velocity did not change, while the centerline values of temperature increased significantly. But adding of hydrogen also led to a transition of the plasma arc discharge into the restrike mode accompanied by higher fluctuations of the plasma jet. It seems that entrainment is not only a process which appears because of density and velocity gradients at the jet fringes but may also be due to a pumping effect caused by arc root movement in the restrike mode. However, the entrainment rate was the same as in a pure argon plasma jet, which can be concluded from the air content profiles. Thus, arc fluctuations do not affect the air entrainment process significantly. In fact velocity gradients play the dominant role.

The radial profiles of mass, momentum and heat flux densities calculated from the measured values of velocity, density and enthalpy of the jet are shown in Figure 4.13. The largest difference was observed in the values of the mass flux, which strongly depends on applied gas and on temperature. The value of the total mass flux, calculated from the mass

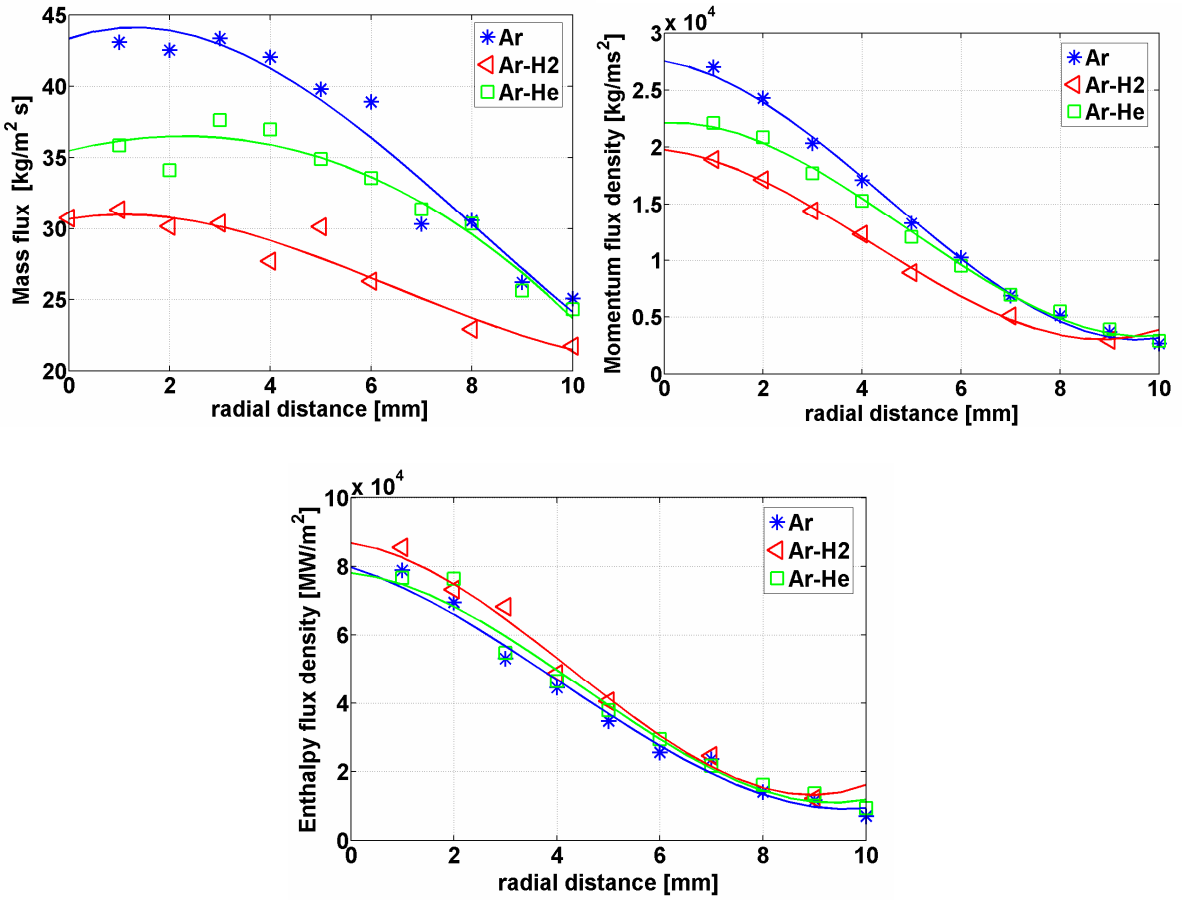

Figure 4.13 Mass, momentum and enthalpy flux density for various plasma gases at the distance 60 mm from the nozzle exit of the torch (plasma gas flow rate – 50 slm, arc power – 20 kW).

flux profiles is given by equation $G = \int 2\pi r \rho V dr$, decreased when helium or hydrogen were added as secondary gas (Table 4.8) which can be explained by the lower density of helium causing a reduction of the total density of the gas. The density of hydrogen is much less than that of pure argon and, therefore, applying of 20 % of hydrogen into the gas mixture leads to a strong density reduction. This can be observed more pronounced for higher temperatures.

The momentum flux density and total momentum flux through the jet cross section $M = \int 2\pi r \rho V^2 dr$ were also highest for the argon plasma jet. This evidences the good ability of the argon plasma to carry injected particles by the jet towards a substrate transferring momentum from plasma gas to the particles.

Table 4.8 Total mass, momentum and heat fluxes through the jet cross section(plasma gas flow rate – 50 slm, arc power – 20 kW).

Plasma gas	Total mass flux, kg/s	Total momentum flux, kg·m/s	Total heat flux, kW
Ar	0.0105	2.94	8.17
Ar-He	0.0098	2.75	8.77
Ar-H_2	0.0079	2.63	11.7

In contrary, the best conditions for heating of particles were observed in an argon-hydrogen jet. Extremely high enthalpy due to the energy of dissociation and ionization of hydrogen molecules affected the heat flux density and the measured values of the total heat flux $H = \int 2\pi r \rho V h dr$ were much higher than for pure argon or for a mixture of argon with helium. Due to the low weight hydrogen has also high heat transfer ability. In conclusion, a mixture of argon with hydrogen seems to be the most appropriate under the studied conditions.

4.3.3 Comparison of the gas and gas-water torches

There are two main differences between the gas and gas-water torches. The first is the strong difference in mass flow rate. In the hybrid gas-water torch the mass flow rate is still low in spite of adding a substantial amount of argon into the gas mixture. The mass flow rate in the gas torch could be several orders of magnitude higher. The second difference is in the principles of stabilization, which allows high thermal loading of the wall in the hybrid torch. Thus, the long arc can be established providing high arc power. The arc power in the hybrid torch can reach as high values as 130 kW under the normal operation conditions, while in the gas torch it is about 40 kW. Thus, very high plasma enthalpy can be achieved in the hybrid torch.

The comparison of the plasma jets of the torches is rather difficult. The normal operation conditions of the gas torch (about 40 kW) corresponds to the critical conditions of the hybrid plasma torch in which such an arc power can be achieved already at 200 A. Under these conditions the hybrid plasma torch has to be supplied with an exit nozzle with smaller diameter. In this case the resulting properties of the plasma jet would differ. Thus, this comparison is rather illustrative than quantitative.

Both plasma torches were operated to reach the net arc power of about 10 kW. The gas torch was supplied with 50 slm of argon and with 54 slm of a mixture of argon with 8 % of hydrogen. The hybrid torch was supplied with 17.5 slm of argon. The total gas flow rate then was almost 3 times less than in the gas torch because half of the steam-argon mixture was exhausted inside the torch chamber. The enthalpy probe measurements were done at the distance 75 mm from the nozzle exit of the torch. The plasma jet generated by the hybrid torch consisted mostly of air at such a distance, while the air amounted only about 17 % of the plasma gas at the jet centerline for the gas torch.

The resulting profiles of the plasma jet characteristics are shown in the Figure 4.14. The temperature and velocity profiles differ considerably in spite of similar conditions at the torch nozzle exit. Velocities were much smaller for the hybrid torch, although they were just little less at the nozzle exit. But the temperature was higher in the jet generated by the hybrid torch even in comparison with argon-hydrogen plasma jets.

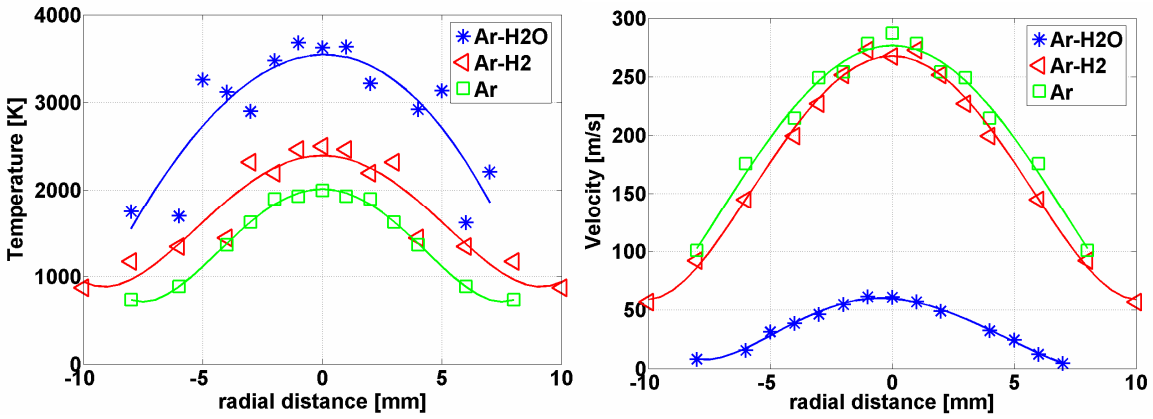

Figure 4.14 Temperature and velocity profiles of the plasma jet generated by gas and gas-water torches (arc power – 40 kW).

It is obvious that the entrainment process was much more intensive in the plasma jet generated by hybrid plasma torch under the present conditions. The main reasons of such a behavior are the strong density gradients existing at the torch exit and the strong fluctuations of the plasma jet caused by unstable operation conditions of the torch particularly around the external anode. Higher arc currents ensure more stable plasma jet generation conditions and minimize the air entrainment in the jet. The hybrid torch must be used under higher arc power generating plasma jets with higher enthalpy, temperature and velocity.

4.4 Plasma jets generated under low pressure conditions

The interesting results published about plasma jets generated under low pressure conditions put an idea to study the behavior of jets generated under such conditions in more detail. Both plasma torches were placed inside the plasma reactor from which gas was pumped out by a pump system. The detailed description of both low pressure chambers is given in Chapter 3.

Plasma jets were photographed. Plasma jet characteristics were measured by the enthalpy probe. The measurements were done in the subsonic region of the plasma flow. There are two limitations hampering measurements by this type of diagnostics in the supersonic regions. The first problem is the too high values of heat fluxes. The heat flux limit onto probe tip amounts to 1200 W, which can be reached very easily in such jets. The probe tip can not survive in such a hot environment and would be damaged. The second problem is caused by fluid dynamics during the supersonic flow past probe tip. A shock wave appears in front of the probe orifice. Thus, the enthalpy probe measures properties of the flow behind the shock, which differs from the properties of the flow itself. The analysis and recalculation must be done to obtain real values of the plasma jet characteristics.

The results were obtained in the regions far from the nozzle exit of the torch where supersonic structure does not exist any longer and the plasma jet is subsonic and fully turbulent. Nevertheless, the obtained information is very interesting not only from the scientific point of view but for applications as well because it shows correlations between supersonic and subsonic regions of the plasma jet.

4.4.1 Jets generated by the gas stabilized plasma torch under low pressures

A plasma torch with gas stabilization of arc was positioned inside the reactor whose pressure could be reduced down to 5 kPa. A transition of the plasma jet from subsonic to supersonic occurred when the internal pressure values inside the reactor were lower than 30 kPa. This was confirmed by observing the change of the plasma flow pattern. The images of the plasma jets generated under different pressures with the same plasma torch operating parameters are shown in Figure 4.15. Pure argon with a flow rate of 50 slm was applied as plasma forming gas for this comparison. The arc current was 600 A.

Two typical jet structures could be observed depending on the pressure. Reducing the pressure in the reactor down to about 30 kPa did not show strong changes in the plasma jet structure. The jet dimensions and shapes remained almost unchanged. Reducing the pressure under 30 kPa resulted first in a plasma jet prolongation, but the exit part of the plasma jet remained almost laminar and only slightly Mach knots in the jet center could be observed.

At 20 kPa the evidence of a supersonic behavior of the jet became more pronounced. The transition from subsonic to supersonic was proved by the presence of two different regions in the plasma jet: a zone with lower luminosity corresponding to a

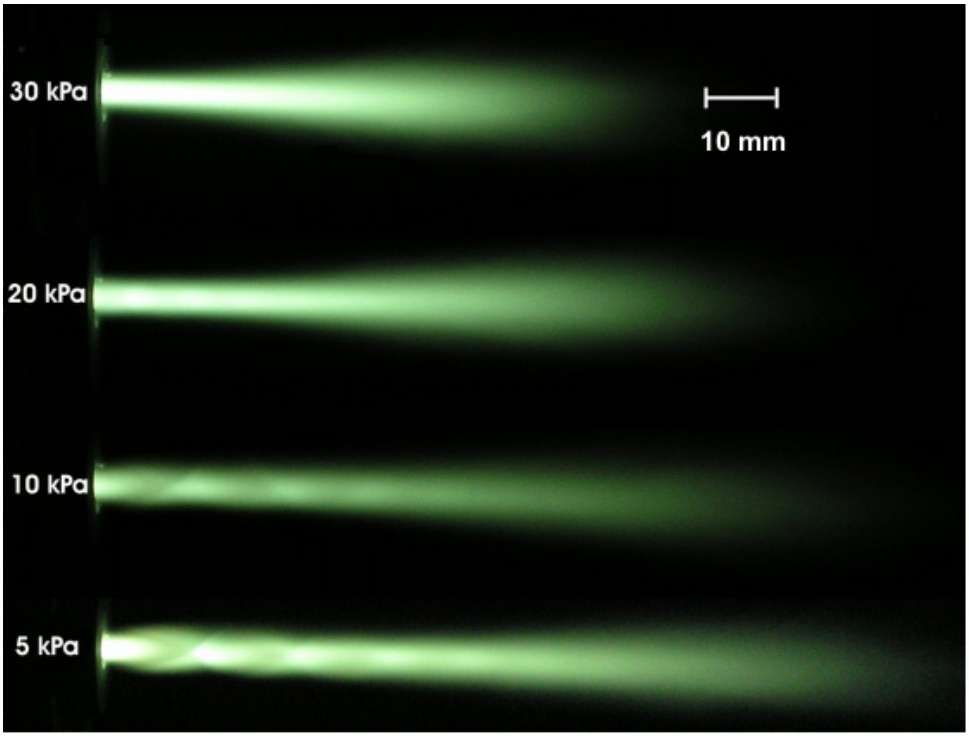

Figure 4.15 Argon plasma jets generated under different pressures in the reactor (arc current – 600 A).

supersonic velocity and lower density followed by a zone with higher luminosity corresponding to higher density, higher temperature and lower velocity. It could be seen that the plasma jet was under expanded, which means that there was a higher pressure in the torch exit than ambient pressure of the outside. Another indication that the plasma jet velocity at the torch exit reached sonic speed was the formation of compression/expansion cells (Mach knots). Starting at the exit of the nozzle a series of expansion waves could be detected downstream causing pressure reduction in the jet until the pressure in the jet is lower than in the ambience. If expansion waves were reflected at the jet's shear layer compression waves were formed. Pressure of the surrounding gas pushed the plasma jet from all sides towards the axis and coalescing compression waves form oblique shock waves, which in turn increase the plasma jet pressure. At 20 kPa it seemed that the process of pressure equalization was finished after the first expansion/compression cell. This effect was weak and an increased brightness had just begun to become distinguishable. There was no visual evidence of a second cell formation. These facts confirmed that 20 kPa seemed to be the critical pressure for the plasma jet for transition from subsonic to supersonic under the studied conditions. After one cell with a weak shock wave the plasma jet became subsonic.

At 10 kPa a shock wave formation could be clearly seen followed by a zone of high luminosity with formed diamonds. The first compression/expansion cell was followed by the second one, which is not as evident as the first, however.

Reduction of the pressure down to 5 kPa resulted in the formation of a series of expansion/compression cells. Here a zone limited by an oblique shock wave where Mach

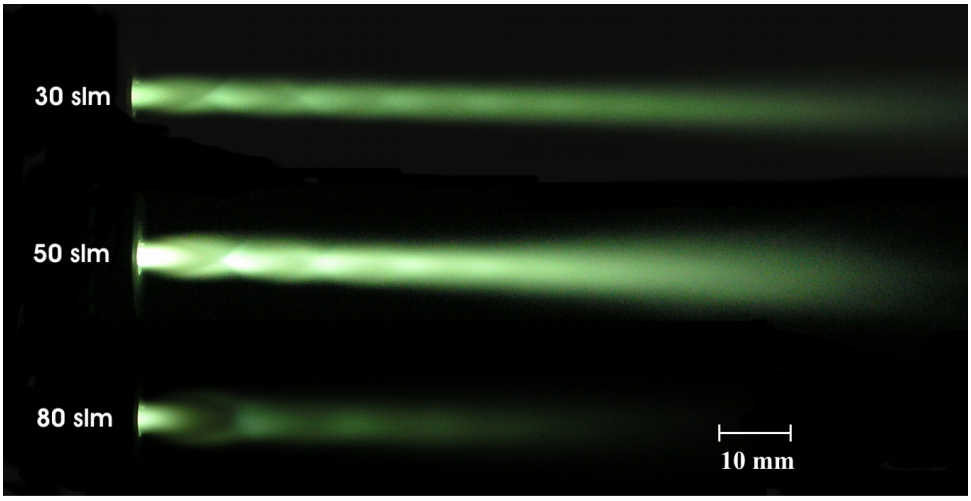

Figure 4.16 Images of plasma jets at 5 kPa for different plasma forming gas flow rates (arc current – 600 A).

number is equal to 1 became distinguishable. The compression/expansion cells extended with the pressure decreased and shock waves were formed also further away from the nozzle exit. This happened because of an increased pressure difference between the plasma jet and the surrounding gas. The jet needed more distance to reach the equilibrium pressure.

An increase of the pressure difference can also lead to another type of flow reflection, the so-called "Mach disc formation". If a plasma gas passes through a shock, its velocity component normal to the shock is greatly reduced but its parallel component remains unchanged. This mechanism is very effective in slowing down the jet and in shortening the plasma plume. The transformation of the flow structure could be observed when the flow rate of the plasma gas was increased. Such a change of the flow structure is shown in Figure 4.16. For argon flow rates of 30 and 50 slm normal reflections were formed, while increasing the argon flow rate to 80 slm a Mach disc formation resulted. For higher argon flow rates the pressure in the jet increased. For 80 slm the pressure difference was so high that an abrupt change in the flow structure occurred resulting in a plasma jet shortening. In contrast to the following ones the edges of the first expansion zone were brighter because of a reflection of the expanding flow at the cold dense surrounding gas (the so-called 'barrel shocks formation').

The experimental study of the supersonic region of the plasma jet was difficult to perform because of the limitations of the diagnostic tools. Nevertheless, the behavior of the plasma jet in subsonic regions is not less interesting than in the supersonic. The process of the jet transition into the turbulent state under the low pressure conditions and the entrainment process in the low density surrounding have the need for a more closed study.

All measurements of the plasma jet characteristics were performed at a distance z = 100 mm from the torch nozzle exit where supersonic structure did not exist any longer and the plasma jet was subsonic and fully turbulent. However, decreasing of the pressure in the reactor lower than 20 kPa caused difficulties for the enthalpy probe measurements because of the impossibility to reach isokinetic sampling conditions. These limitations

were given by the pumping capacity of the pumping system of the enthalpy probe, which provides gas sampling. In the range of the performed experiments an isokinetic ratio between 0.6 and 1 can be supposed to be reliable corresponding to an extent of error following from enthalpy probe analysis (Figure 3.19). Measurements with an isokinetic ratio lower than 0.6 were not taken into consideration.

Figure 4.17 represents the values of the dynamic pressure $p_d = \frac{V^2}{2}\rho$ (ρ - density, V - velocity) at the jet axis depending on reactor pressure, which were measured directly and were not affected by recalculations by means of tables of thermodynamic properties. In fact these values reflect the momentum flux of the plasma jet at the given point. The dynamic pressure increased slowly when the ambient pressure is reduced down to 10 kPa. The most significant changes in the dynamic pressure and momentum flux happened when the pressure was reduced under 10 kPa. The dynamic pressure at 5 kPa was two times higher than that at 10 kPa. Such a rise can be explained by a strong increasing of the plasma jet velocity (Figure 4.18). Plasma jet velocity and temperature changed in the same way. A transition of the plasma flow to supersonic became apparent in formerly subsonic regions only at pressures below 10 kPa. The plasma velocity started increasing more quickly at pressures below 20 kPa and a drastic velocity rise occurred at pressures lower than 10 kPa. For pressures higher than 10 kPa the supersonic structure rapidly broke down. At the same time downstream regions of the plasma jet almost did not suffer that

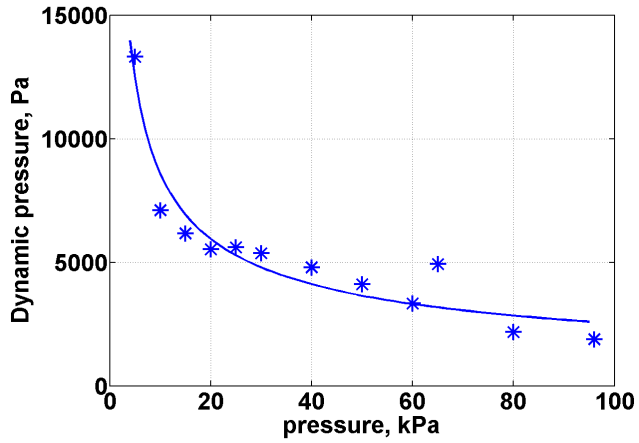

Figure 4.17 Development of the dynamic pressure in the jet center with the pressure changes at position z = 100 mm (arc current – 600 A, argon flow rate – 40 slm).

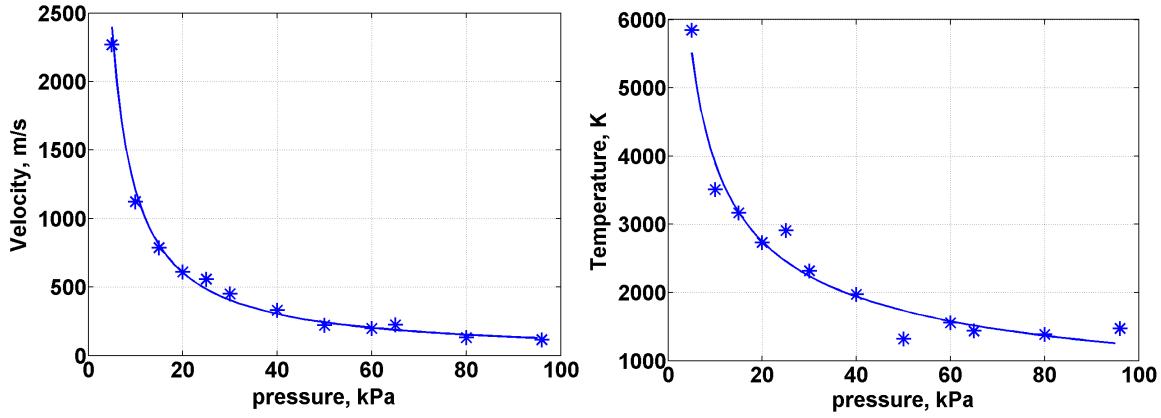

Figure 4.18 Dependence of the plasma jet properties at the jet centerline on pressure at position z = 100 mm (arc current – 600 A, argon flow rate – 40 slm).

transition.

Plasma jet temperature increased with pressure reduction. This was caused by the reduction of the density of the ambient gas which was entrained into the jet. Less energy from the plasma flow was consumed by entrained low density cold gas and the plasma temperature remained higher for the longer distance.

The radial profiles of the plasma jet characteristics measured at a distance of z = 100 mm from the nozzle exit are shown in Figure 4.19. The radial recording of the plasma jet velocity showed a plasma jet expansion for lower pressures. Velocity profiles of the jets for 20 kPa and 30 kPa differed slightly, which corresponds to the visual impressions of the plasma jets (Fig. 4.19) showing a plasma jet transition to supersonic behavior for pressures below 20 kPa. The radial dimensions of the high temperature plasma jet region were not altered, while the centerline temperature increased from 2500 K for 30 kPa to 6000 K for 5 kPa. Thus, the temperature gradients increased. However, the temperature at the plasma jet fringes remained independent from the ambient pressure. Plasma jet fringes contained mostly warmed up entrained ambient air, whose temperature was independent of the chamber pressure.

Hence, all facts mentioned here indicate a prolongation of the plasma jet hot core at reduced chamber pressures and a decreasing of the ambient air entrainment.

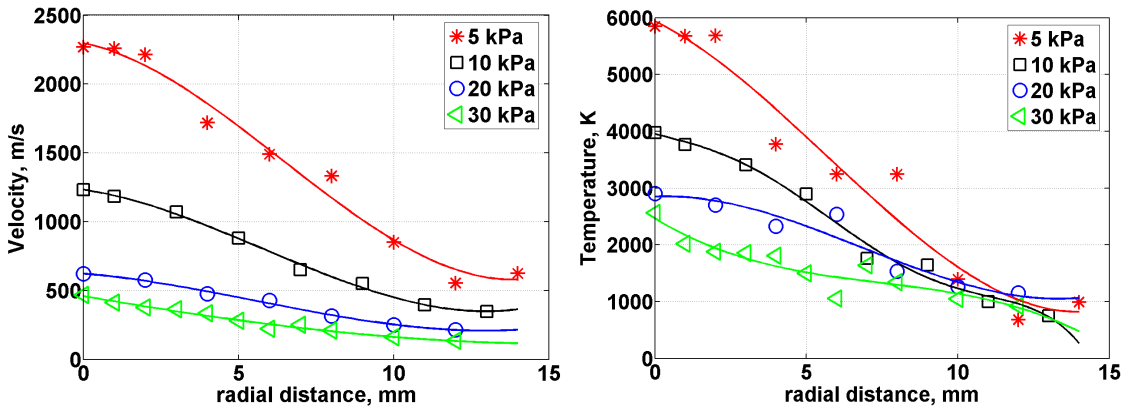

Figure 4.19 Radial profiles of the plasma jet characteristics dependent on ambient pressure at the position z = 100 mm (arc current – 600 A, argon flow rate – 40 slm).

4.4.2 Jets generated by hybrid gas-water torch under low pressures

Plasma jets generated by hybrid gas-water stabilized torch substantially differ from jets generated by gas stabilized torches, especially concerning plasma jet temperature, velocity and density at the plasma torch exit as it was shown above. That is why the results obtained for jets generated by gas stabilized torches cannot be simply used for the hybrid torch. These differences could lead to a different gas dynamic behavior of the jets and their different interactions with low pressure surrounding. Moreover, a plasma torch with hybrid

stabilization of the arc has the anode outside the torch chamber. This means that arc operation could be affected by ambient pressure.

The plasma torch with hybrid water-argon stabilization of the arc was attached to the reactor. Pressure inside the reactor was varied in the range of 4 to 100 kPa.

Three different structures of the plasma flow were observed. For pressures from atmospheric to 40 kPa plasma jet remained subsonic without significant changes in the jet shape and length. Only the plasma jet brightness was reduced for lower pressures. For pressures below 40 kPa the plasma jet started transiting into the supersonic flow (Fig. 4.20). Similarly to the gas torch, visualization shows underexpanded character of the supersonic flow with higher pressures at the torch nozzle exit comparing to the ambient gas pressure. A high luminosity region at the nozzle exit was followed by a low luminosity region characterized by supersonic velocities. The plasma jet pressure was adapting to the ambient pressure resulting in the formation of the expansion/compression cell. Unlike with the investigations of gas-stabilized jets, there was no evidence of the second compression/expansion cell formation. It seems that the process of pressure equalization was finished after the first cell and the plasma jet became subsonic.

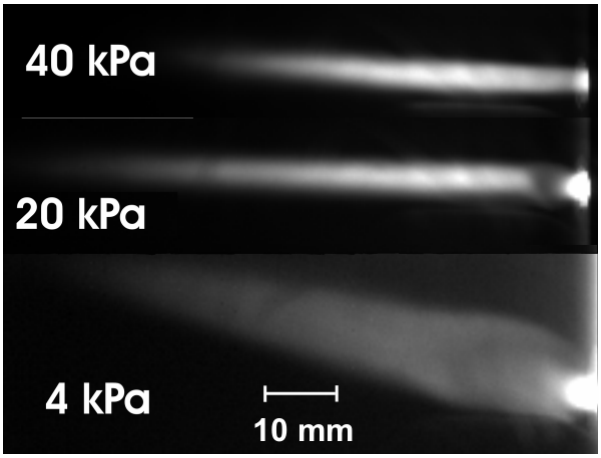

Figure 4.20 Images of plasma jets generated by hybrid torch at different pressures (arc current – 150 A, argon flow rate – 12,5 slm).

Reduction of the pressure down to 4 kPa resulted in the formation of another flow structure. Because of the high difference in the pressures the plasma jet underwent a strong expansion. The jet diameter rapidly increased right at the nozzle exit forming the low brightness of the supersonic zone. It seems that compression waves could not coalesce to form a shock wave. A zone of high pressure and temperature did not exist. The plasma jet becomes subsonic. Such a jet behavior corresponds to so-called ‘scattering regime’, which is characterized by disappearance of well-delimited shock waves.

The specific development of the jet with pressure reduction and fast break down of the supersonic structure may be caused by two factors. The first is strong interaction with ambient gas even under low pressure conditions. The shear layer between the plasma jet and ambient gas grows fast due to extremely high velocity and density gradients. The second reason may be the arc which passes through the supersonic zone of the plasma jet.

Dissipation of energy into the plasma jet and interaction of the main jet with the anodic jet may affect the flow dynamics of the supersonic flow.

Properties of the plasma jet were measured in the subsonic region by the enthalpy probe. The main results are represented in the Appendix B. Dependences of the plasma jet characteristics on pressure, arc current and flow rate of plasma forming gas were studied.

The results showed similar behavior of the plasma jet generated by the hybrid gas-water torch and the plasma jet generated by the gas torch under low pressure conditions. Both the plasma temperature and the velocity increased when the pressure was reduced. Velocity increase was substantially more significant for pressures below 20 kPa, when the transition to supersonic flow behaviour took place. The reduction of the entrainment was the main reason of the observed increase of plasma temperature and velocity accompanied by a decrease of the oxygen content. The plasma jet characteristic profiles were smoother without sharp gradients at the fringes. Fluctuations of the plasma jet were decreasing as well. The study showed that the hybrid torch operated under low pressure could provide a wide range of conditions for applications.

4.5 Investigation of shroud gas effect on plasma jet properties

4.5.1 Shrouding of the plasma jet generated by hybrid torch

Shielding system for hybrid gas-water stabilized torch

Usually in nontransfered arc plasma torches shroud nozzles are attached to the plasma torch exit [99-105]. The external anode applied in the hybrid plasma torch makes it difficult to apply such a construction. That is why the shielding system was positioned at a distance of 25 mm from the torch nozzle exit right after the anode (Fig. 4.21).

The system for shielding consisted of a ring for shroud gas distribution and supply, and a ceramic tube. The ring was 78 mm in diameter and 10 mm in width of the front part (Fig. 4.22). It was made of stainless steel and was not cooled. Several holes with diameters of 1 mm each were made in the ring to distribute the shroud gas around the plasma jet. The shroud gas flow was directed parallel to the torch axis. The solid wall was made from a ceramic tube 100 mm in length, which was placed downstream the ring. The tube was removable and was not cooled. The ceramic tube protected the surrounding of the plasma jet from air entrance altering the surrounding atmosphere. The shielding system was centered with respect to the exit nozzle. First, the feeding of the shroud gas was made through one port entering to the distributing ring at its top (Fig. 4.22 a)). But this arrangement turned out to be unsatisfactory as it could not provide proper distribution of the shroud gas around the jet. As a result the flow rate of the shroud gas at the bottom part of the ring was higher than at the top part. The ring was divided then inside into three sections by partitions and shroud gas was now supplied through three ports from different sides to avoid improper shroud gas distribution (Fig. 4.22 b)).

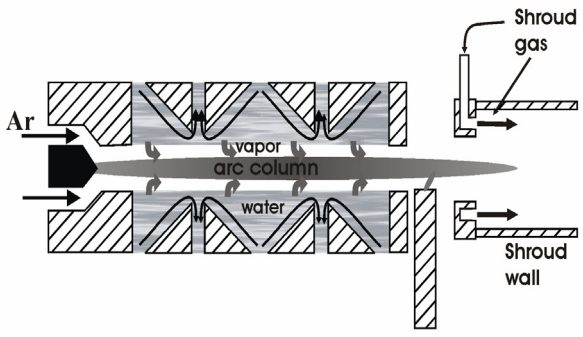

Figure 4.21 Hybrid argon-water torch with the system for shielding.

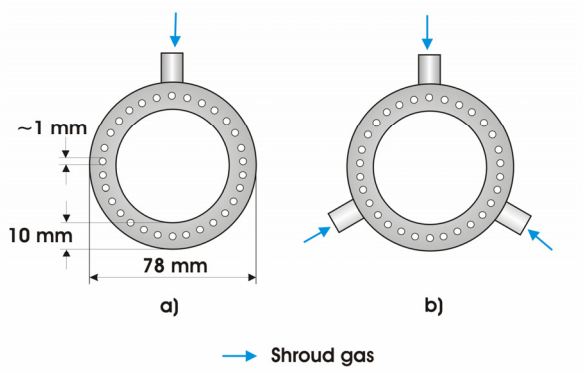

Figure 4.22 The ring for gas shroud distribution: a) one gas entrance; b) three gas entrances.

Several gases were applied. First, effect of nonreactive argon was studied. Further, argon was replaced with reactive acetylene, methane, and a safety mixture of hydrogen with nitrogen (5% of H_2). The choice of the shroud gases was dictated not only by the necessity to reduce the oxygen content entrained from the surrounding, but also by oxygen

contained in the plasma gas from the products of dissociation and ionization of water. The problem with gas distribution appeared when pure acetylene was used as a shroud gas. At temperatures about 400 °C the pyrolysis of acetylene starts. As the ring was not cooled its temperature rose fast during acetylene combustion. Carbon precipitated inside the ring blocking the holes. To avoid this effect acetylene was mixed with nitrogen, which enabled a cooling of the ring.

The present measurements were done under atmospheric pressure conditions. In all experiments the argon flow rate was 17.5 slm and the arc current 300 A. The arc voltage under these conditions was about 250 V, which corresponded to an arc power of 75 kW. The enthalpy probe scanned the jet at a distance of 200 mm from the nozzle exit, which corresponded to 65 mm from the end of the ceramic tube.

The effect of the shroud gas was studied for two cases – with and without ceramic tube.

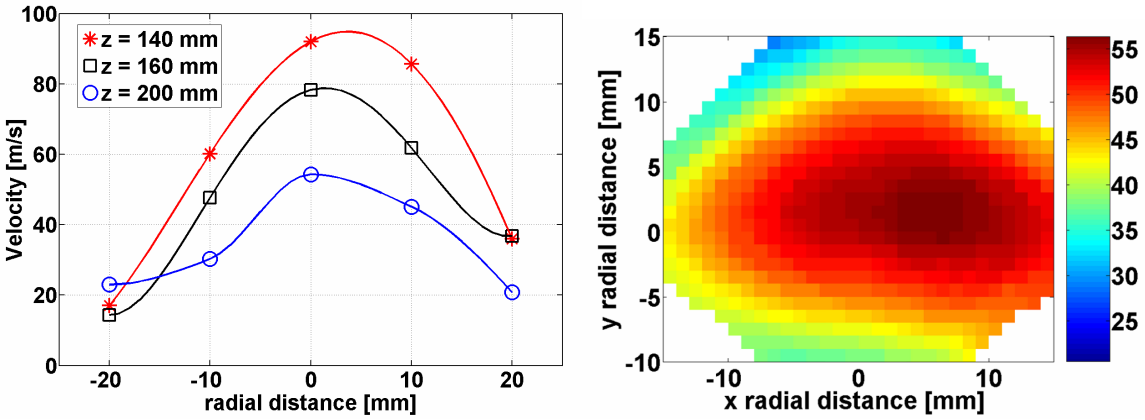

a) b)

Figure 4.23 Vertical velocity profiles along the jet a) and distribution of velocity at the distance z = 200 mm b) The jet was shrouded by a C_2H_2/N_2 mixture. Colorbar in b) depicts values of the plasma jet velocity (argon flow rate – 17.5 slm, arc current – 300 A).

Shielding by wall and gas

Figures 4.23 and 4.24 represent properties of the plasma jet when the ceramic wall was applied. The application of the shielding system heavily affected the plasma flow. As it was mentioned before plasma jets generated by the hybrid torch are not axisymmetric and the axis does not concur with the plasma torch axis because of interaction of the main flow with the anode jet. Radial velocity profiles made during vertical scanning of the jet show the deflection of the jet centerline (maximum values of velocity) from the plasma torch axis (Fig. 4.23 a). In the measurements the shielding system with ceramic wall and a mixture of 20 slm of C_2H_2 and 20 slm of N_2 was applied. The deflection of the jet inside the ceramic tube existed in spite of applying 40 slm of shroud gas around the jet. The deflection made up several millimeters at the distance of 200 mm, which is confirmed by the highest values of velocity on Figure 4.23 b). The Figure 4.23 b) represents the map of the velocity in the plasma jet cross section at the distance 200 mm from the nozzle exit. The x distance means the horizontal direction of the plasma jet scanning and the y stays for

vertical scanning. The velocity distribution shows how the shielding wall could affect the plasma flow. The plasma jet was not round but flattened out from the top which could be the result of the jet interaction with the ceramic wall of the tube, which represents a barrier not allowing an unaffected flowing of the plasma gas. The flow pattern could have been

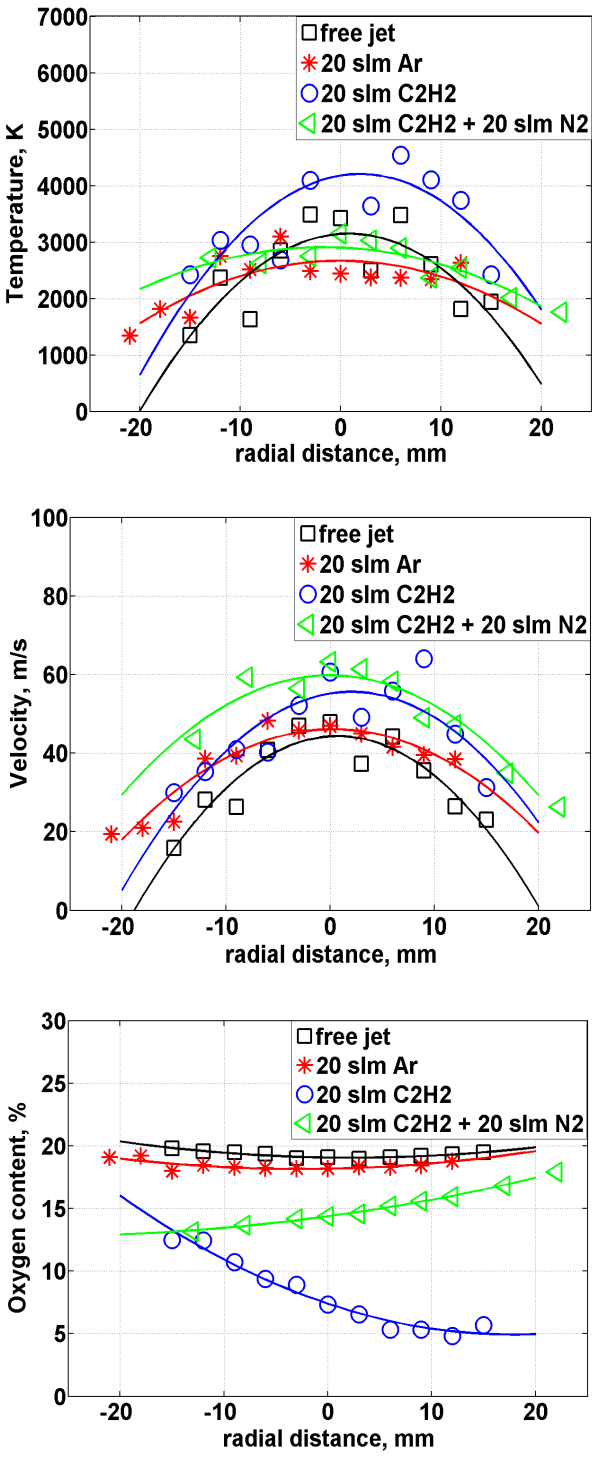

Figure 4.24 Properties of the plasma jet at the distance 200 mm without shroud gas and with argon and acetylene shrouding (shrouding with the ceramic tube).

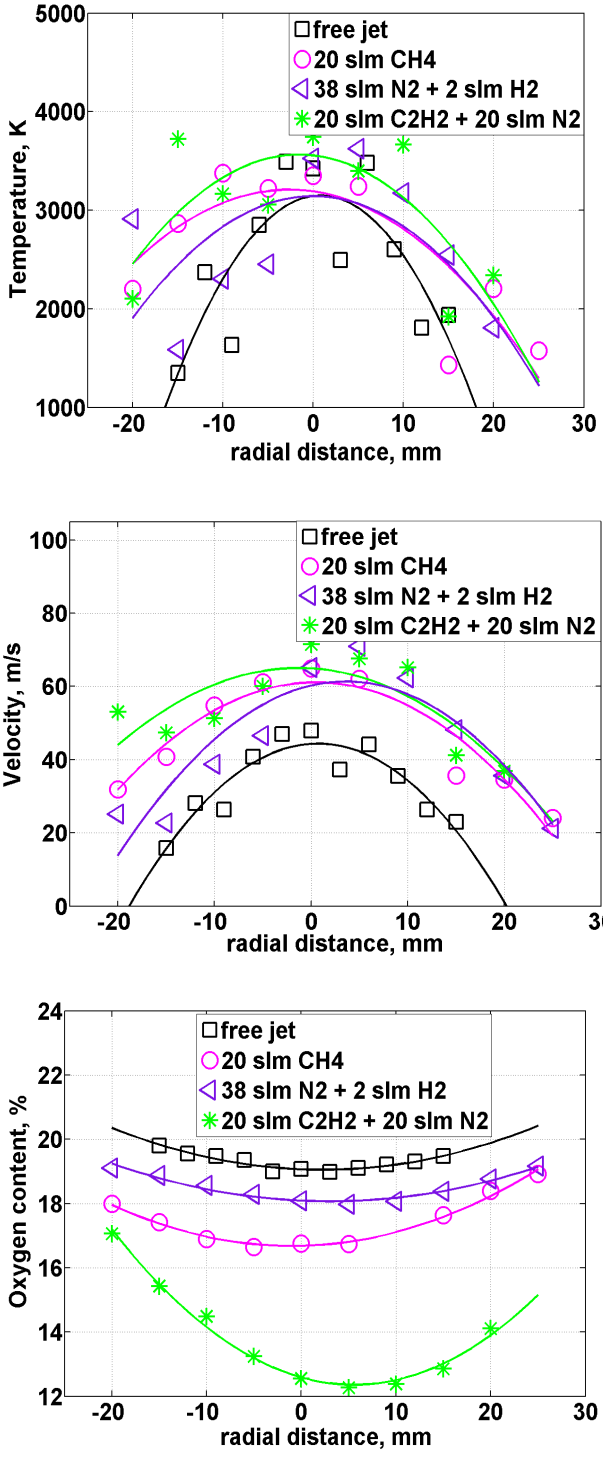

Figure 4.25 Properties of the plasma jet at the distance z = 200 mm without shroud gas and with CH_4, N_2/H_2 and C_2H_2/N_2 shrouding (shrouding without the ceramic tube).

also influenced by the shroud gas itself. Being exited from the holes the shroud gas formed small jets flowing not parallel to the jet centerline and, moreover, spreading around the jet. Both flows ran into each other mixing and disrupting one another. Furthermore, shroud gas contained reactive acetylene which by burning could result in disturbances of the plasma flow. All mentioned factors together with the effect of the rotating anode resulted in the jet deflection and flattening.

Temperature, velocity and oxygen content in the jet are shown in Figure 4.24 for free jet, when no shroud gas was applied, and for the cases of shrouding by argon and acetylene and the mixture of acetylene with nitrogen as well. The oxygen percentage in the free jet shows that the jet consisted mostly of heated air. The zero point on the x axis corresponds to the centerline of the jet.

The results showed just small effect of the argon shrouding on the properties of the plasma jet. The profiles of the plasma jet characteristics show that the shroud gas improved the free stream region as the plasma jet became wider without strong gradients at the jet fringes. The temperature values of the jet went down slightly because of the influence of cold argon consuming a part of energy from the jet for its heating. The velocity of the jet remained unchanged. The concentration of oxygen decreased just a little. Further increasing of the argon flow rate up to 120 slm resulted just in minor changes of the oxygen content in the jet center accompanied by a minor temperature reduction. These results indicate that air entrainment is most intensive in the part of the jet close to the nozzle exit, which was not protected by the gas shielding while in the region, where shroud gas acted, entrainment rates already slowed down.

Argon shroud gas was replaced by reactive acetylene. The acetylene reacts very intensively with the oxygen already at temperatures close to 300 °C. A reaction of acetylene with oxygen results in the formation of carbon oxides. Moreover, the injection of acetylene introduces a further energy source as the combustion heat of 58.6 MJ/m^3 will be released. The results showed strong changes of the plasma jet characteristics when acetylene was applied. The oxygen content was reduced when the acetylene flow rate was increased and already 20 slm of acetylene allowed a reduction of the oxygen content to values about 5 %. Temperature and velocity of the jet increased. This effect was caused by a reaction of oxygen with acetylene accompanied by heat release. Consequently, the high-temperature high-velocity region was extended significantly. This is expected to provide better particle heating and acceleration with reduced particles oxidation, and thus improving spraying process efficiency and deposition quality. The shifted profile of the oxygen content was caused by nonuniform distribution of the shroud gas due to the holes, which became cluttered because of acetylene pyrolysis.

Mixing of acetylene with the same amount of nitrogen resulted in better distribution of the shroud gas around the jet. As nitrogen is a diatomic gas it consumes energy from the plasma flow for the dissociation. Thus, adding of nitrogen causes a reduction of the temperature. Moreover, a higher total shroud gas flow rate results in a higher discharge velocity of the shroud gas through the holes. This could affect process of acetylene combustion. On the other hand, a higher shroud gas flow rate leads to smaller velocity

gradients at the jet fringes, which in turn reduces the process of plasma jet deceleration caused by entrainment. Thus, the plasma jet velocity was increased.

Shielding by gas

In Figure 4.25 there are results of the experiments where the ceramic tube was removed and only the effect of the shroud gas was studied. In addition to a mixture of acetylene with nitrogen, methane and the mixture of nitrogen with hydrogen were examined. Methane is also combustible, but it is more stable and its pyrolysis starts at much higher temperatures, which allowed to use it without addition of other gases. Like acetylene, methane is also a source of heat as its combustion is accompanied by a release of 37 MJ/m^3 of heat. In the combustion reaction one molecule of methane binds 2 molecules of O_2, whereas a molecule of acetylene 2.5. In spite of this, methane is preferable as shroud gas since it is better to store and to handle. In addition, a safety mixture of hydrogen with nitrogen was examined in the experiments with 5 % of H_2.

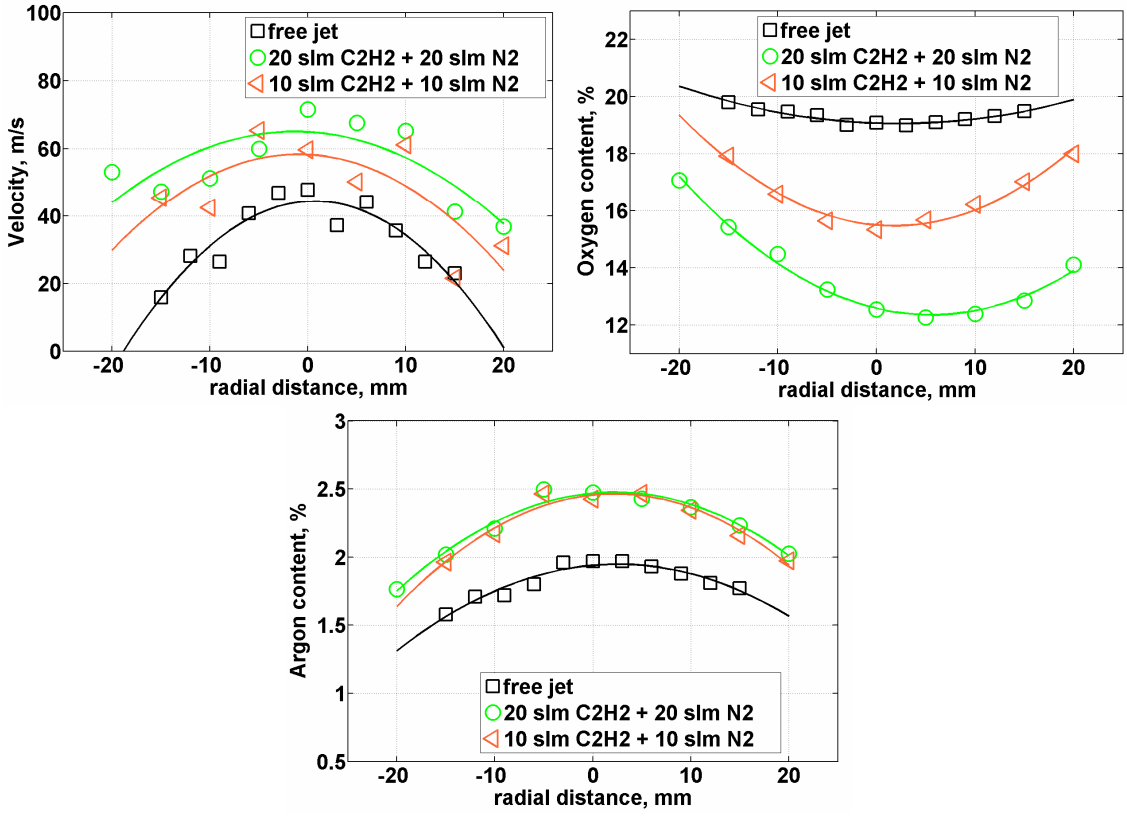

Figure 4.26 Effect of shroud gas flow rate on the properties of the plasma jet at a distance z of 200 mm without the ceramic tube.

Similarly as in the case of the ceramic tube, the shroud gas application resulted in the flattening of the plasma jet characteristics for all shroud gases. Using of the H_2/N_2 mixture led to an increase of the temperature at the plasma jet fringes, while the centerline temperature was unchanged. The temperature of the jet was a little bit higher when acetylene and methane were used because of the released heat of the combustion. The velocity increased for all shroud gases, the centerline velocity increased by almost 30 %

from 45 m/s to near 60 m/s. The results show that H_2/N_2 shrouding only replaces air from the ambient atmosphere and thus reduces available oxygen to be entrained from the surrounding. Hydrogen binds oxygen atoms but its amount is too small to provide proper oxygen elimination. The increase of the hydrogen flow rate to 4 slm, so that the hydrogen content amounted to10 % in the mixture, had no effect on the oxygen content in the plasma jet and was not studied deeply, therefore. Acetylene and methane not only replace air but also consume a significant amount of oxygen by the combustion process. Acetylene shrouding provided the best results concerning oxygen reduction together with improvement of the plasma jet characteristics.

Effect of shroud gas flow rate

The effect of shroud gas flow rate is illustrated in Figure 4.26. Acetylene was mixed with nitrogen in a ratio of 50 % to 50 %. The shroud gas flow rate was set to the values 20 and 40 slm. The oxygen content decreased for higher flow rates of the shroud gas, while the velocity increased. The argon content reflects the amount of plasma in the jet. The argon content increased when C_2H_2/N_2 shrouding was used, but it was almost independent on shroud gas flow rate. Increasing of the shroud gas flow rate had no effect in the center of the jet and had only negligible effect at the plasma jet fringes. The results confirmed that the entrainment process was slowed down by shroud gas supply which could be the consequence of two factors. As the shroud gas exits from the holes it immediately starts to react intensively with air. The reaction of the acetylene with oxygen is accompanied by heat release, which results in heating of the plasma jet surrounding. Thus, ambient gas bubbles getting into the plasma jet in the process of the entrainment and cooling and slowing down the jet has a lower density and could travel and mix up quicker in the plasma jet in comparison with cold air bubbles. The process of the plasma jet velocity reduction slows down. Moreover, in contrast to stagnant air surrounding, shroud gas moves in the same direction as the plasma jet reducing velocity gradients at the jet fringes and slowing down the process of bubble formation.

4.5.2 Shroud nozzle application in the gas stabilized torch

For the experiments described in the following a specially designed shroud nozzle was fixed onto the exit of the quick connectable plasma torch both installed within the plasma reactor. In most experiments the shroud gas was supplied in parallel to the jet axis direction. Only a few experiments were performed with a swirl shrouding. The experimental setup and main results are shown in Appendix C. Additionally obtained results are presented in the subsequent section.

In all experiments presented in this section the arc power of the plasma torch was 20 kW. Most of the measurements were done under a chamber pressure of 40 kPa, which eased the performing of the experiments. Furthermore, they are giving simultaneously valuable information for normal pressure operation of the shroud arrangement. Some few

measurements were done under atmospheric pressure conditions. These will be specified for each experimental result.

Effect of shroud gas

Effects of the nature of the shroud gas (nitrogen and argon) and the shroud gas flow rate were tested (a more extended description is given in Appendix C). Nitrogen affected the plasma jet more than argon, which particularly became apparent at the jet fringes. Therefore, argon seemed to be more suitable for shroud purposes. The flow rate of the shroud gas was varied from 10 to 120 slm. The results confirmed that an injection of shroud gas diminishes the interaction of the jet with surrounding air and delays the drop of plasma jet temperature and velocity. The optimum shroud gas flow rate seemed to be 80 slm of argon. For this case the centerline temperature was considerably increased while air content was decreased correspondingly. Increasing the flow rate of the shroud gas up to

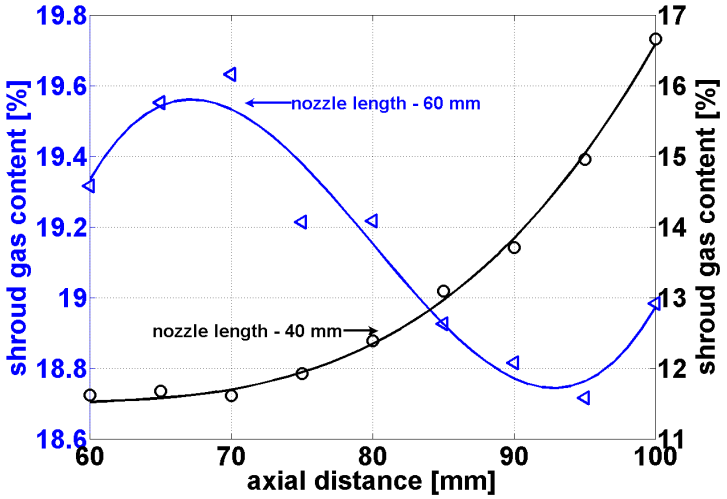

Figure 4.27 Axial distribution of the shroud gas in the jet (shroud gas – nitrogen, shroud gas flow rate – 20 slm).

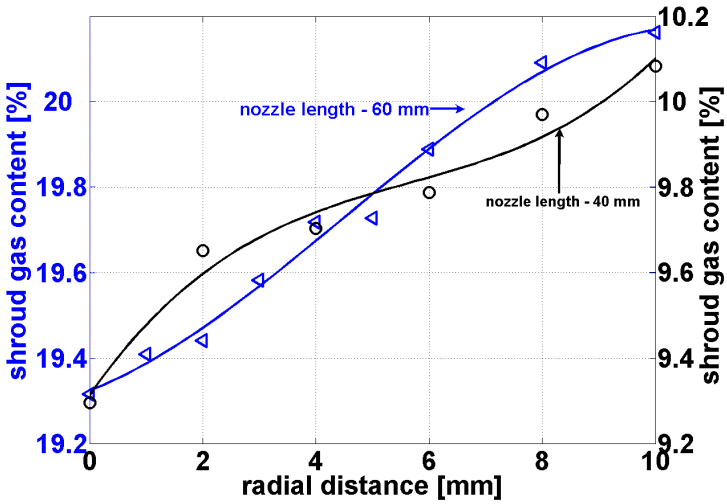

Figure 4.28 Radial distribution of the shroud gas in the jet (shroud gas – nitrogen, shroud gas flow rate – 20 slm).

120 slm disturbed the plasma jet too much causing a reduction of plasma jet temperature and velocity.

In Figures 4.27 and 4.28 the axial and radial concentrations of the shroud gas in the plasma jet are shown for two shroud nozzle lengths, 40 and 60 mm. The flow rate of the shroud gas was 20 slm and the gas was supplied under an angle of 135° with respect to the plasma jet axis in both cases. Nitrogen was used as shroud gas to discriminate from plasma gases, which did not contain N_2. Nitrogen contribution from air was eliminated by recalculating the air amount in the jet from the concentration of oxygen.

Another variable parameter was the width of the slot through which the shroud gas was supplied. In case of the shorter 40 mm nozzle it was 2 mm, while the longer nozzle was tested with a 1 mm slot. Smaller slot widths for the same shroud gas flow rate resulted in higher shroud gas outlet velocity.

The results showed a totally different behavior of the shroud gas mixing with the plasma jet with this device. The amount of shroud gas in the jet was lower for the shorter shroud nozzle. The percentage of shroud gas rose along the centerline although the change was not significant and amounted to 1% on the distance from 60 to 100 mm from the nozzle exit of the torch.

The amount of shroud gas at the centerline of the jet changed differently when a longer nozzle with a smaller slot width was applied. Doubled outlet velocity of the shroud gas directed under an angle with respect to the jet centerline caused disruption of the plasma flow. This could be confirmed experimentally as the shroud gas percentage increased at the jet centerline up to 70 mm from the nozzle exit. At distances higher than 70 mm the amount of shroud gas decreased probably because of a distribution of the shroud gas over the whole jet.

The radial distribution of the shroud gas for different shroud nozzles showed also different behavior. Such differences may be attributable to the place of measurement. Both measurements were done at the same distance of 60 mm, which corresponded to the exit of the longer nozzle.

The results showed that shroud gas could disturb the main plasma flow. To eliminate such a plasma jet disturbance it should be better to reduce the angle of shroud gas injection. The shroud gas should be supplied directly around the jet in the least intrusive way to eliminate altering of the original flow field of the jet.

The slot width for the shroud gas plays also an important role. Increasing the slot width resulted in two opposite effects for the same gas flow rate. On one hand a wider slot leads to a decreasing of the outlet shroud gas velocity. On the other hand the shielding thickness increased. However, these interchangeable effects only showed a slight influence on the plasma jet properties, which is confirmed by Figures 4.29 and 4.30. In these experiments the nozzle with a length of 60 mm was used and 40 slm of shroud argon was applied. In axially direction no influence on the air content and velocity could be detected by varying the slot width. By using a 1 mm slot the temperature was higher in the regions inside and close to the shroud nozzle. This could be explained by a lowering of the convective cold air suction from the surrounding gas inwards the shroud nozzle due to a pressure gradient between the inner and outer part of the nozzle. Otherwise, the effect of

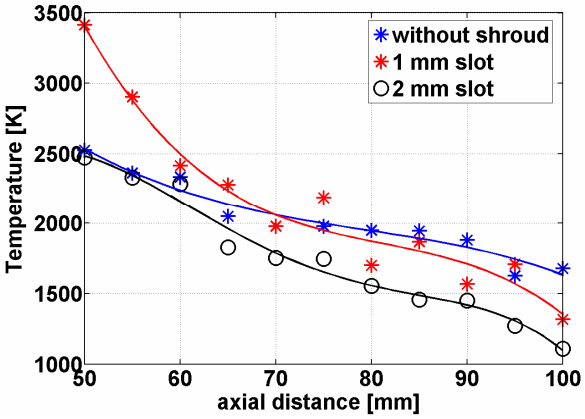

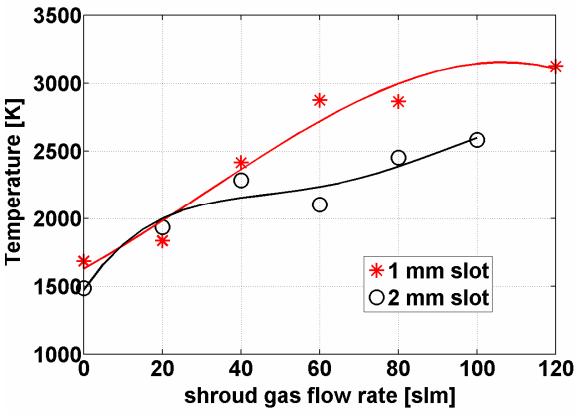

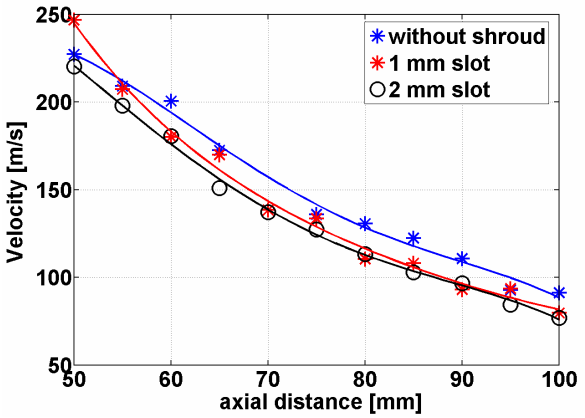

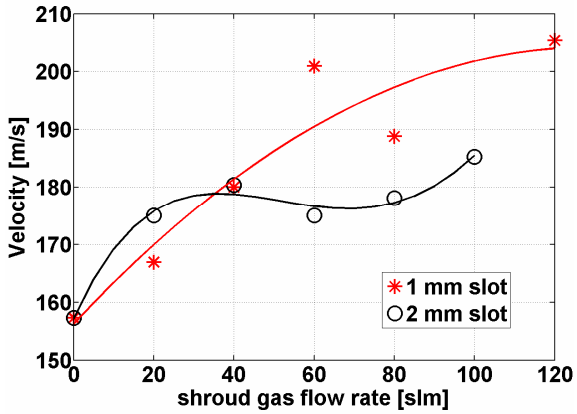

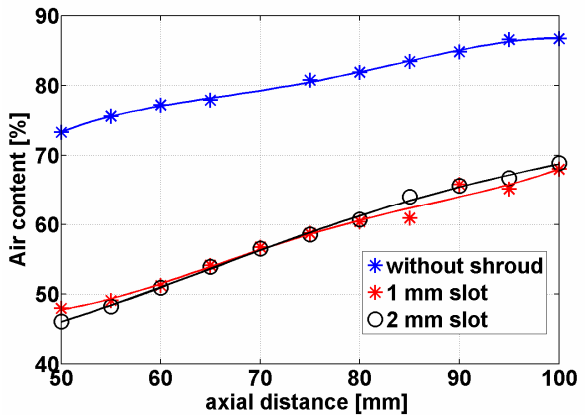

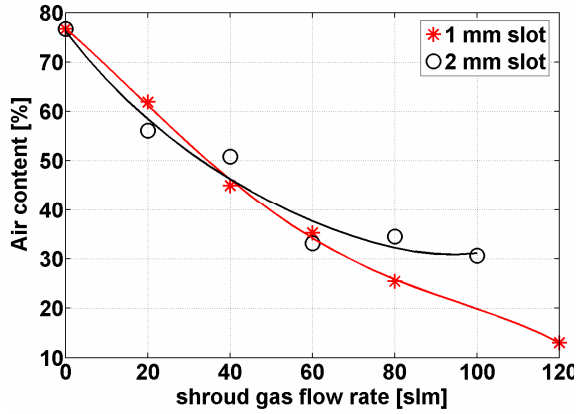

Figure 4.29 Properties of the plasma jet dependent on slot width of the shroud nozzle at the jet centerline (shroud gas – argon, shroud gas flow rate – 40 slm).

Figure 4.30 Properties of the plasma jet at the centerline position z = 60 mm dependent on shroud gas flow rate for two slot widths of the shroud nozzle (shroud gas – argon)

slot width became more pronounced for shroud gas flow rates higher than 40 slm. The dependence of the plasma jet characteristics on shroud gas flow rate was measured at point z = 60 mm on the centerline of the jet. The shroud gas flow rate was varied between 0 and 120 slm. The centerline temperature and velocity were higher when the slot width was decreased from 2 mm to 1mm, as well as the air content decreased being the evidence of a reduced air entrainment.

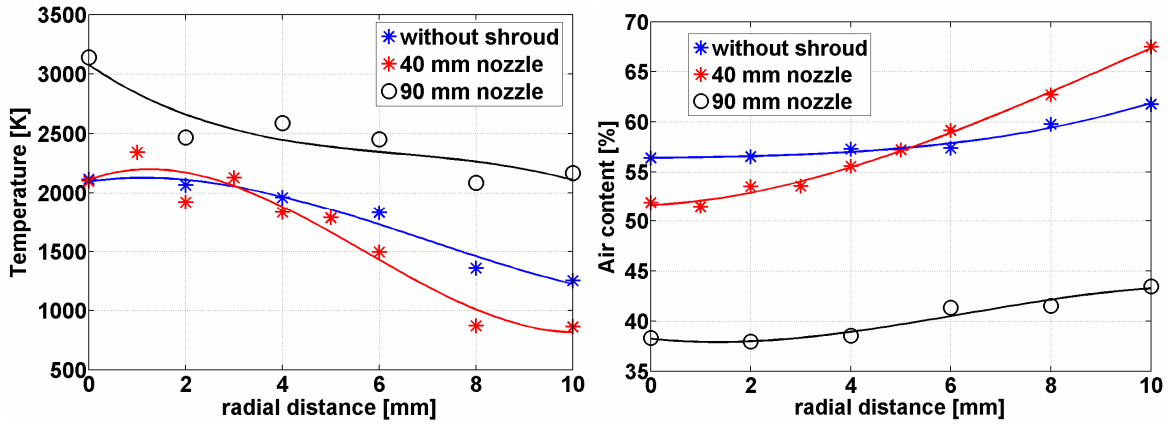

Figure 4.31 Radial profiles of the plasma jet temperature and air content without shrouding and with shroud nozzles of 40 and 90 mm length at the distance z = 60 mm from the nozzle exit (shroud gas flow rate – 40 slm).

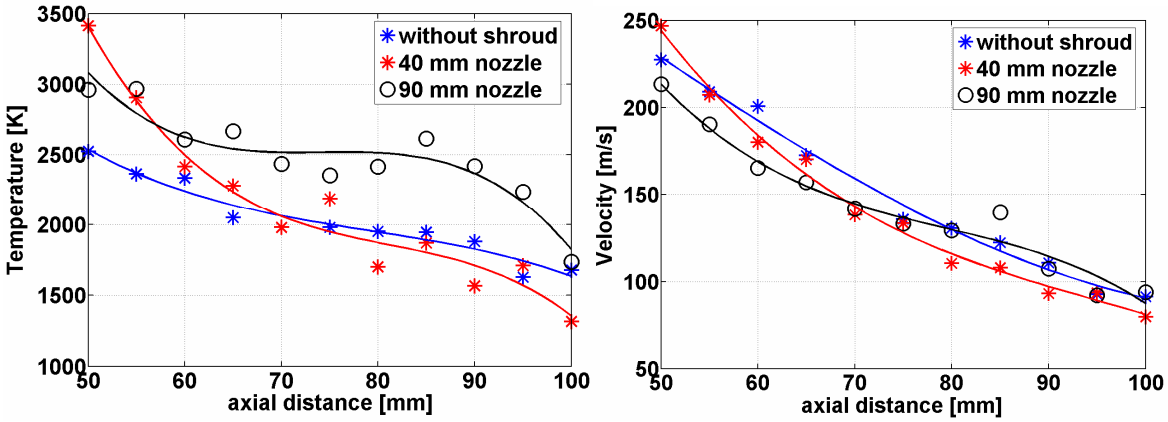

Figure 4.32 Temperature and velocity at the plasma jet centerline without shroud gas and with shroud nozzles of 40 and 90 mm length (shroud gas flow rate – 40 slm).

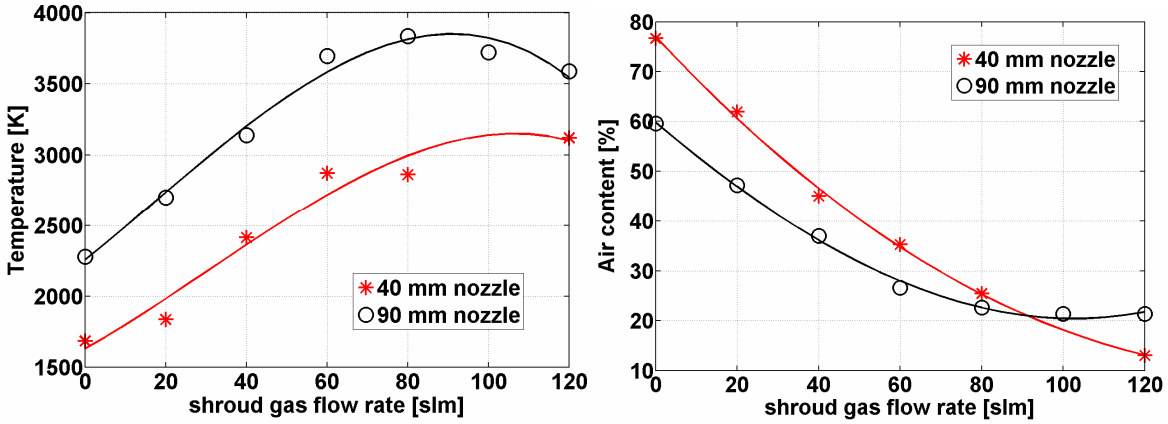

Figure 4.33 Temperature and air content as a function of shroud gas flow rate at the plasma jet centerline at the position z = 60 mm from the nozzle exit for 40 and 90 mm shroud nozzles (shroud gas flow rate – 40 slm).

As a conclusion the smaller slot width appeared to be better, which means the shielding effect depends on the mass flux of the applied shroud gas.

Effect of nozzle length

The effect of nozzle length on air entrainment is depicted in Figures 4.31, 4.32 and 4.33. Experiments were carried out under atmospheric pressure. The flow rate of argon shroud gas was set to 40 slm and was equal to the plasma gas flow rate.

The results showed that the length of the shroud nozzle represents an important factor. The first pair of graphs shows radial profiles of the plasma jet temperature and air content at a distance z = 60 mm from the nozzle exit of the torch (Fig. 4.31). In case of the longer nozzle (nozzle length - 90 mm) the measurements were done inside the nozzle, while in the case of the shorter nozzle at a distance 20 mm outside from the end of the shroud nozzle. Temperature and air content in the plasma jet differed heavily for both shroud nozzles. For the longer nozzle temperature was much higher and air content was much lower than without shrouding, while in the case of shorter nozzle, the centerline temperature remained the same and the air content was just slightly reduced at the centerline position. The situation changed at the jet fringes, where temperature went down and the air content with the shorter shroud nozzle was higher than without it. This effect was caused by the interference of the shrouding gas with the plasma flow. In case of a longer nozzle the plasma jet at this region was not disturbed by the gas flow and the wall of the shroud nozzle protected the jet surrounding from shroud gas. Air observed in the jet was entrained through leakages in the place of shroud nozzle bracing and because of air circulation within the nozzle. At the same time, velocity was almost unchanged, which is confirmed by the axial velocity evolution from Figure 4.32. It seems that in the central part of the plasma jet the velocity evolution was independent on the presence of the shroud gas.

The axial values of temperature and velocity at the jet centerline confirmed a positive influence of the solid shielding on the plasma jet. Velocity values were not affected, but the effect on temperature was significant. For the longer shroud nozzle the temperature changed slightly only at the fringes inside the nozzle. At distances from 50 mm up to 90 mm the temperature decreased by 500 K. A stronger temperature reduction started at the exit of the nozzle. The behavior of the plasma jet differed when the shorter nozzle was applied. There was a strong temperature drop at a distance of 60 mm from the nozzle exit close to the exit of the shroud nozzle. Here, the plasma jet reached the temperature value of the plasma jet without shrouding.

In additional experiments the shroud gas flow rate was varied from 0 to 120 slm. Figure 4.33 shows the dependence of temperature and air content in a plasma measured at the jet centerline at a distance z = 60 mm from the nozzle exit. For the shorter shroud nozzle the temperature increased for higher shroud gas flow rates while the air content decreased. A temperature rise was caused by removing air from the jet surrounding. Instead of heating and dissociating the molecular gases of air the heat withdrawn from the plasma was utilized only for heating of the shroud gas now.

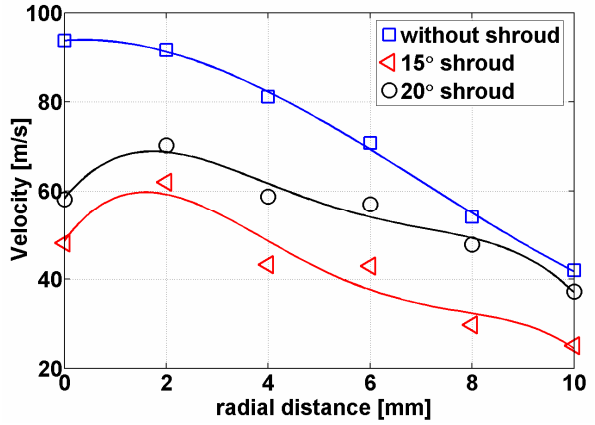

Figure 4.34 Velocity profiles of jets without shrouding and with swirl shrouding (shroud gas flow rate – 40 slm).

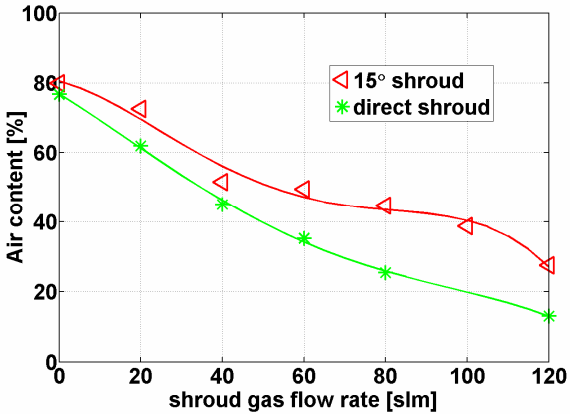

Figure 4.35 Dependence of air content in plasma jet on shroud gas flow rate with direct and swirl shrouding at the jet centerline.

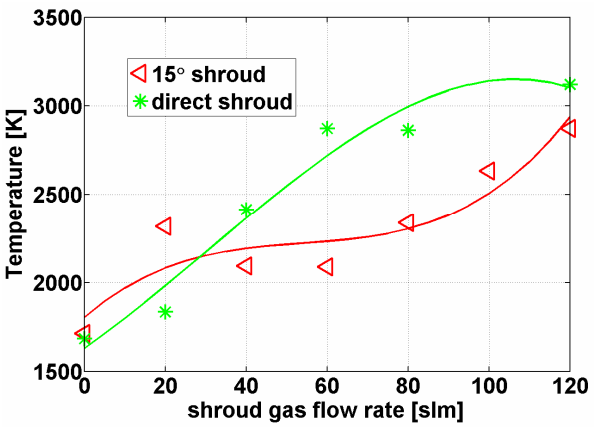

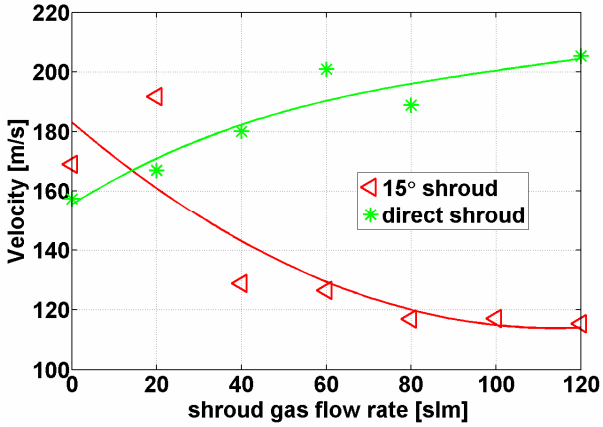

Figure 4.36 Dependence of plasma jet characteristics on shroud gas flow rate with direct and swirl shrouding at the jet centerline.

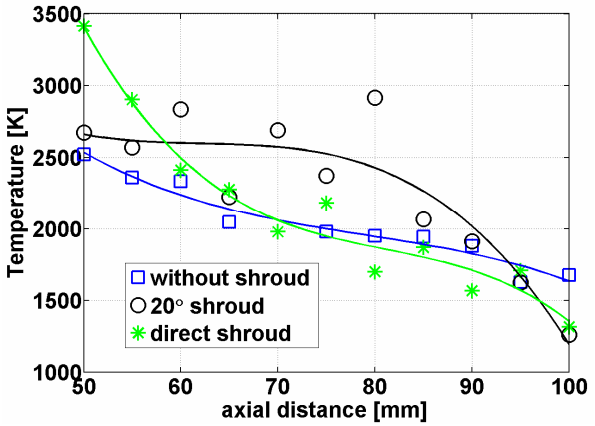

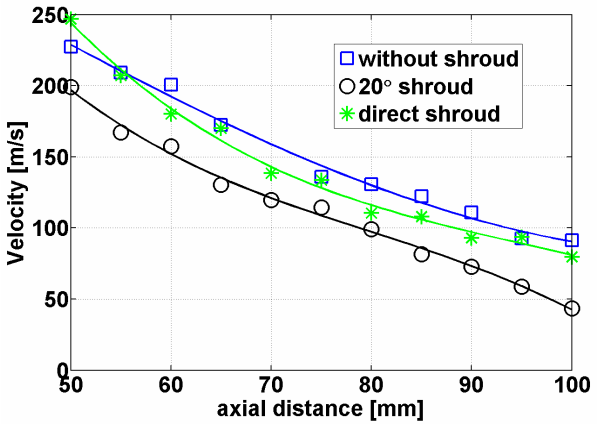

Figure 4.37 Development of plasma jet characteristics at the jet centerline without shrouding and with both methods of shrouding – direct and swirl (shroud gas flow rate – 40 slm).

The temperature and air content curves describing the development of the plasma jet shrouded by a longer nozzle showed that the behavior of the upstream part of the plasma jet affected its downstream part. In spite of applying shroud gas at 90 mm from the nozzle exit the plasma jet characteristics changed in the upper parts of the jet. The temperature values without any shroud gas were higher because the solid wall shielded the jet surrounding from cold air entering. The same held true when lower shroud gas flow rates were used in the case of the longer nozzle. The plasma jet temperature level changed with the shroud gas flow rate. The strong temperature changes were accompanied by a reduction of the air content in the jet observed for flow rates of the shroud gas lower than 80 slm. For shroud gas flow rates higher than 80 slm the plasma characteristics remained almost unchanged. It seems that the air content for higher shroud gas flow rates was due to the sucking of ambient gas by the plasma jet through leakages. Air entered inwards the shroud nozzle because of the lower static pressure inside the nozzle in comparison to the pressure in the reactor. This demands to apply restrictions in the production of the removable parts, which must excellently fit into the holder preventing air sucking.

All presented facts add up to prefer a longer nozzle to be used for gas shrouding. Such a nozzle combines simultaneously solid and gas shielding, resulting in a better plasma jet protection against the entrainment of ambient air.

Swirl shrouding

An injection of the shroud gas through several holes 1 mm in diameter located concentrically around the plasma jet was tested. The simulations and results of experiments performed by Thomson et al. [84] showed that shroud gas injected axially through holes do not mix completely and do not form a perfect envelope of gas around the jet. Therefore, a swirl shrouding was tested. An azimuthal component of the shroud gas flow was superposed on its axial component and thus, the flow pattern around the jet changed. It was supposed that a more uniform distribution of the shroud gas around the plasma flow could be reached with the help of such an arrangement. A special ring with holes drilled under angles of 15° and 20° was worked out. The shroud gas was injected under these angles. The direction of the shroud gas swirling coincided with the direction of the plasma jet swirling caused by a swirl injection inside the plasma torch. In the case of inversely directed flows of plasma gas and shroud gas the formation of vortices in the boundary layer between both flows can be generated.

The results of these measurements are shown by Figure 4.34 to 4.37. The different behavior of a plasma jet with swirl shrouding is evident. The swirling shroud gas had the strongest influence on the plasma jet velocity, which decreased rapidly. Figure 4.34 shows radial profiles of the plasma jet velocity for a free jet and for swirling under 15° and 20°. The highest values of plasma jet velocity were not observed at the jet centerline any longer but were shifted and observed at 2 mm distance. The swirling caused additional penetration of air into the plasma jet and the reduction of the air content is not as efficient as in the case of direct shrouding (Fig. 4.35). The plasma jet was more unstable with more intensive fluctuations. Moreover, the higher the flow rate of the shroud gas the more evident was the

plasma jet swirling. Although the plasma jet temperature increased with higher shroud gas flow rate, the plasma jet velocity dropped more rapidly (Fig. 4.36). The plasma jet temperature rose because the shroud gas argon as admixture to the plasma gas consumed less energy for heating in contrary to the replaced air. The axial component of the plasma jet velocity measured by the enthalpy probe was also reduced as it was influenced by the azimuthal forces of the shroud gas.

Figure 4.37 shows the axial development of the plasma jet characteristics for a plasma jet without shroud, for direct shroud and for 20° shroud gas injection. Argon shroud gas was supplied with a flow rate of 40 slm in both cases. These measurements confirmed that direct shrouding was better than shrouding with swirl components. Although the temperature was a little bit higher in the case of swirl shrouding, the plasma jet fluctuated much more compared to direct shrouding. Along the jet stream the centerline plasma jet velocity was lower for swirl shrouding, while for the direct one it was almost the same as without shrouding.

All mentioned facts prove favorable effects of the shroud gas on plasma jet characteristics and mainly a reduction of the air entrainment process. The direct shrouding through the concentric slot appeared to be better than swirl shrouding through several holes located concentrically around the plasma jet. Shrouding with rotating gas resulted in strong changes of the plasma flow pattern. As a result the whole plasma jet started to rotate. This effect could lead to dragging off the particles injected into the jet to be sprayed. The particles could loose their momentum towards the substrate and would hit the substrate with insufficient velocity, or could even be lost resulting in a strong reduction of the deposition efficiency.

4.6 Influence of the carrier gas injection onto the plasma jet

The present section is connected with the application of the thermal plasma jets for plasma spraying applications. In the plasma spraying powder particles are transported to the jet with the help of a carrier gas through an injector. Choice of the injector and injection parameters is very important. Injection parameters controls the distribution of the powder within the jet, their trajectories, and thus their heating and acceleration [147]. Powder particles could be injected at the some distance from the nozzle exit or directly inwards the nozzle. The injector location should be chosen with respect to the heat flux of the jet and particles melting temperature. Internal injection provides a better heat and momentum transfer to the particles as particles are injected directly into the plasma flame. However, the internal injection disturbs the plasma jet by cold carrier gas more than in the external case.

Type of the carrier gas and its flow rate must be adjusted in such a way to provide the introduction of the maximum number of the powder particle into the hot core of the plasma jet in order to get an optimum acceleration and heating. Sometimes gas is replaced by liquid if fine powder particles have to be sprayed.

Consequently, the proper choice of the injection parameters is a key feature in the achievement of the optimum deposition efficiency.

The effect of the carrier gas injection into the plasma jet generated by the gas stabilized plasma torch was investigated. The main results are represented in Appendix D.

In the publication several injection conditions are discussed. The influence of the internal injection was studied under low pressure conditions. The carrier gas was supplied without powder particles to study its effect on the plasma jet characteristics. The characteristics of the plasma jet were investigated by means of the enthalpy probe technique. The powder injection conditions were varied by changing:

- injection angle (perpendicular and inclined);
- carrier gas flow rate;
- carrier gas type (nitrogen and helium).

The results showed that the injection led to plasma jet disturbances and the centerline of the primary axis-symmetrical jet was shifted to the direction opposite of the injection port and the displacement of the jet was proportional to the carrier gas flow rate: the higher the gas flow rate the stronger the displacement accompanied by higher jet perturbations. In case of the inclined injection the carrier gas acted as a shroud gas opposing to the air entrainment, while perpendicular injection just pushed the jet into the opposite direction. Inert helium was found to be more suitable as a carrier gas as it affected the plasma jet less than molecular nitrogen.

4.7 Influence of plasma generation conditions on the shape of the plasma jet

The investigation of the plasma jet shape and its dependence on the plasma generation conditions was studied by means of Schlieren imaging. The influence of the arc power and pressure was investigated as well as how the spraying parameters affect the plasma jet behavior. The plasma gas was a mixture of argon with hydrogen (40 slm Ar/ 3 slm H_2).

Figure 4.38 represents the visualization of the plasma jet generated under two arc powers – 27 and 32 kW - under the pressure of 30 kPa. The black region on the left side of the photos corresponds to the nozzle exit of the torch. There was no significant difference in the plasma jet behavior. For the higher arc power the plasma jet was narrower at the upstream part. But in the downstream part the width of both jets was the same, which is in correlation with results obtained by the enthalpy probe measurements.

Figure 4.39 represents plasma jets generated under different pressures. 10 kPa was the pressure limit for the method and for lower pressures it was impossible to recognize variations of density in the plasma jet and the jet itself from the surrounding. The pressure increase allowed a better distinction of the plasma jet fringes and observation of the transition of the flow from laminar to turbulent behavior accompanied by the formation of vortices. The spreading of the plasma jet as a result of entrainment is evident. The plasma jets for the whole investigated pressure range had conical shapes but the cone was better drawn for lower pressures. For the higher pressures the plasma jet fringes are more unstable because of higher level of turbulence. The zone right after the nozzle exit of the torch with weak contrast variations corresponds to the laminar flow region. The laminar part of the jet is quite long and clearly seen for the 10 kPa. Increase of the pressure to 30 kPa resulted in its abridgement and the formation of the vortices can be recognized. Further increase of the pressure led to the disappearance of the well-defined laminar part. The laminar part could still exist in the center of the plasma jet but only the plasma jet fringes were investigated by means of this method. The formation of the vortices began very close to the exit nozzle.

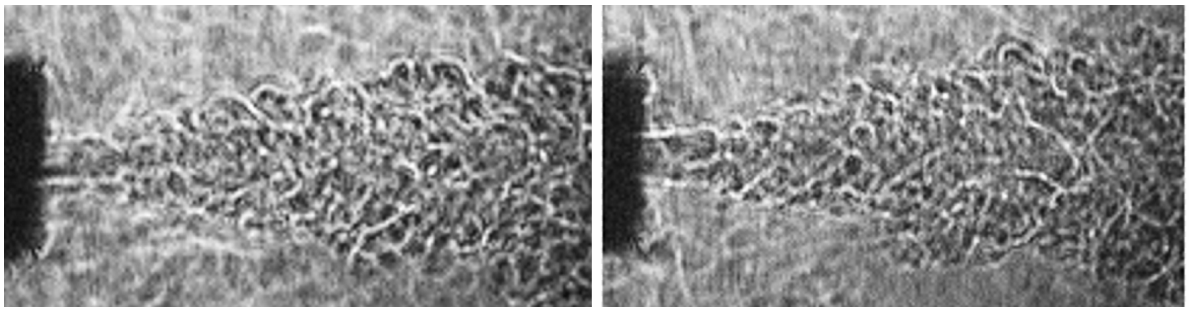

27 kW 32kW

Figure 4.38 Influence of the arc power on the plasma jet shape (plasma gas - 40 slm Ar/ 3 slm H_2, pressure – 30 kPa).

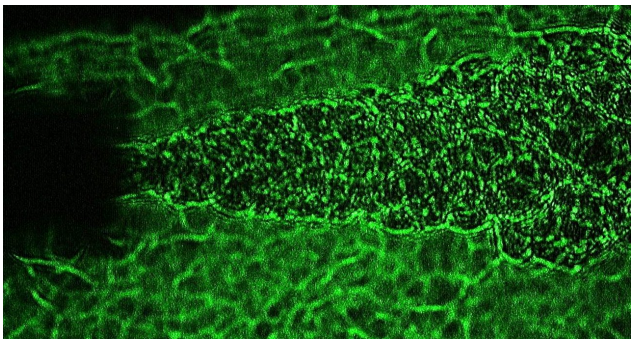

80 kPa

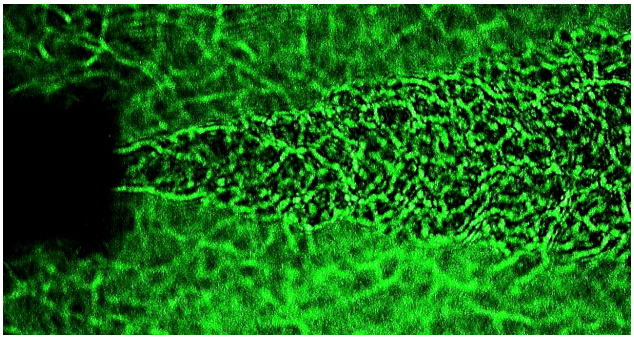

50 kPa

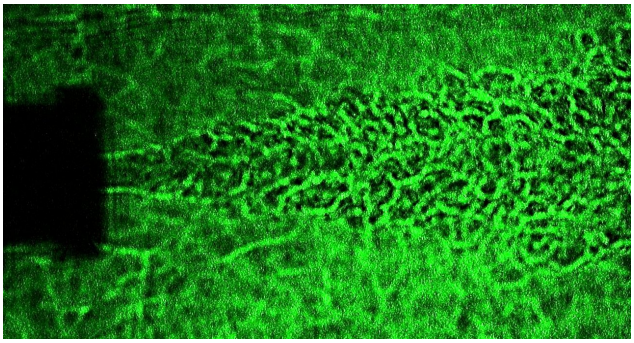

30 kPa

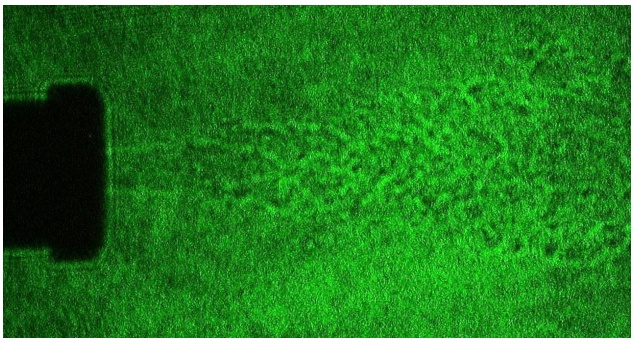

10 kPa

Figure 4.39 Effect of the pressure reduction on the plasma jet shape (plasma gas - 40 slm Ar + 3 slm H_2, arc power – 20 kW).

The injection of the powder particles into the plasma jet strongly affects the flow pattern. The influence of the carrier gas without particles on the shape of the plasma jet was also studied. The carrier gas was injected perpendicularly to the main plasma flow through the different injectors very close to the torch exit nozzle. The injectors 1.5 and 3 mm in diameter were studied. Nitrogen and helium were applied as carrier gases. The resulting images are shown in Figure 4.40. The injection port can be seen on the bottom part of the photo so the injection direction was bottom-up. The axis of the plasma torch is shown by the straight line. The plasma jet fringes are marked by the dotted line.

The plasma jet flow was affected for all carrier gas injection conditions. The cone shape of the jet was altered mainly from the side where the injection took place. The plasma jet itself was shifted in the opposite direction of the injection port. Helium used as carrier gas perturbed the plasma jet less than nitrogen. Increase of the carrier gas flow rate from 5 to 10 slm resulted also in higher jet perturbation, which becomes apparent in the abrupt change in the plasma jet cross section. The place of this change of the flow diameter was even closer when the injector diameter was decreased from 3 to 1.5 mm. The decrease of the injector diameter meant increase of the velocity of the carrier gas while its flow rate stayed unchanged.

Thus, the injection of the carrier gas affected the plasma jet shape a lot indicating changes in the plasma jet diameter and consequently change in the volume of the useful plasma to be favorite for the processing.

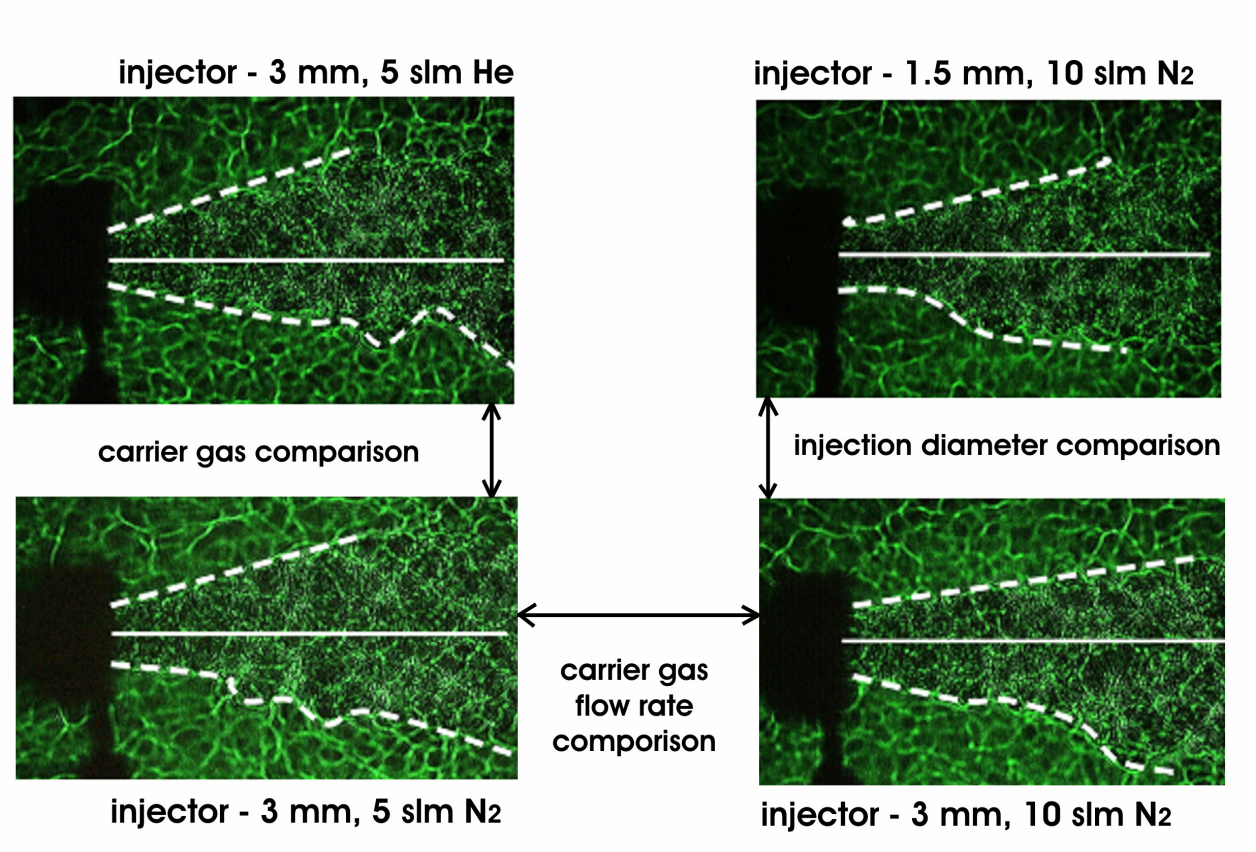

Figure 4.40 Influence of carrier gas on the plasma jet shape (plasma gas - 40 slm Ar + 3 slm H_2, arc power – 20 kW).

Summary of the research

The thesis examines the process of ambient air entrainment into the plasma jets generated by DC arc plasma torches. The study considers two DC arc plasma torch types. The main difference between the torches is the way of arc stabilization. In the plasma torch with gas stabilization an arc is stabilized by the gas supplied into the torch chamber. In the hybrid torch two principles are combined. In the cathode part the arc is stabilized by gas flow supplied along a cathode, while the main part of the arc is generated inside a water vortex allowing high thermal load and thus providing higher arc power. The differences in the principles of stabilization result in big differences in the properties of the generated plasma jets. The observation of the plasma jets generated under different conditions was the main subject of the present research.

The present work was mainly experimental. The experimental work around the hybrid gas-water torch was conducted during the period from the end of the year 2000 to the middle of year 2005. As this is a completely new type of a torch, the main work during the first two years was focused on the development and improvement of the plasma torch itself. The main experimental results were obtained during the last three years.

One of the main aims of the experimental part was to work out the method of the application of the enthalpy probe system for diagnostics of the plasma jet containing water steam. The main restriction of the enthalpy probe application is that any liquid from the sampled gas has to be eliminated. The method of the enthalpy probe application is based on the recalculation of the real plasma jet properties from the values obtained by the enthalpy probe measurements. Water vapor obtained in the plasma jet is frozen out in the gas sample line of the enthalpy probe. Then the analysis of the obtained data and the evaluation of the plasma jet characteristics becomes a complex problem. The analysis is based on the assumption of the absence of demixing processes and on the measurement of the plasma jet composition close to the exit nozzle of the torch obtained by means of emission spectroscopy. This type of diagnostics had been applied for such a type of plasma for the first time and thus these measurements are unique.

The experiments on the gas stabilized plasma torch were carried out during my several stays with the DLR-Stuttgart in the years 2003-2004. The same enthalpy probe diagnostics system from Tekna inc. (Sherbrooke, Canada) was applied but without freezing as there was no any liquid in the plasma.

The main contribution of the present work is the detailed description of the air entrainment process in relation to the plasma jet generation conditions. The behavior of the plasma jet generated by the hybrid argon-water torch differs from the jet generated by the torch with gas stabilization of the arc. This distinction was caused by a large difference between density of the plasma jet, which is extremely low in the case of the hybrid torch, and ambient air density as well as by strong interaction of the main flow with the anodic jet. Such an interaction results not only in deflection of the main plasma flow from the torch chamber axis but an anodic jet strongly perturbs the main plasma flow as well causing more intensive cold ambient air entrainment. Increase of both arc current and

argon flow rate led to a reduction of the anodic jet influence and to straightening of the jet because of the increased momentum flux of the main plasma flow.

The effect of arc current, plasma gas composition, surrounding pressure and shrouding on the cold air entrainment was studied. The behavior of the plasma jet exhibits strong linking of the entrainment process to the velocity and density gradients. The higher the gradients are the higher the entrainment rate is. The development of the plasma flow depends on the initial conditions right at the plasma torch exit. The plasma jet temperature and velocity at the nozzle exit increased for higher arc currents. The temperature rise was connected with higher Joule heating being released by the arc. Moreover, in the hybrid torch the increase of evaporation rate for higher arc currents resulted in increase of the mass flow rate at the nozzle exit of the torch causing increase of the plasma jet velocity. In spite of higher gradients at the jet fringes, the temperature and velocity of the plasma in the downstream regions of the jet increased with increasing arc current for both torches [XI, XVI]. Increase of argon content in argon-steam plasma led to a substantial increase of the plasma density and subsequently the density ratio of plasma to ambient gas was reduced and the entrainment was slowed down [III, V, VI].

The composition of the plasma forming gas play also an important role in the jet behavior, particularly adding of hydrogen to argon resulted in strong changes of the plasma jet generated by the gas stabilized torch. Presence of hydrogen led to a transition of the plasma torch to the restrike mode accompanied by higher fluctuations of the plasma jet [IV]. Entrainment is not only a process which appears because of density and velocity gradients at the jet fringes but may also arise because of a pumping effect caused by arc root movement in the restrike mode. However, the measurements showed that arc fluctuations did not affect the air entrainment process significantly. In fact velocity gradients play the dominant role.

Under low pressure conditions a transition of the plasma flow from subsonic to supersonic takes place. The critical value of the surrounding pressure for the transition was close for both torches and was about 30 kPa. The transition to supersonic flow also affects the behavior of the plasma jet in it downstream regions. The obtained results indicate a prolongation of the plasma jet hot core at reduced pressures and a decreasing of the ambient air entrainment [XVI-XVIII].

The application of shrouding around the plasma jet has favorable effect on the plasma jet. The results confirmed that the entrainment process is slowed down when the shroud gas is supplied which could be the consequence of three factors. The shroud gas replaces air from the jet surrounding. The bubbles, which contain shroud gas and are getting into the plasma jet in the process of the entrainment, have a lower density and could travel and mix up quicker in the plasma jet in comparison with cold air bubbles. The process of the plasma jet velocity reduction slows down. Less heat from the jet would be spent for the heating of the entrained shroud gas in comparison with air. Thus, the plasma jet temperature reduction is less intensive. Moreover, in contrast to stagnant air surrounding, shroud gas moves in the same direction with the plasma jet reducing velocity gradient at the jet fringes and slowing down the process of the bubble formation [XIV, XX, XXI, XXVI].

The main results of the present study could be summarized in such a way:

- The entrainment process was much more intensive in the plasma jet generated by hybrid plasma torch. The main reasons of such a behavior are the strong density gradients existing at the torch exit and the strong fluctuations of the plasma jet caused by arc root movements.
- The main factors determining air entrainment are gradients of the plasma jet density and velocity at the nozzle exit of the torch.
- The fluctuations of the arc produced by arc root movements, which also cause pumping of the ambient gas into the plasma jet, do not play a dominant role in the process of air entrainment.
- The main method for reducing the entrainment rate is the reduction of velocity and density gradients. The main way how to obtain such conditions is either the application of a gas shroud around the plasma jets (reduction of the velocity gradients) or the generation of the plasma jets under low pressure conditions (reduction of the density gradients because of the low density of the surrounding).

The results of the thesis could be used for analytical description of the entrainment phenomenon as well as for numerical studies. Heat and momentum transfer from plasma to materials can be estimated. As enthalpy and momentum fluxes determine plasma-particles interaction in the plasma spraying process, the plasma characteristics could be applied for the evaluation of the particles behavior in the jet. The evaluation of the plasma jet characteristics along the jet and their dependence on the torch parameters should help to optimize the application of such torches for the treatment of hazardous waste. The project devoted to gasification of wastes by the hybrid torch is presently being started in the Thermal Plasma Department in Prague.

The obtained results are interesting not only from the phenomenological point of view but they are of great importance for practical applications. The user of the torches should decide which plasma torch operation conditions are favorable for the certain application allowing the optimization of the industrial process.

In spite of the wide range of obtained dependences there is still a lot to do about the entrainment effect. The complete description of the entrainment phenomena is still missing. Further studies of the entrainment process will be continued not only in our laboratory but surely in other laboratories around the world.

Literature

1. M. I. Boulos, P. Fauchais and E. Pfender: Thermal Plasmas: Fundamentals and Applications Vol.1, Plenum Press, New York, (1994)
2. M.F. Zhukov, A.S. Koroteev and B.A. Urjukov: Prikladnaja dinamika termicheskoj plazmy, Nauka, Novosibirsk (1975)
3. X. Zhou, J. Heberlein, *Plasma Sources Sci. Technol.* **3**, 564 (1994)
4. M.S. Benilov, *J. Phys. D: Appl. Phys.* **32**, 257 (1999)
5. J. Haidar, *J. Phys. D: Appl. Phys.* **32**, 263 (1999)
6. A.B. Murphy, J. *Phys. D: Appl. Phys.* **34**, 151 (2001)
7. J.J. Lowke and A.B. Murphy: The hand book of Fluid Dynamics, ed. R.W. Johnson CRC press, Boca Raton (1998).
8. P.W. Atkins: Physical Chemistry, Oxford University Press, Oxford (2001)
9. S. Chapman and T.G. Cowling: The Mathematical Theory of Non-uniform Gases, 3rd ed., Cambridge University Press, Cambridge (1970)
10. H. Schlichting and K. Gersten: Boundary Layer Theory, Springer-Verlag, Berlin Heidelberg (2000)
11. Y. Raizer: Fizika gazovogo razryada, Nauka, Moscow (1987)
12. J. Heberlein; Heat and mass transfer under plasma conditions, (Ed.) Fauchais et al., The New York academy of science, New York, 14 (1999)
13. M.I. Boulos; *J. of Visualization* **4** (1), 19 (2001)
14. K. Mailhot, F. Gitzhofer and M. I. Boulos, In Thermal Spray: A United Forum for Scientific and Technological Advances, (Ed.) C. C. Berndt, ASM International, Materials Park, OH, 21 (1997)
15. H. Nowakowska, Zakrzewski and M. Moisan, *J. Phys. D: Appl. Phys.* 22, 789 (1990)
16. M. Moisan and Z. Zakrzewski, *J. Phys. D: Appl. Phys.* **24**, 1025 (1993)
17. L.L. Alves, *Eur. Phys. J. Appl. Phys.* **26**, 195 (2004)
18. P. Fauchais and A. Vardelle, *IEEE Transactions on Plasma Science* **25** (6), 1258 (1997)
19. R. McPherson, *Thin Solid Films* **83**, 297 (1981)
20. R. McPherson, *Surf. Coat. Technol.* **39/40**, 173 (1989)
21. P. Fauchais, A. Vardelle and B. Dussoubs, *J. Therm. Spray Technol.* **10** (1), 44 (2001)
22. T. Yoshida, *Pure Appl. Chem.* **66** (6), 1223 (1994)
23. M. Kelkar and J. Heberlein, *J. Phys. D: Appl. Phys.* 33, 2172 (2000)
24. D. J. Varacalle, D. P. Zeek, G. S. Cox, D. Benson, K.W. Couch, E. Sampson and V. Zanchuck, *J. Therm. Spray Technol.* **7** (1998)
25. E. Pfender, H. Zhu and Y.C. Lau, *Mater. Sci. Eng*. **A139**, 352 (1991)
26. E. Bouyer, G. Schiller, M. Muller and R.H. Henne, *Plasma Chem. Plasma Process.* **21** (4), 523 (2001)
27. K. Takeda, M. Ito and S. Takeuchi, *Pure Appl. Chem.* **62** (9), 1772 (1990)

28. S. L. Girshick and J.M. Larson, *Pure Appl. Chem.* **70** (2), 485 (1998)
29. S L Girshick, *Plasma Sources Sci. Technol.* **3**, 388 (1994)
30. L. Fulcheri, T.M. Gruenberger and J. Gonzalez-Aguilar, Proc. ISPC-17, August 5-14, 2005, Toronto, Canada, ID572 (2005)
31. G. Van Oost, C. Leys and M. Joos, *Czechoslovak J. Phys.* **52**, D784 (2002)
32. P.G. Rutberg, Progr. Plasma Process. Of Mat. (Ed. P. Fauchais), Begell House, New-York-Wellington, 745 (2001)
33. E. Pfender, *Plasma Chem. Plasma process.* **19** (1), 1 (1999)
34. A.M. Howatson: An introduction to gas discharges, Atomizdat, Moscow (1980)
35. J. F. Coudert, M.P. Planche, and P. Fauchais, *Plasma Chem. Plasma Process.* **16**, 211S (1996)
36. J.Heberlein, *J. High Temp. Mater. Process*. **6**, 321 (2002)
37. S.A. Wutzke, E. Pfender and E. Eckert, *AIAA J*. **5**, 707 (1967)
38. M. Hrabovský, O. Chumak, T. Kavka and V. Kopecký, Proc. of 12th Workshop on Plasma Technology, September 2004, TU Ilmenau, 15 (2004)
39. O. Chumak, M. Hrabovský, T. Kavka, V. Kopecký, *Proc. ISPC-17*, August 5-14, 2005, Toronto, Canada, ID282 (2005)
40. J. Heberlein, Annals New York Academy of Science 891, 14 (1999)
41. R.H. Henne, V. Borck, W. Mayr, K. Landes and A. Reush, *Proc.* 8th National Thermal Spray Conference, (Ed.) C.C. Berndt and S. Sampath, ASM international, OH – USA, 67 (1995)
42. R. F. Bunshah, J.M. Blocher and D.M. Mattox: Deposition Technologies for films and coatings, Noyes Publications, Park Ridge, New Jersey, USA (1982)
43. H. Gerdien and A.Lotz; Wiss. Veroffentlichungen Siemenswerk 2, 489 (1920)
44. H. Gerdien and A. Lotz; *Z. Tech. Phys.* **4**, 157 (1923)
45. H. Maecker; *Z. Tech. Phys.* **129**, 108 (1951)
46. F. Burnhorn and H. Maecker; *Z. Tech. Phys.* **129**, 369 (1951)
47. Burnhorn, H. Maecker and T. Peters, *Z. Tech. Phys*. **131**, 28 (1951)
48. B. Gross, B. Grycz and K. Miklossy: Plasma Technology, Iliffe Books Ltd., London (1968)
49. P. Chraska and M. Hrabovsky; Proc. ITSC1992, May 28-June 5, Orlando, USA, 81 (1992)
50. M. Hrabovsky, M. Konrad, V. Kopecky and V. Sember, Thermal Plasma Torches and Technologies Vol.1, (Ed.) O.P. Solonenko, Cambridge, Cambridge Int. Sci. Publ., 242 (2000)
51. V. Brezina, M. Hrabovsky, M.Konrad, V.Kopecky and V.Sember, *Proc*. ISPC-15 (ed. A.Bouchoule et al.) Vol.III, July 9-13, 2001, Orleans, 1021 (2001)
52. J.M. Beer and N.A. Chigier: Combustion aerodynamics, Applied Science Publishers LTD, London, England (1972)
53. W.R. Howthorne, D.S. Weddell and H.C. Hottel; 3rd Symposium on Combustion, Flames and Explosion Phenomena, 1951, Baltimore, 266 (1951)
54. C. Boguslavski and O. Popiel, *J. Fluid Mech.* **90**, 531 (1979)
55. S.C. Crow and F.H. Champagne, *J. Fluid Mech.* **48**, 549 (1970)

56. G. Birkgof: Gidrodynamika, Izdatelstvo inostrannoj literatury, Moscow (1963)
57. S. Terrade: Overview of hydrodynamic instabilities, http://www.enseeiht.fr/
58. A.A. Townsend, *J. Fluid Mech.* **26**, 689 (1966)
59. H.L. Grant, *J. Fluid Mech*. **4**, 149 (1958)
60. P. Bradshaw, D.H. Ferriss and R.E. Johnson, *J. Fluid Mech.* **19**, 591 (1964)
61. J.C. Lau, M.J. Fischer and H.V. Fuchs, *J. Sound Vib.* **22** (1972)
62. J.C. Lau and M.J. Fischer, *J. Fluid Mech.* **67**, 299 (1974)
63. W.J.A. Dahm and P.E. Demotakis, AIAA Journal **25**, 1216 (1987)
64. G. L. Brown and A. Roshko, *J. Fluid Mech.* **64**, 775 (1974)
65. A.J. Yule, *J. Fluid Mech.* **89** (3), 413 (1978)
66. G.E. Mattingly and C.C. Chang, *J. Fluid Mech.* **65**, 541 (1974)
67. F.P.Ricou and D.B.Spalding; *J. Fluid. Mech.* **11**, 21 (1961)
68. I.H.Tombach, Ph.D Thesis, California Institute of Technology (1969)
69. P.A. Monkewitz, B.Lehmann and B.Barsikow, *J. Fluid. Mech*. **213**, 446 (1989)
70. S.Russ, P.J.Strykowski, E.Pfender, *Experiments in Fluids* **16**, 397 (1994)
71. J. R. Fincke, C. H. Chang, W.D. Swank and D.C. Haggard, *Int. J. Heat Mass Transfer.* **37** (11), 1673 (1994)
72. J.R. Fincke, R. Rodriquez and C.G. Pentecost, Proc. 3^{d} National Thermal Spray Conference, May 20-25, 1990, Long Beach, CA, USA, 45 (1990)
73. O. Lagnoux, J.F. Coudert, K. Wittman and P. Fauchais, Thermal Spray 2003: Advancing the Science & Applying the Technology, (Ed.) C. Moreau, B. Marple, ASM International, Materials Park, Ohio, USA, 71 (2003)
74. E. Pfender, J. Fincke and R. Spores, *Plasma Chem. Plasma Process.* **11** (4), 529 (1991)
75. E. Pfender, W.L.T. Chen and R. Spores; *Proc. 3^{d} National Thermal Spray Conference*, May 20-25, 1990, Long Beach, CA, USA, 1 (1990)
76. R.Spores and E.Pfender, *Surf. Coat. Technol.* **37**, 251 (1989)
77. J. Lesinski and M. Boulos, *Plasma Chem. Plasma Proc.* **8** (2), 113 (1988)
78. P.C. Huang, J. Heberlein and E. Pfender, *Plasma Chem. Plasma Proc*. **15** (1), 25 (1995)
79. M.Brossa and E.Pfender, *Plasma Chem. Plasma Process.* **8**, 75 (1988)
80. A. Vardelle, P. Fauchais and N.J. Themelis, Advances in Thermal Spray and Technology, (ed.) C.C. Berndt, ASM international, 175 (1995)
81. K. Volenik, F. Hanousek, P. Chraska, J. Ilavsky and K. Neufuss; Mater. Sci. Eng. **272**, 199 (1999)
82. A.A. Syed, A. Denoirjean, P. Denoirjean, J.C. Labbe and P. Fauchais, Thermal spray 2003: Advancing the science & Appliing the Technology, (ed.) Moreau and B. Marple, ASM international, 985 (2003)
83. O. Lagnoux, J.F. Coudert, K. Wittman and P. Fauchais, Thermal Spray 2003: Advancing the Science & Applying the Technology, (Ed.) C. Moreau, B. Marple, ASM International, Materials Park, Ohio, USA, 71 (2003)
84. P. Roumilhac, J.F. Coudert and P. Fauchais, Proceedings of 3rd Thermal Spray Conference, May 20-25, 1990, Long Beach, CA, USA, 11 (1990)

85. D.R. Mash, , N.E. Weare and D.L. Walker, *J. of Metals* **13**, 473 (1961)
86. A. R. Stetson and C. A. Hauck, *J. of Metals* **13**, 34 (1961)
87. B. Jodoin and P.Proulx, *J. High Temperature Material Process.* **4**, 21 (2000)
88. Jodoin, M. Gindrat, J.-L. Dorier, Ch. Hollestein, M. Loch and G. Barbezat, Proceedings ITSC 2002, Essen, Germany, 716 (2002)
89. Steady-state Jets, Los Alamos Science (1985)
90. R. Bolot, D.Klein and C. Coddet, Thermal spray 2003: Advancing the science & Appliing the Technology, (ed.) Moreau and B. Marple, ASM International, Materials Park, Ohio, USA, 1087 (2003)
91. M. Gindrat, J.-L. Dorier, Ch. Hollestein, M. Loch, A. Refke, A. Salito and G. Barbezat, Proc. ITSC 2002, Essen, Germany, 459 (2002)
92. S.E. Selezneva, M. Rajabian, D. Gravelle and M.I. Boulos, *J. Phys. D: Appl. Phys*. **34**, 2862 (2001)
93. O. Chumak, M. Hrabovsky, V. Kopecky, M. Konrad and T. Kavka, Proc. WDS'2004, Prague, Czech Republic, 388 (2004)
94. G. Schiller, R. Henne, P. Mohr and M. Lang, Proc. SOFC-V, (Ed.) U. Stimming et al., The Electrochemical Society Inc., NJ, USA, 635 (1997)
95. J. Laimer, H. Pauser, H Störi, R. Haubner and B. Lux; *Diamond Relat. Mater.* **6**, 406 (1997)
96. J. Laimer, H. Pauser, C. G. Schwärzler and H Störi, *Surf. Coat. Technol.* **98**, 1066 (1998)
97. K. Foelsch, *Journal of the Aeronautical Sciences*, 161 (1949)
98. R. Henne, E. Bouyer and V. Borck, Proc. ITSC2001, (Ed.) C.C. Berndt, K.A. Khor and E.F. Lugscheider, ASM International , OH, USA, 471 (2001)
99. I. Thomson, V. Pershin, J. Mostaghimi and S. Chandra, *Plasma Chem. Plasma Process*. **21** (1), 65 (2001)
100. M. Jankovic and J. Mostaghimi, *Plasma Chem. Plasma Process.* **15** (4), 607 (1995)
101. J. E. Jackson; US Patent No 3470347 (1969)
102. D.T. Gawne, T. Zhang and B. Liu, *Surf. Coat. Technol*. **153**, 138 (2002)
103. K. D. Kang and S. H. Hong, *J. Appl. Phys.* **85** (9), 6373 (1999)
104. M.S. Novotarski, US Patent 5486383 (1996)
105. J.H. Harrington, US Patent No 4121082 (1978)
106. G.R. Jones and S.R. Naidu, *J. Phys. D: Appl. Phys*. **7**, 2254 (1974)
107. A. Chapman and G.R. Jones, *IEEE Trans. On Plasma Science*, PS-6, 300 (1978)
108. M. Hrabovsky and V. Kopecky; *Proc. SPPT-16*, April 27-29, 1993, Prague, Czech Republic, 236 (1993)
109. M. Brossa and E. Pfender, *Plasma Chem. Plasma Process*. **8** (1), 75 (1988)
110. W. D. Swank, J.R. Fincke and D.C. Haggard, *Rev. Sci. Instrum.* **64** (1), 56 (1993)
111. W.L.T. Chen, J. Heberlein and E. Pfender, *Plasma Chem. Plasma Process.* **14** (3), 317 (1994)
112. M. Rahmane, G. Soucy and M. I. Boulos, *Rev. Sci. Instrum.* **66** (6), 3424 (1995)

113. J. Hlina, J. Gruber and J. Sonsky, *Proc. ISPC-17*, August 7-12, 2005, Toronto, Canada, ID434 (2005)
114. I. Serbetci and H.T. Nagamatsu, *IEEE Trans. Plasma Sci.* **18**, 102 (1990)
115. S. Raghu and G. Goutevenier, *Exp. Fluids* **19**, 136 (1995)
116. S.P. Mates, D. Basak, F.S. Biancaniello, S.D. Ridder and J. Geist, *J. Therm. Spray Technol.* **11**, 195 (2002)
117. J. Grey, P. F. Jacobs and M. P. Sherman, *Rev. Sci. Instrum.* **33** (7), 738 (1962)
118. A.A. Ovsyannikov and M.F. Zhukov: Plasma diagnostics, Cambridge international science publishing, Cambridge (2000)
119. P.W. Atkins: Physical Chemistry, Oxford University Press, Oxford (1998)
120. R. Hejzlar: Mechanika tekutin, Vydavatelsti ČVUT, Praha (2001)
121. M. Hrabovsky, M. Konrad, V. Kopecky and V. Sember, *IEEE Trans. Plasma Sci.* **25** (5), 833 (1997)
122. V. Sember, Progress in Plasma Processing of Materials 2003 (Ed. P. Fauchais), New York, Begell House Inc., 41 (2003)
123. E. Hoffmann, J. Charette, A. Stroobant: *Mass Spectrometry Principles and Applications*; V., Wiley & Sons, New York, NY (1996)
124. Quadrupole mass spectrometer, Balzers Instruments User's manual, Balzers
125. P.H. Dawson: Quadrupole mass spectrometry and its applications, Elsevier Science Publishing Company, Amsterdam (1976)
126. A.L. Hare, *Proc*. ISPC-3, UIPAC, g.3.2. (1977)
127. J.R. Fincke, S.C. Snyder and W.D. Swank, *Rev. Sci. Instrum*. **64**, 711 (1993)
128. M. Jankovic and J. Mostaghimi, *Plasma Chem. Plasma Process.* **18** (1), 53 (1998)
129. J.R. Fincke, W.D. Swank, S.C. Snider and D.C. Haggard, *Rev. Sci. Instrum.* **64** (12), 3585 (1993)
130. J.B. Cox and F.J. Weinberg, *J. Phys. D: Appl. Phys.* **4**, 877 (1971)
131. L. Foucault, *Ann. Obs. Paris* 5, 203 (1859)
132. A. Toepler, Ein Beitrag zur Experimentalphysik, Cohen & Son, Bonn (1864)
133. C. Gruenig and E. Mayinger, *Chem. Eng. Technol.* **23**, 909 (2000)
134. S. Chan, S. Torii, and T. Yano, *Int. J. Energy Res.* **25**, 1091 (2001)
135. J.F. Camacho, D.E. Bliss, and S.M. Cameron, *IEEE Trans. Plasma Sci.* **30**, 42 (2002)
136. O. Iwase, W. Süss, D.H.H. Hoffmann, M. Roth, C. Stöckl, M. Geissel, W. Seelig and L. Bock, *Phys. Scr.* **58**, 634 (1998)
137. S.O. Macheret, Y.Z. Ionikh, N.V. Chernysheva, A.P. Yalin, L. Martinelli and R.B. Miles, *Phys. Fluids* **13**, 2693 (2001)
138. I.H. Hutchinson: Principles of plasma diagnostics, Cambridge University Press (1987)
139. W. Merzkirch: Flow visualization, 2nd edition, Academic Press, London (1987)
140. M. Mitchner and C. Kruger: Partially Ionized Gases, Wiley&Sons, New York (1973)
141. F.P. Incropera and G. Leppert, *ISA Trans*. **6**, 35 (1967)

142. J.R. Fincke, S.C. Snyder and W.D. Swank; *Rev. Sci. Instrum.* **64**, 711 (1993)
143. http://ttwinner.free.fr/
144. L. Krejci and F. Marsik; Proc. International Conference on Fluid Mechanics (2003)
145. F.P. Ricou and D.B. Spalding, *J. Fluid Mech*. **2**, 21 (1961)
146. O. Chumak, M. Hrabovsky, V. Kopecky and T. Kavka, Proc. PLTP2003, May 2-6, 2004, Kyiv, Ukraine, 6.11.111-p (2004)
147. J.R. Fincke, W.D. Swank and D.C. Haggard, Proc. 1st United Thermal Spray Conference, (Ed.) C.C. Berndt, ASM International, OH, USA, 335 (1998)

List of published papers

I. T. Kavka, J. Gregor, V. Sember, M. Hrabovsky, Investigation of Heat and Mass Fluxes in Thermal Plasma Jet Generated in Water and Water-Argon Plasma Torches, Proceedings of contributed papers,WDS'2001, Prague, Czech Republic (2001) pp. 312-317

II. T. Kavka, M. Hrabovsky, Development of Plasma Properties along Thermal Plasma Jet Generated by Hybrid Water-Argon Torch, *Czechoslovak Jour.of Physics* **52** (2002)

III. T. Kavka, M. Hrabovsky, V. Sember, Properties of Electric Arc and Plasma Jet in the Plasma Torch with Water-Argon Stabilization, Proceedings of contributed papers, WDS'2002, Prague, Czech Republic (2002) pp. 381-387

IV. T. Kavka, E. Bouyer, R.H.Henne, Studying of Cold Gas Entrainment Process in Thermal Plasma Jet under Soft Vacuum Conditions, Proceedings of contributed papers, PLPT-03, Kiev, Ukraine (2003) 5.12.108-p

V. T. Kavka, M. Hrabovsky, M. Konrad, V. Kopecky, V. Sember, O. Chumak, Entrainment of ambient air into H2O/Ar Arc Plasma Jet, Proceedings of contributed papers, ISPC-16, June 22-27, 2003, Taormina, Italy

VI. T. Kavka, M. Hrabovsky, V. Sember, M. Kopecky, Effect of Gas Flow on Plasma Jet Generated by Hybrid H2O-Ar Torch, Proceedings of contributed papers, FSO2003, September 22-26, 2003, Nove Mesto na Morave, Czech Republic, pp. 85-88

VII. M. Hrabovsky, V. Kopecky, V. Sember, A. Chumak, T. Kavka, Properties of Hybrid Water/Argon DC Arc Torch under Reduced Pressure, ICOPS 2003, June 2-5, Jeju, Korea

VIII. M. Hrabovsky, V. Kopecky, T. Kavka, A. Chumak, V. Sember, Properties of New Plasma Spraying Torch with Hybrid Gas/Liquid Arc Stabilization, 48. Internationales Wissenschaftliches Kolloquium, September 22-25 2003, Ilmenau, Germany, pp. 319-320

IX. V. Sember, T. Kavka, V. Kopecky, M. Hrabovsky, Spectroscopic and Enthalpy Probe Diagnostics of Fluctuating H_2O-Ar Thermal Plasma Jet, Proceedings of contributed papers, FSO2003, September 22-26, 2003, Nove Mesto na Morave, Czech Republic, pp. 211-214

X. V. Sember, T. Kavka, V. Kopecky, M. Hrabovsky, Comparison of Spectroscopic and Enthalpy probe measurements in H2O-Ar Thermal Plasma Jet, Proceedings of contributed papers, ISPC-16, June 22-27, 2003, Taormina, Italy

XI. T. Kavka, J. Gregor, O. Chumak, M. Hrabovsky, Effect of arc power and gas flow rate on properties of plasma jet under reduced pressures, *Czechoslovak Jour. of Physics* **54** (2004) pp. 753-758

XII. T. Kavka, A. Maslani, J. Arnold, R. Henne, Influence of injection mode on properties of DC plasma jets for thermal plasma spraying, *Czechoslovak Jour. of Physics* **54** (2004), pp. 766-771

XIII. O. Chumak, V. Kopecky, M. Konrad, M. Hrabovsky, T. Kavka, Powder particle penetration into steam–argon plasma jet and its relation with particle parameters, *Czechoslovak Jour. of Physics* **54** (2004) pp. 931-936

XIV. T. Kavka, J. Arnold, R. Henne, M. Hrabovsky, Experimental investigation of shroud gas effect on properties of thermal plasma jets, Proceedings of contributed papers, 12th Workshop Plasmatechnik, September 23-24 2004, Ilmenau, Germany, pp. 49-54

XV. M. Hrabovsky, O. Chumak, T. Kavka, V. Kopecky, Study of the anode restrike processes in DC arc plasma torch, 12th Workshop Plasmatechnik, September 23-24 2004, Ilmenau, Germany, pp. 15-24

XVI. T. Kavka, J. Gregor, O. Chumak, V. Kopecky, M. Hrabovsky, Enthalpy Probe Study of the Expanding Thermal Plasma Jet; *J. High Temperature Material Process.* **9** (2005) pp. 45-54

XVII. M. Hrabovsky, V. Kopecky, O. Chumak, T. Kavka, M. Konrad, Properties Of Plasma Jet Generated In Hybrid Gas/Water Torch Under Reduced Pressures, *J. High Temperature Material Process.* **8** (4) (2004) pp. 575-584.

XVIII. T. Kavka, J. Gregor, O. Chumak, V. Kopecky, M. Hrabovsky, Study of the expansion thermal plasma jet by enthalpy probe, Proceedings of contributed papers, WDS'2004, Prague, Czech Republic, pp. 378-383

XIX. O. Chumak, M. Hrabovsky, V. Kopecky, M. Konrad, T. Kavka, Behaviour of Anode Attachment of DC Arc Plasma Jet at Reduced Pressures, Proceedings of contributed papers, WDS'2004, Prague, Czech Republic, pp. 388-393

XX. R. H. Henne, T. Kavka, J. Arnold, G. Schiller, Improvement of DC Thermal Plasma Spraying by Reducing the Cold Gas Entrainment Effect, Proc. International Thermal Spray Conference ITSC2005, May 2-4, 2005, Bassel, Switzerland, pp. 615-621

XXI. T. Kavka, M. Hrabovsky, O. Chumak, A. Maslani, Reduction of Oxygen Content in Atmospheric Plasma Jet: Shrouding by Reactive and Nonreactive Gas, Proceedings of contributed papers, ISPC-17, August 6-14, 2005, Toronto, Canada, ID-690

XXII. O. Chumak, M. Hrabovský, T. Kavka, V. Kopecký, Study of anode phenomena in dc arc plasma torch by electric probes, Proceedings of contributed papers, ISPC-17, August 6-14, 2005, Toronto, Canada, ID-282

XXIII. M. Hrabovsky, V. Kopecky, M. Konrad, M. Hlina, T. Kavka, G. van Oost, E. Beeckman, J. Verstraeten, J. Ledecky, E. Balabanova, Gasification of Biomass in Water-Stabilized DC Arc Plasma, Proceedings of contributed papers, ISPC-17, August 6-14, 2005, Toronto, Canada, ID-298

XXIV. T. Kavka, O. Chumak, V. Kopecky, M. Hrabovsky, Influence of Shroud Gas on DC Arc Plasma Jet and Injected Particles, Proceedings of contributed papers, CAPPSA 2005, August 30 – September 2, 2005, pp. 89-92

XXV. O. Chumak, M. Hrabovsky, T. Kavka, V. Kopecky, Investigation of Arc Fringes in Anode Region of DC Plasma Torch by Electric Probes, Proceedings of contributed papers, CAPPSA 2005, August 30 – September 2, 2005, pp. 73-76

XXVI. M. Hlina, M. Hrabovsky, V. Kopecky, M. Konrad, T. Kavka, G. van Oost, E. Beeckman, J. Verstraeten, Production of Syngas by Pyrolysis of Biomass in Thermal Plasma, Proceedings of contributed papers, CAPPSA 2005, August 30 – September 2, 2005, pp. 230-234

XXVII. O. Chumak, M. Hrabovsky, T. Kavka, V. Kopecky: Investigation Of Diffuse Current In Arc Boundary By Electric Probes, Proceedings of contributed papers, FSO XVI, September 5-9, 2005, pp. 73-76

XXVIII. M. Hrabovsky, V. Kopecky, V. Sember, T. Kavka, O. Chumak: Properties of Hybrid Water/Gas DC Arc Plasma Torch; *IEEE Transitions on Plasma Science*, in process

XXIX. G. Van Oost, M. Hrabovsky, V. Kopecky, M. Konrad, M. Hlina, T. Kavka, E. Beeckman, J. Verstraeten, Treatment of waste using a hybrid gas-water stabilized torch, *Advances in Applied Science* **5** (2005) pp. 7-12.

List of the attached publications

A. T. Kavka, M. Hrabovsky, M. Konrad, V. Kopecky, V. Sember, O. Chumak, Entrainment of Ambient Air into H2O/Ar Arc Plasma Jet, Proceedings of contributed papers, ISPC-16, June 22-27, 2003, Taormina, Italy

B. T. Kavka, J. Gregor, O. Chumak, V. Kopecky, M. Hrabovsky, Enthalpy Probe Study of the Expanding Thermal Plasma Jet, *J. High Temperature Material Process.* **9** (2005) pp. 45-54

C. T. Kavka, J. Arnold, R. Henne, M. Hrabovsky, Experimental investigation of shroud gas effect on properties of thermal plasma jets, Proceedings of contributed papers, 12th Workshop Plasmatechnik, September 23-24 2004, Ilmenau, Germany, pp. 49-54

D. T. Kavka, A. Maslani, J. Arnold, R. Henne, Influence of injection mode on properties of DC plasma jets for thermal plasma spraying, *Czechoslovak Jour. of Physics* **54** (2004) pp. 766-771